Dynamic Modeling and Analysis of Circumferential and Spiral Waves in Piezoelectric Cylinders

By: Ibrahim Muhammad

Supervised by Dr. Hao Bai, Department of Mechanical Engineering

Co-Supervised by Dr. Meilan Liu, Department of Mechanical Engineering

December, 2011

A Thesis submitted in partial fulfillment of the requirement of

The M.Sc. Eng. Degree in

Control Engineering

Faculty of Engineering

Lakehead University

Thunder Bay, Ontario

Copyright Exceptions

Abstract

Understanding the dynamic characteristics of ultrasonic guided wave in structures is important, as it is one of the methods that are widely used in many different areas of industrial sectors and inspections, such as Non-Destructive Testing (QNDT). The ultrasonic guided wave is transmitted and reflected at the surface of the wave materials. A detailed study and interpretation of mode conversion in guided wave is required.

The current research presents a theoretical study of guided wave in piezoelectric cylinders based on the theory of elasticity. Two different methods were employed to study dispersion relations in piezoelectric cylinders. One of them is a finite element method and the other is an analytical method. In the analytical method, three displacement potentials are introduced to obtain dispersion relation of guided wave modes. This method is developed primarily to cross check finite element results.

In the finite element method, the dispersion equation has been formulated as a generalized eigenvalue problem by treating mechanical displacements and electric potential with one dimensional (quadratic) finite element model through the thickness of the cylinder. Computer codes have been developed and verified by comparing with limited published results. The numerical results are presented for different cylinders and electric boundary conditions. In the numerical studies, three dimensional wave spectrum surfaces were generated. Discussion of guided wave propagating in different direction in cylinders was given as well.

Acknowledgement

I would take this chance to thank all the people that helped me to accomplish this research. First of all I would like to thank Almighty God for giving the power and health to achieve this task. I would like to thank my supervisor Dr. H. Bai for all his support and help during these past two years. He has provided me with lots of insight on how to become a good researcher. I would like to thank my co-supervisor Dr. M. Liu. I would also like to thank NSERC for all the funding I have received. Also, I would like to thank my thesis examiner Dr. W. Wang and Dr. B. Ismail. The Lakehead University graduate department also helped me financially and I would like thank them for all their support. I would also like to thank and show my appreciation to all the faculty and staff of the Masters of Science in Control Engineering. Last but not least I would like to greatly thank family (Father, mother, my two brothers and 3 sisters) and all my dear friends. Combined together they have given me the strength and will power to accomplish what I have accomplished. Without them I would definitely not have made it this far.

Table of Contents

List of Figures

List of Tables

Nomenclature

$A, B, C = mechanical\ scalar\ potentials$

$c_T = shear\ wave\ velocity$

$c^0 = elastic\ modulus$

$[C] = matrix\ representing\ the\ conglomeration\ of\ [\boldsymbol{C^*}], [\boldsymbol{e}]\ and [\boldsymbol{\varepsilon}]$

$[\boldsymbol{C^*}] = matrices\ of\ elastic\ anisotropic\ moduli$

$\boldsymbol{D_i}\ (1,2,3) = components\ of\ electric\ displacement$

$E^0 = electric\ field\ constant$

$e^0 = piezoelectric\ constant$

$[\boldsymbol{e}] = matrices\ of\ piezoelectric\ constants$

$h = non - dimensional\ cylinder\ thickness$

$H = electric\ enthalply$

$J_m = Bessel's\ function\ of\ order\ m\ type\ J$

$k = non -\ dimensional\ axial\ wave\ number$

$[\boldsymbol{K_{ij}}](i = j = 1,2,3) = stiffness\ matrices$

$KE = kinetic\ energy$

$[\boldsymbol{L}] = differential\ Operator$

$m = non - dimensional\ circumferential\ wave\ number$

$[\boldsymbol{M}] = mass\ matrix$

$[\boldsymbol{N}] = Finite\ element\ interpolation\ matrix$

$P_i(i = 1,2,3,4,5,6) = integration\ constants$

$r = radial\ direction\ coordinate$

$r_i = non - dimensional\ inner\ radius\ of\ a\ cylinder$

$r_o = non - dimensional\ outter\ radius\ of\ a\ cylinder$

$\{\boldsymbol{S_i}\}(1,2,3,4,5,6) = components\ of\ mechanical\ strain$

$\{\boldsymbol{T_i}\}(i = 1,2,3,4,5,6) = stress\ components$

$t = time\ (seconds)$

$\{\boldsymbol{u}\} = mechanical\ displacements$

$\{\ddot{\boldsymbol{u}}\} = second\ time\ derivative\ of\ mechanical\ displacements$

$\{\boldsymbol{v}\} = the\ field\ variables\ of\ nodal\ displacement\ and\ electric\ potential$

$\{\boldsymbol{V_e}\} = the\ nodal\ displacement\ and\ electric\ potential\ in\ an\ element$

$\{\boldsymbol{V}\} = wave\ propogation\ harmonic\ solution$

$\omega = non - dimensional\ angular\ frequency$

$\omega^* = angular\ frequency\ (\frac{rad}{s})$

$\omega_0 = relative\ angular\ frequency\ \left(\frac{rad}{s}\right)$

$Y_m = Bessel's\ function\ of\ order\ m$ type Y

$z = axial\ direction\ coordinate$

Greek Letters

$\zeta = FEM\ coordinate\ system$

$\rho = normalized\ mass\ density$

$[\boldsymbol{\varepsilon}]$ = matrices of dielectric permittivities

$\varepsilon^0 = dieelectric\ constant$

$\varphi = electric\ potential$

$\theta = circumerentail\ direction\ coordinate$

$\nabla = Differntial\ operator$

Acronyms

FEM=Finite Element Method

FGM=Functionally Graded Material

FGPM=Functionally Graded Piezoelectric Material

QNDT=Qualitative Non-Destructive Testing

Superscripts

T=matrix transpose

Chapter 1: Introduction

1.1 Background

Ultrasonic Qualitative Non-Destructive Testing (QNDT) is mainly dependent through an understanding of the propagation and evanescent waves in the material or specimen under investigation. The main purpose of QNDT is to detect and identify mechanical failures without causing damage to the product under investigation. Finding such failures is an important task to insure that catastrophic failure does not occur. Figure 1 shows a typical experimental setup for QNDT. Basically, an ultrasonic transducer is used to generate a guided wave by converting electrical energy into mechanical vibrations. The wave travels and it reflects off the surface of the test material (where flaws exist). The reflected pulses can be reconverted into electrical energy using a transducer. The reflected pulses can be measured and analyzed using the time of travel and size of these pulses. This information can lead to the detection of position and size of the cracks or defects. The research in this thesis will be a benchmark for understanding what happens to the reflected waves (mode conversion) and the detection of defects.

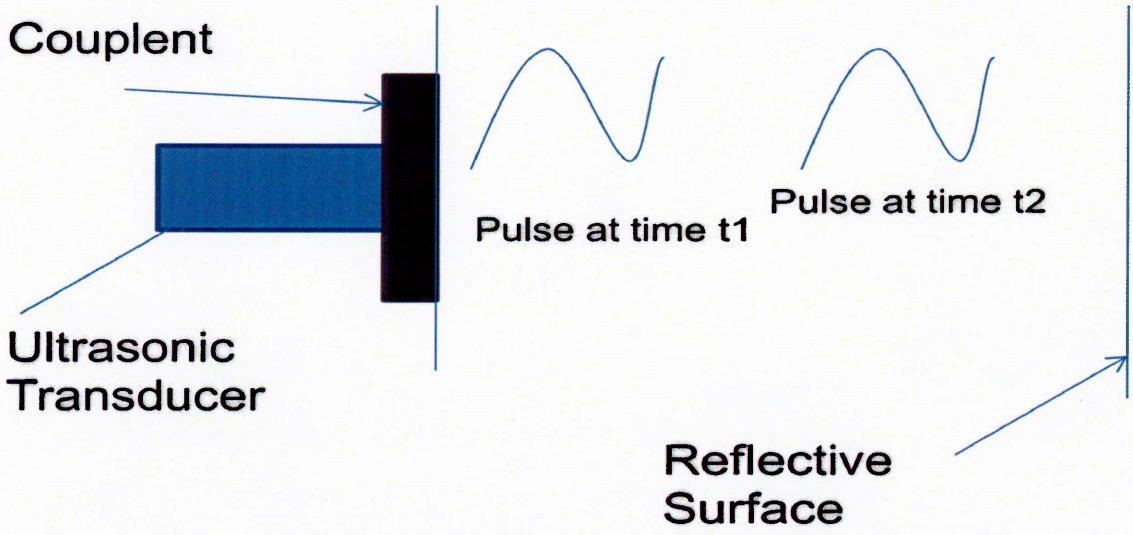

Figure 1: QNDT typical experimental setup

Many mechanical parts undergo a series of failures in a lifetime. Fatigue cracks are one of these failures, they have been found to initiate and grow in the radial direction in many annulus shaped

components [1]. It has also been proposed by Liu et al. [2] that guided circumferential waves may be used to detect radial fatigue cracks. Many circular mechanical parts are used in the industry. For example, a helicopter's rotor shaft system consists of many circular hollow parts that are not accessible for visual inspection. In addition, in the nuclear power plant generation, the reactors and most of their components are circular in shape such as fuel rods and the core. Accessibility of such parts can be difficult and also hazardous due to radiation. A helicopter rotor hub is composed of an inner and outer cylinder and this is where fatigue cracks form and propagate. Therefore, developing more accurate, reliable and robust techniques is needed since the conventional techniques are not as reliable for detection of defects. For example, Pulse echo is used today and it is hard for this technique to interrogate such parts because the problem of the curvature, complicated nature of the reflected mode and the accessibility. Other methods of investigating fatigue cracks rely predominantly on visual inspection as well as methods of ultrasonic imaging. The problem with conventional ultrasonic imaging, in the case of annulus type, is that access to the inner surface is usually unavailable. That is why waves are only generated from the outside surface. Radial cracks are known to initiate from the exterior [2]. In turn, it is needed to selectively generate particular wave modes for the concentration of energy is near the inner surface to increase signal to noise ratio. Non-destructive testing is critical determining remaining life and structure integrity.

The results in this thesis may also serve as the basis for designing piezoelectric transducers, for which standing wave modes resulting from reflections of travelling waves off cross-section boundaries of the cylinders play an important role.

1.2 Literature Review

Many types of wave propagations have been studied in the past. Mindlin and McNiven developed wave propagation in the axial direction of a circular cross section [3]. Mindlin and Fox [4] also looked into the axial propagation of waves of a rectangular cross section bar. Gazis [5] studied axial propagation on a circular hollow cylinder. Miklowitz [6] reviewed all the above studies. Ditri and Rose [7] solved the problem of transient wave propagation in the axial direction of a hollow cylinder subjected to surface tractions.

Numerous researchers have studied wave propagation in hollow and solid cylinders. Many studies have mainly concentrated on isotropic materials. Pochhammer [8] was one of the

first to analyze axisymmetric waves in isotropic cylinders. When analyzing waves that propagate in the axial or the circumferential direction, one must first look at the studies of Cook and Valkenburg [9]. They observed that the Rayleigh surface wave could exist on a cylindrical surface. A greater comprehensive analysis was developed by Viktorov [10], Grace et al. [11]. Frequency dispersion takes place for surface waves propagating along a curved surface, which is not like the Rayleigh on a planar surface. This was found by the above-mentioned research [10, 11]. Brekhovskikh [12] also found that in the case of curvilinear boundary of a solid, it is possible for other type of waves to occur close to the curved boundary. Cerv [13] investigated the dispersion of elastic waves and Rayleigh type waves in a thin circular annulus. Dispersion equations for time harmonic circumferential waves in a circular annulus were developed by Qu et al. [14]. It was found that multiple reflections can occur and surface waves between the outer and inner surfaces can propagate in the radial direction as well.

Mirsky [15] studied the propagation of a free harmonic wave in transversely isotropic circular cylinders. Experimental work on the analysis of anisotropic cylinders first appeared in [16, 17]. Kaduchak and Loeffler [18] developed some theoretical work on acoustic wave scattering from composite cylindrical shells that are made up of isotropic and transversely isotropic layers. Tsai [19, 20] investigated cylindrically guided waves in transversely isotropic shafts and thick hollow cylinders. Transversely isotropic cylinders that are immersed in water were analyzed by Dayal [21]. Dayal's approach was later corrected by Nagy [22]. The analytical formulation of wave propagation in fluid loaded transversely isotropic cylinders and cylinder shells was developed by Berliner and Solechi [23, 24].

Piezoelectric cylinders have been widely used in electro-optics, communications, measurement techniques, and many other acoustics applications. The Currie brothers first discovered the term piezoelectricity in 1880 and work has been extensively documented in many literatures [25-27]. Mathematical models have been formulated and the governing equations are presented but exact solutions and techniques are difficult to obtain for a variety of much more complex problems. Shaw [28] has presented the first experimental studies. He used optical interference techniques to measure resonant and antiresonant frequencies. Approximate solutions were presented since exact solutions are not widely available. EerNisse [29] developed a solution technique that was based on the Ritz method. This technique used a trail function that

was based on Bessel's and Sine Functions. The results of EerNisse [29] were compared to those of Shaw [28] and were found to be higher than the measured odd modes of fully electrode barium titanate discs. Allik and Hughes [30] used a finite element method that was based on the variation principles used by EerNisse [29].

Allik and Hughes [30] found that the finite element method can be used to solve the elastic equations of motion for complex geometries but the work did not present any numerical work. Many more researchers used the finite element method to analyze the vibration characteristics of piezoelectric objects. Many also extended to the three-dimensional finite element method but this required high computing cost for data storage and computational time. The solutions of Ostergaard and Pawlak [31] allowed them to solve static and electroelastic vibration of different piezoelectric devices, they did this using the finite element method presented in ANSYS engineering analysis system theoretical manual. Cheng [32] developed a one-dimensional static analysis of the axisymmetric 6m2 piezoelectric crystal class, which also solved the axisymmetric dynamic vibration of piezoelectric cylinders.

The vibrations of electrostatic cylinders of infinite length were first studied by Paul [33]. He was the first to find the frequency equation of a cylindrical shell of the hexagonal 6 mm piezoelectric crystal class. Wilson and Morrison [34] extended Paul's work by solving the exactly the equations of motion for cylindrical rods belonging to $6, \overline{6}$, 622 and 6 mm piezoelectric crystals. They solved the equations for both the free and clamped surfaces for the elastic boundary conditions and short and open circuit electrical boundary conditions. Paul and Raju [35] used Ambardor and Ferris [36] unfinished work, due to complexity, to solve wave propagation in long bone such as the femur. They used asymptotic analysis to solve this problem. Paul and Venkatesan [37] used the same method to solve the axisymmetric frequencies of a long cylinder guided by a thin gold coat. The results [37] proved that frequencies are higher for the coated cylinder in comparison to the uncoated cylinder. They also found the torsional frequencies of hexagonal 622 class crystals using the Fourier expansion collection method. Circular and elliptic solutions were also obtained by the above-mentioned source for cylinders of Beta quartz. A finite element method was used by Buchanan and Peddison [38] to find frequencies over a wider range of wavelengths than those presented by Paul and Vankatesan [37]. In addition, their method was simpler in comparison with Paul's findings. Their findings

contradict Paul's since they found that increasing the thickness of the coating decreased the frequency.

Piezoelectric ceramics were studied by Adelman et al. [39]. The vibration of radially polarized piezoelectric transducers' governing equations was solved for the PZT-4 transducers subjected to different boundary conditions. The resonant and antiresonant frequencies along with the radial displacement and electric potential, for long tubes and circular annuli were also presented.

Siao et al, [40] solved the problem of wave propagation in a laminated piezoelectric cylinder using the finite element method. There is a misprint in these results so this makes it hard to compare with these results. Bai et al. [41] later corrected this shortcoming. They studied the electro mechanic response of a laminated piezoelectric hollow cylinder by means of a semi analytical FEM and their results have been confirmed by Shatlov et al. [42].

Circumferential Wave Propagation

Liu et al, [43] considers a two-dimensional circular annulus as a waveguide and studies the propagating waves in the circumferential direction. The dispersion equation is derived analytically and the dispersion curves are plotted. Displacement profiles are presented for the wall thickness. A comparison is made between a flat plate and an annulus with infinite curvature.

It was found by this study that at high frequencies for different inner to outer surface radii, the first propagating mode is almost a straight line that means it is almost non-dispersive. In addition, there exists a crossover point between neighboring modes. Such crossover points exist in the case of a flat plate; and can be used to identify symmetric and anti-symmetric modes (for flat plate only). The presented phase velocities confirmed the results obtained from the dispersion curves. The group velocities plots established that the dispersion equations only depend on the ratio of the inner to the outer surface not only outer radius. By approximating the dispersion curves of a thin cylinder to that of a flat plate (shrinking the radius to zero) the solutions to a solid circular annulus cannot simply be obtained.

Tyutekin [44] examines helical waves and their properties using Kirchhoff's-Love equations. Tyutekin [44] reduced the complexity of the problem to an equivalent plane wave on a plate. After the dispersion equation is derived, a conclusion is made about the anisotropy of shell properties. Dispersion curves are plotted for different propagating angles and the

displacements are calculated. After analyzing different angles of propagation, it was concluded that for an isotropic media the wave number of free waves do not depend on the angle of propagation.

Liu et al, [2], the solution of the three dimensional equations of motion and quasi-electrostatic equations are given in terms of eight mechanical and three electrical potentials. The dispersion curves are presented for propagation and evanescent waves for PZT-4 and PZT-7 for circumferential waves numbers m=1, 2 and 3. When analyzing the PZT-4 material for the short circuit boundary conditions, it was observed that the first mode asymptotes to the surface waves propagation and the second mode tends to the asymptote to the shear wave. When comparing the short circuit with the open circuit boundary condition, it was found that the curves of the open circuit are much steeper than the short circuit boundary conditions. For the PZT7 material, it was found that the first bending mode is not sensitive to the type of electrical boundary conditions on the lateral cylindrical surface and not sensitive to the measure of electro mechanical coupling. Nevertheless, higher modes seem to be more sensitive to both the type of electrical boundary conditions and the measure of electro-mechanical coupling.

In Jiangong et al, [45] the wave characteristics of Functionally Graded Piezoelectric Material (FGPM) hollow cylinders are studied. Dispersion curves for FGPM and non-piezoelectric hollow cylinders are considered for showing the piezoelectric effect. It was found that FGPM hollow cylinders has no real change on the dispersion curves, but the gradient field can change the piezoelectricity effect considerably. One major effect to the characteristics of the guided waves is caused by the ratio of radius to thickness. In addition, it was found that the FGPM can weaken the dispersion effect unlike the regular piezoelectric material.

Jiangon [46] studied piezoelectric-piezomagnetic functionally graded material (FGM). A comparison is made between piezoelectric-piezomagnetic FGM and non-piezoelectric non-piezomagnetic material to show the influences of piezoelectric-piezomagnetic effect. The independent SH (shear wave) wave is found not to be effected by the electric field and the magnetic field when the cylindrical curved plate is orthotropic and is polarized in the thickness direction. The piezoelectric effect is much stronger on the Ba2 TiO3-CoFe2O4 FGM in a cylindrical curved plate when compared with the effect of the magneto-electric coefficient.

Finally, it was found that both piezoelectric and piezomagnetic cylindrical curved plates (guided waves) are influenced by varying the ratio of radius to the thickness.

Previous research on piezoelectric cylinders has mainly concentrated on assigning the circumferential wave number to an integer. To fully understand the wave propagation one needs to study the effects of assigning m to a real non-integer and complex number. To be able to fully understand wave propagation and how this can be related to crack detection, we need to better understand mode conversion at the reflected surface. For example, circumferential cracks are easy to detect by axial waves, on the other hand axial cracks are easy to detect with the circumferential waves. Therefore, reflected and transmitted waves are sensitive to the geometry and orientation of the crack. This here is why we are studying wave propagation in both the axial and circumferential direction.

1.3 Objective

The main objective of the current research is to study guided ultrasonic waves propagation, in both the circumferential and axial directions, in an infinitely long piezoelectric circular cylinder. The circumferential wave number m is taken as a real non-integer and complex number. Therefore, the periodicity property does not hold in the circumferential direction. The circumferential wave propagation in an annulus is studied first. The dispersion equation is obtained analytically by solving the equations of motion. The equations of motion should be decoupled when they are expressed by the displacement and electric potential. A semi-analytical FEM (Finite Element Method) is introduced here as well. Solutions, including exact and numerical, will be severed as a benchmark for further involved future research. Then the circumferential wave propagation along a piezoelectric circular cylinder is studied. In the study, the waveform solution is represented by the expression: $e^{i(kz+m\theta-\omega t)}$ where m and k are the circumferential and axial wave numbers and ω is the circular frequency of the wave. Not like most the studies that m is limited as an integer, both m and k can take a real and complex number. The analytical solution for the PZT4 was introduced and the dispersion relations were developed after considering various mechanical and electrical boundary conditions in the cylinder's surfaces. A finite element procedure is presented here. Numerical results are presented for different geometries of the cylinder.

The thesis is divided into four chapters. The introduction is presented in chapter one. The development and analysis of circumferential wave in an annulus is presented and discussed in chapter two. A more general and complicated analysis of circumferential waves (spiral waves) in a circular cylinder is presented in chapter three. Finally, the conclusions and recommendations for further studies are outlined in chapter four.

Chapter 2: Circumferential Wave in an Annulus

The propagation of the circumferential wave in a circular cylinder is considered in this chapter. Here, the motion is assumed to be independent on the axial direction of the cylinder and the axial displacement is assumed to be zero. To have a pure circumferential wave one needs to assign $w = 0$ and $k = 0$. Two methods are developed here: analytical method and the finite element approximation method. In the analytical method, the explicit analytical solution is derived to archive the frequency equation of the cylinder. On the other hand, in the FEM, Hamilton's principle is employed to obtain the equation of motion, and the wave spectra can be constructed by solving the eigenvalue problem.

Computer codes based on FORTRAN language are developed for both solutions. To validate the effectiveness and the accuracy of the computer codes, comparison with published results of an isotropic cylinder is done. Numerical results for thick and thin cylinders are also presented here.

2.1 Equations of Motion

Consider an infinitely long cylinder. The symmetrical axis of the material coincides with the symmetrical axis of the cylinder. Since the motion is independent to the axial direction ($k = 0$, $w = 0$) of the cylinder, the motion in the cylinder will be a plane strain. The polar coordinates (r, θ) with origin located at the centre of the annulus are employed here as shown in Figure 2.

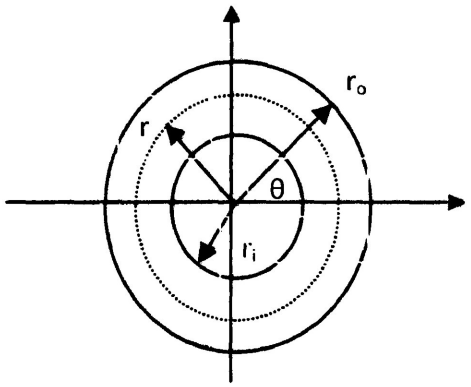

Figure 2: An annulus with inner radius r_i and outer radius r_o.

The variables involved in the study are the mechanical displacements , stress , strain electric displacements and electric fields . They are defined as follows:

$$\{\boldsymbol{u}\} = \{u, v\}^T \tag{2.1}$$

$$\{\mathbf{T}\} = \{T_{rr}, T_{\theta\theta}, T_{r\theta}\}^T = \{T_1, T_2, T_6\}^T \tag{2.2}$$

$$\{\boldsymbol{S}\} = \{S_{rr}, S_{\theta\theta}, S_{r\theta}\}^T = \{S_1, S_2, S_6\}^T \tag{2.3}$$

$$\{\boldsymbol{D}\} = \{D_r, D_\theta\}^T = \{D_1, D_2\}^T \tag{2.4}$$

$$\{\boldsymbol{E}\} = \{E_r, E_\theta\}^T = \{E_1, E_2\}^T = -\nabla\phi \tag{2.5}$$

Where, $u = u(\mathrm{r}, \theta, \mathrm{t})$, $v = v(\mathrm{r}, \theta, \mathrm{t})$ are the mechanical displacement components in the radial and circumferential direction, respectively, and $\phi = \phi(\mathrm{r}, \theta, \mathrm{t})$ is the electric potential, and t is the time.

The strain displacement [49] relations are:

$$S_1 = \frac{\partial u}{\partial r} \tag{2.6}$$

$$S_2 = \frac{1}{r}\left(u + \frac{\partial v}{\partial \theta}\right) \tag{2.7}$$

$$S_6 = \frac{1}{r}\left(\frac{\partial u}{\partial \theta} - v\right) + \frac{\partial v}{\partial r} \tag{2.8}$$

The electric field [48] components are:

$$E_1 = -\frac{\partial \phi}{\partial r} \tag{2.9}$$

$$E_2 = -\frac{1}{r}\frac{\partial \phi}{\partial \theta} \tag{2.10}$$

The coupled constitutive [48] equations are given by:

$$\{\boldsymbol{T}\} = [\boldsymbol{C}^*]\{\boldsymbol{S}\} \tag{2.11}$$

$$\{\boldsymbol{D}\} = [\boldsymbol{\varepsilon}]\{\boldsymbol{E}\} \tag{2.12}$$

$$[\boldsymbol{C}^*] = \begin{bmatrix} C_{11} & C_{12} & 0 \\ C_{12} & C_{11} & 0 \\ 0 & 0 & C_{66} \end{bmatrix} \tag{2.13}$$

$$[\varepsilon] = \begin{bmatrix} \varepsilon_{11} & 0 \\ 0 & \varepsilon_{11} \end{bmatrix} \tag{2.14}$$

Where, $C_{11}, C_{12}, C_{66} = (C_{11} - C_{12})/2$, are the elastic stiffness constants at constant electric field and ε_{11} is the clamped dielectric constant at constant strain.

The equations of motion [49] are given by

$$\frac{\partial T_1}{\partial r} + \frac{1}{r}\frac{\partial T_6}{\partial \theta} + \frac{T_1 - T_2}{r} = \rho \ddot{u} \tag{2.15}$$

$$\frac{\partial T_6}{\partial r} + \frac{1}{r}\frac{\partial T_2}{\partial \theta} + 2\frac{T_6}{r} = \rho \ddot{v} \tag{2.16}$$

The double dot notation is the second time derivative. The charge equation of electrostatics [48] is given by:

$$\frac{\partial D_1}{\partial r} + \frac{1}{r}\frac{\partial D_2}{\partial \theta} + \frac{D_1}{r} = 0 \tag{2.17}$$

The traction free, open circuit and closed circuit boundary conditions are given as follows:

Traction free boundary conditions

$$T_1 = T_6 = 0 \ @ \ r = r_i, r_o \tag{2.18}$$

Open circuit boundary conditions

$$D_1 = 0 \ @ \ r = r_i, r_o \tag{2.19}$$

Closed Circuit boundary conditions

$$\phi = 0 \ @ \ r = r_i, r_o \tag{2.20}$$

Non-dimensionalization will be used here in order to scale down all the different variables. All the variables are given in terms of the dimensional terms. In order to non-dimensionalize, four key parameters are required:

- The thickness, h
- Elastic moduli, c^0
- Piezoelectric constant, e^0

- Mass density, ρ^0

The reference parameters are the dielectric constant ε^0 and the electric field E^0 which can be defined by the following equations respectively:

$$\varepsilon^0 = (e^0)^2/c^0 \tag{2.21}$$

$$E^0 = \frac{c^0}{e^0} \tag{2.22}$$

All the dependent variables, independent variables and material properties are now normalized as follows:

$$r^* = \frac{r}{h}\,,\ t^* = \frac{t}{h}\sqrt{\frac{c^0}{\rho^0}} \tag{2.23}$$

$$u^* = \frac{u}{h}\,, v^* = \frac{v}{h},\ T_p{}^* = \frac{T_p}{c^0},\ S_p{}^* = S_p \tag{2.24}$$

$$D_i{}^* = \frac{D_i}{e^0},\ E_i = \frac{E_i}{E^0} \tag{2.25}$$

$$c_{pq}{}^* = \frac{c_{pq}}{c^0},\ \varepsilon_{ip}{}^* = \frac{\varepsilon_{ip}}{\varepsilon^0},\ e_{ip}{}^* = \frac{e_{ip}}{e^0},\ \rho^* = \frac{\rho}{\rho^0} \tag{2.26}$$

Since the normalized equations have the same form as their counterpart before normalization, in the following, the * will removed for the purpose of simplifying the notation.

2.2 Analytical Solution Formulation

The mechanical displacements [49] are represented by two scalar potentials, namely:

$$u = \frac{\partial B}{\partial r} + \frac{1}{r}\frac{\partial C}{\partial \theta} \tag{2.27}$$

$$v = \frac{1}{r}\frac{\partial B}{\partial \theta} - \frac{\partial C}{\partial r} \tag{2.28}$$

The strains are then derived using the above two potentials and Equations (2.6-2.8), and are given by the following equations:

$$S_1 = \frac{\partial^2 B}{\partial r^2} - \frac{1}{r^2}\frac{\partial C}{\partial \theta} + \frac{1}{r}\frac{\partial^2 C}{\partial \theta \partial r} \tag{2.29}$$

$$S_2 = \frac{1}{r}\left[\frac{1}{r}\frac{\partial^2 B}{\partial \theta^2} - \frac{\partial^2 C}{\partial \theta \partial r} + \frac{\partial B}{\partial r} + \frac{1}{r}\frac{\partial C}{\partial \theta}\right] \tag{2.30}$$

$$S_6 = \frac{2}{r}\frac{\partial^2 B}{\partial \theta \partial r} - \frac{2}{r^2}\frac{\partial B}{\partial \theta} + \frac{1}{r^2}\frac{\partial^2 C}{\partial \theta^2} - \frac{\partial^2 C}{\partial r^2} + \frac{1}{r}\frac{\partial C}{\partial r} \tag{2.31}$$

The stresses are also derived by applying the definitions of the strain displacement in the above Equations (2.29-2.31).

$$T_1 = C_{11}\left[\frac{\partial^2 B}{\partial r^2} - \frac{1}{r^2}\frac{\partial C}{\partial \theta} + \frac{1}{r}\frac{\partial^2 C}{\partial \theta \partial r}\right] + C_{12}\frac{1}{r}\left[\frac{1}{r}\frac{\partial^2 B}{\partial \theta^2} - \frac{\partial^2 C}{\partial \theta \partial r} + \frac{\partial B}{\partial r} + \frac{1}{r}\frac{\partial C}{\partial \theta}\right] \tag{2.32}$$

$$T_2 = C_{12}\left[\frac{\partial^2 B}{\partial r^2} - \frac{1}{r^2}\frac{\partial C}{\partial \theta} + \frac{\partial^2 C}{\partial \theta \partial r}\right] + C_{11}\frac{1}{r}\left[\frac{1}{r}\frac{\partial^2 B}{\partial \theta^2} - \frac{\partial^2 C}{\partial \theta \partial r} + \frac{\partial B}{\partial r} + \frac{1}{r}\frac{\partial C}{\partial \theta}\right] \tag{2.33}$$

$$T_6 = C_{66}\left[\frac{2}{r}\frac{\partial^2 B}{\partial \theta \partial r} - \frac{2}{r^2}\frac{\partial B}{\partial \theta} + \frac{1}{r^2}\frac{\partial^2 C}{\partial \theta^2} - \frac{\partial^2 C}{\partial r^2} + \frac{1}{r}\frac{\partial C}{\partial r}\right] \tag{2.34}$$

The electric displacements [48] in terms of the scalar potential ϕ are:

$$D_1 = -\varepsilon_{11}\left[\frac{\partial \phi}{\partial r}\right] \tag{2.35}$$

$$D_2 = -\varepsilon_{11}\left[\frac{1}{r}\frac{\partial \phi}{\partial \theta}\right] \tag{2.36}$$

By substituting Equations (2.27, 2.28) and (2.32-2.36) into the equations of motion (2.15-2.17), the following Equations are obtained:

$$c_{11}\nabla^2 B = \rho \ddot{B} \tag{2.37}$$

$$c_{66}\nabla^2 C = \rho \ddot{C} \tag{2.38}$$

$$\nabla^2 \phi = 0 \tag{2.39}$$

Where, $\nabla^2 = [\,]_{,rr} + \frac{1}{r}[\,]_{,r} + \frac{1}{r^2}[\,]_{,\theta\theta}$. (2.40)

The wave-like form solutions [49] are employed here as

$$B = B_0 e^{i(m\theta - \omega t)} \tag{2.41}$$

$$C = C_0 e^{i(m\theta - \omega t)} \tag{2.42}$$

$$\emptyset = \emptyset_0 e^{i(m\theta-\omega t)} \tag{2.43}$$

Where, m is the circumferential wave number and ω is the circumferential frequency. Substituting Equations (2.41-43) into Equations (2.37-2.39), respectively, will yield the following differential Equations:

$$B_0^{"} + \frac{1}{r}B_0' + \left(\alpha_1^2 - \frac{m^2}{r^2}\right)B_0 = 0 \tag{2.44}$$

$$C_0^{"} + \frac{1}{r}C_0' + \left(\alpha_2^2 - \frac{m^2}{r^2}\right)C_0 = 0 \tag{2.45}$$

$$\emptyset_0^{"} + \frac{1}{r}\emptyset_0' - \frac{m^2}{r^2}\emptyset_0 = 0 \tag{2.46}$$

Where, the double-prime superscript indicates the 2nd derivative with respect to r.

The solutions to Equations (2.44-2.46) are given by [50]:

$$B_0 = P_1 J_m(\alpha_1 r) + P_2 Y_m(\alpha_1 r) \tag{2.47}$$

$$C_0 = P_3 J_m(\alpha_2 r) + P_4 Y_m(\alpha_2 r) \tag{2.48}$$

$$\emptyset_0 = P_5 r^m + P_6 r^{-m}, \qquad \text{for } m \neq 0 \tag{2.49}$$

and

$$\emptyset_0 = P_5 \ln r + P_6, \qquad \text{for } m = 0 \tag{2.50}$$

Where

$$\alpha_1 = \frac{\omega}{c_1},\ \alpha_2 = \frac{\omega}{c_2},\ c_1 = \sqrt{\frac{c_{11}}{\rho}}, c_2 = \sqrt{\frac{c_{66}}{\rho}} \tag{2.51}$$

and P_1, ..., P_6 are unknown constants to be determined by the mechanical and electrical boundary conditions.

By substituting the solutions into the stress and electric displacement or electric potential boundary conditions, the linear homogeneous equations are derived as

$$[\boldsymbol{Q}]_{6\times 6}\begin{Bmatrix} P_1 \\ P_2 \\ P_3 \\ P_4 \\ P_5 \\ P_6 \end{Bmatrix} = 0 \tag{2.52}$$

Where, the elements of the $\boldsymbol{Q}$ matrix are given in Appendix A. The frequency spectra can be obtained by finding the non-zero solution of the above equation which is given by

$$|Q| = 0 \tag{2.53}$$

If $\boldsymbol{\omega}$ is given, the circumferential wave number m can be computed. The circumferential wave number m can be real, imaginary or complex wave numbers. The real wave numbers are representing the propagating waves. The imaginary and complex wave numbers represent non-propagating modes.

2.3 Finite Element Method (FEM) Formulation

Siao et al. [40] developed a Rayleigh-Ritz type approximation in laminated composite media. In their solution procedure, the displacement and electric potential along the radial direction were represented by the interpolation of quadratic functions of radial variable. Three-node elements were used along a radius of the cylinder.

Introducing the Hamilton's principle to include piezoelectric effects in a body of volume B which has the form [40]

$$\delta \int_{t_0}^{t_1} (KE - H)dt = 0 \tag{2.54}$$

Where KE and H are the kinetic energy [49] and the electric enthalpy [48], respectively, given by:

$$KE = \frac{1}{2} \iiint \{\dot{\boldsymbol{v}}\}^T [\boldsymbol{\rho}] \{\dot{\boldsymbol{v}}\}\, dB \tag{2.55}$$

$$H = \frac{1}{2} \iiint \{\boldsymbol{q}\}^T [\boldsymbol{C}] \{\boldsymbol{q}\}\, dB \tag{2.56}$$

Where,

$$[\boldsymbol{C}] = \begin{bmatrix} [\boldsymbol{C}^*] & 0 \\ 0 & -[\boldsymbol{\epsilon}] \end{bmatrix} \tag{2.57}$$

$$\{v\} = \begin{Bmatrix} u \\ \varphi \end{Bmatrix} \tag{2.58}$$

$$\{q\} = \begin{Bmatrix} S \\ E \end{Bmatrix} \tag{2.59}$$

The displacements and electric potential in a typical element can be expressed as

$$\{v\} = [N]\{V_e\} \tag{2.60}$$

Where, $\{V_e\}$ is the nodal value vector containing the displacement u, v and electric potential φ at the three nodes.

$$[N] = \begin{bmatrix} n_1(\zeta) & n_2(\zeta) & n_3(\zeta) & 0 & 0 & 0 & 0 & 0 & 0 \\ 0 & 0 & 0 & n_1(\zeta) & n_2(\zeta) & n_3(\zeta) & 0 & 0 & 0 \\ 0 & 0 & 0 & 0 & 0 & 0 & n_1(\zeta) & n_2(\zeta) & n_3(\zeta) \end{bmatrix} \tag{2.61}$$

and

$$n_1(\zeta) = \frac{1}{2}\zeta(\zeta - 1), \quad n_2(\zeta) = 1 - \zeta^2, \quad n_3(\zeta) = \frac{1}{2}\zeta(\zeta + 1) \tag{2.62}$$

$$\{q\} = [\mathrm{B_1}]\{V\} + [B_2]\{V_{,\theta}\} \tag{2.63}$$

Where,

$$[B_1] = [L_r][N], [B_2] = [L_\theta][N] \tag{2.64}$$

$$[B_1] = \begin{bmatrix} N_{,r} & 0 & 0 \\ \frac{1}{r}N & 0 & 0 \\ 0 & N_{,r} - \frac{N}{r} & 0 \\ 0 & 0 & -N_{,r} \\ 0 & 0 & 0 \end{bmatrix} \tag{2.65}$$

$$[B_2] = \begin{bmatrix} 0 & 0 & 0 \\ 0 & \frac{1}{r}N_{,\theta} & 0 \\ 0 & 0 & \frac{1}{r}N_{,\theta} \\ \frac{1}{r}N_{,\theta} & 0 & 0 \\ 0 & 0 & -\frac{1}{r}N_{,\theta} \end{bmatrix} \tag{2.66}$$

Take the second time derivative of (2.60) and substitute into (2.55) will results in the following:

$$KE = \frac{1}{2}\iint \{\dot{V}\}^T [M]\{V\} d\theta dz \tag{2.67}$$

Substitution of Equation (2.63) into Equation (2.56) yields the following:

$$H = \frac{1}{2}\iiint \left[[B_1]^T\{V\}^T + [B_2]^T\{V_{,\theta}\}^T\right][C]\left[[B_1]\{V\} + [B_2]\{V_{,\theta}\}\right] dB \tag{2.68}$$

The definitions of $[K_{11}]$, $[K_{12}]$, $[K_{21}]$ and $[K_{22}]$ can be found in Appendix C.

Substituting (2.68) and (2.67) into (2.54) results in the following equation:

$$\delta \int_{t_0}^{t_1} dt \frac{1}{2}\iint [\{\dot{V}\}^T [M]\{V\} - \{V\}^T[K_{11}]\{V\} - \{V\}^T[K_{12}]\{V_\theta\} - \{V_\theta\}^T[K_{21}]\{V\} - \{V_\theta\}^T[K_{22}]\{V_\theta\}]d\theta\, dz = 0 \tag{2.69}$$

Carrying out the variation in (2.69) leads to the following system of partial differential equations of motion:

$$[M]\{\ddot{V}\} + [K_{11}]\{V\} + [K_{12}]\{V_\theta\} - [K_{21}]\{V_\theta\} - [K_{22}]\{V_{\theta\theta}\} = 0 \tag{2.69}$$

Equation (2.70) can be solved by introducing the following wave form solution [50] solution:

$$\{V\} = \{V_0\}e^{i(m\theta-\omega t)} \tag{2.70}$$

Substitution of the wave solution in Equation (2.70) yields the following:

$$0 = ((\,[K_{11}] - [M]\omega^2) + im([K_{12}] - [K_{21}]) + m^2[K_{22}])\{V_0\} \tag{2.71}$$

When the values of ω^2 are assigned, Equation (2.72) becomes a quadratic Eigen problem in terms of m. Real wave numbers represent propagating waves while complex conjugate pairs describe the standing vibrations with spatially decaying amplitudes.

2.4 Computer Programming

Computer programs are developed in order to obtain the numerical results of both the finite element method and analytical solution. The FEM program was obtained from previous research work and modified for the purpose of this research. For the analytical method computer code was developed to solve the determinant of the 6x6 Q matrix given in Equation (2.53).

Figure 3(a), shows the flow chart of the developed FEM program. The program starts out by reading the input provided by the user. The input includes the material properties, geometry, load, boundary conditions, assigned ω or m, and the FEM parameters such as number of elements, Gauss sampling points etc. Then the program will assemble the global matrix by first forming the element matrix. The eigenvalue problem is now formed and solved and the results can be obtained to draw the wave spectra.

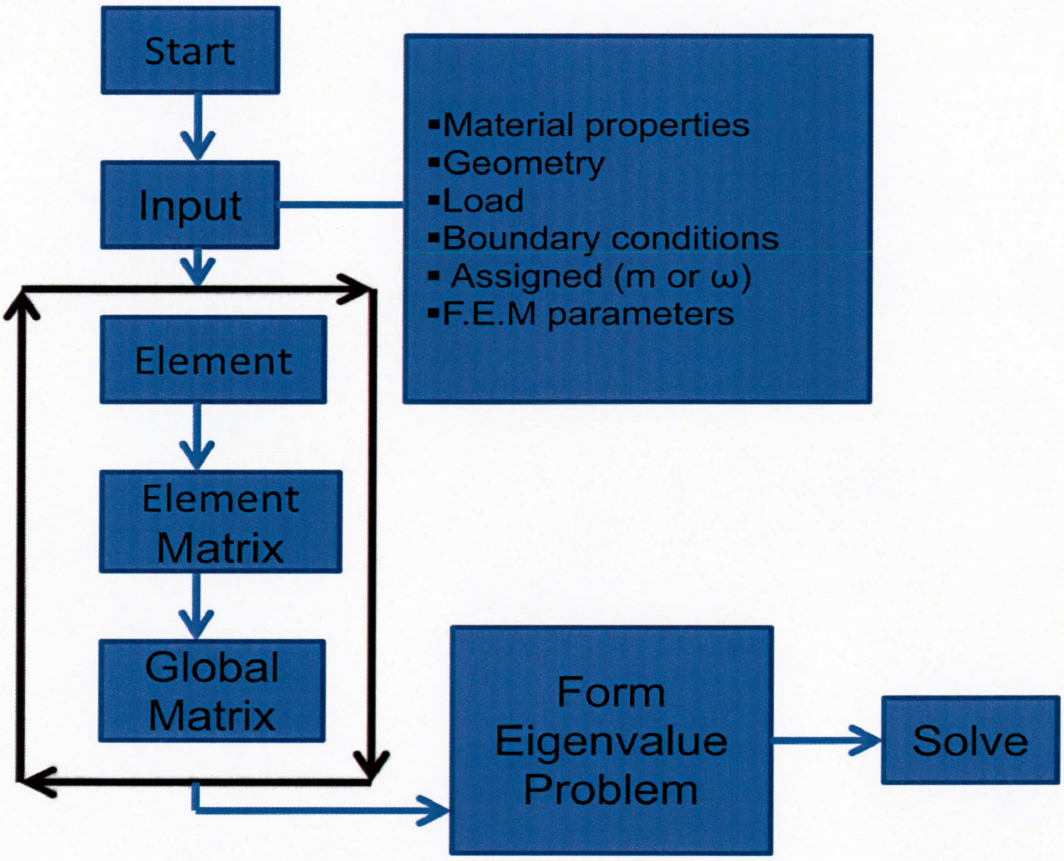

Figure 3(a): FEM program flow chart.

Figure 3(b), shows the flow chart of the FORTRAN program for the analytical solution. The program starts out by reading the input provided by the user. The material properties, geometry, load, boundary conditions, assigned ω and m (obtained from the results of the FEM). Followed by, performing a root finding method to determine the roots of the determinant of the Q matrix. The program will evaluate the Bessel functions which are required to calculate the elements of

the Q matrix. After the Q matrix is assembled, the determinant of the Q matrix is computed. The refined ω or m are found. This procedure is repeated depending on how many roots are provided by the user.

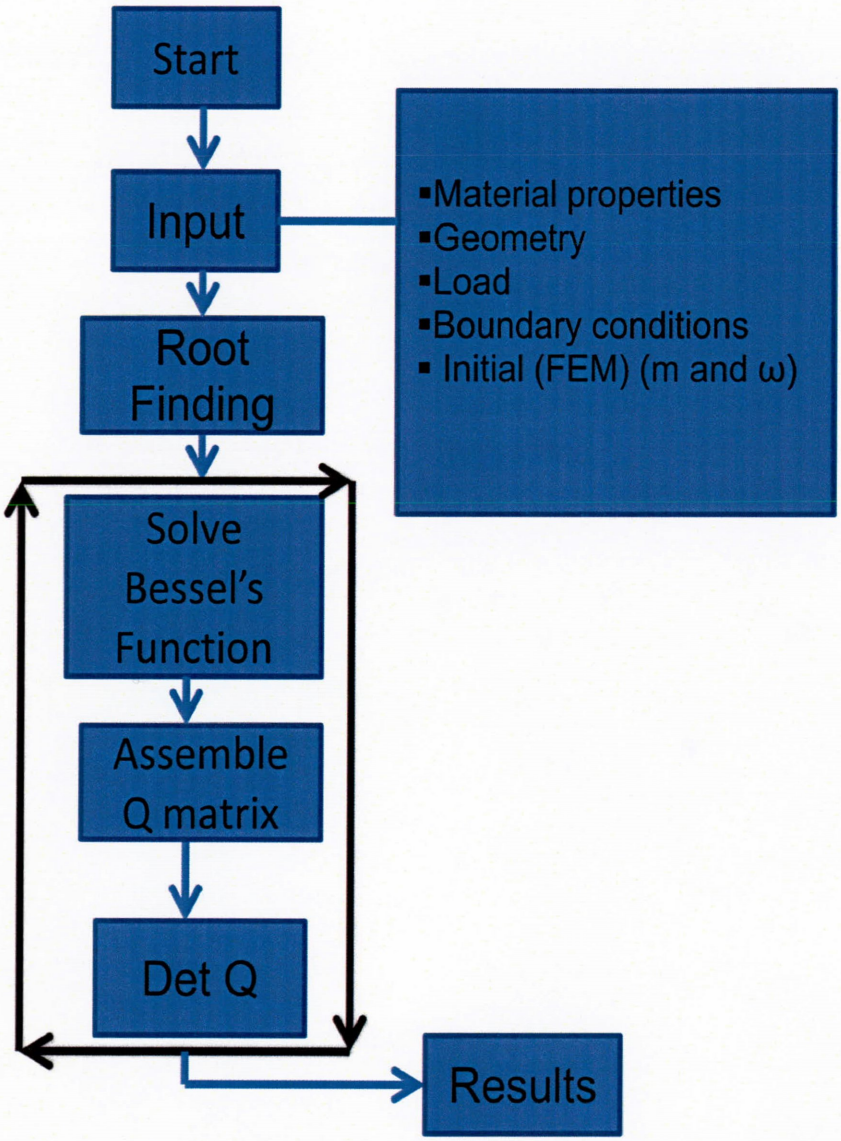

Figure 3(b): Analytical solution program flow chart.

2.5 Numerical Results and Discussion

This section provides numerical examples that illustrate the findings in the dispersion curves of the guided circumferential waves in an annulus. The graphs are presented for open and closed electric boundary conditions and traction free mechanical boundary condition. Two types of cylinder are used to draw the dispersion curves, the thin cylinder and the thick cylinder. All the material properties and geometry parameters used in the calculation are given below.

2.5.1 Comparison Study

The next step here is to validate the correctness of developed computer codes. To do this we must simulate trusted published results. Reference [2] was chosen to be simulated in order to validate the results. The program was developed for a piezoelectric cylinder and the reference [2] presents results for a non piezoelectric cylinder. The program's input data are modified accordingly, therefore the piezoelectric, electric field and the dielectric constants are set to be zero.

For simulation purposes, the following quantities are fixed h=1, r_i=0.11111, r_o=1.111111, $c^0 = 102.4\ GPA = c_{44}$. The same material properties and geometry is used here which are given by:

$$[\boldsymbol{C}^*] = \begin{bmatrix} 3.12848 & 1.12848 & 0 \\ 1.12848 & 3.12848 & 0 \\ 0 & 0 & 1 \end{bmatrix} \tag{2.72}$$

$$[\boldsymbol{\varepsilon}] = \begin{bmatrix} 0 & 0 \\ 0 & 0 \end{bmatrix} \tag{2.73}$$

The results were simulated using both the analytical solution and the FEM using the developed programs.

Figure 4 shows the comparison results between the published results (dashed line) and the simulated results (solid line). There are some discrepancies between those results. For example, the first propagating mode, after k=2 the dashed line and the solid line start to deviate from each other. This discrepancy is mainly due to the fact that the dashed lines (published results) were traced manually

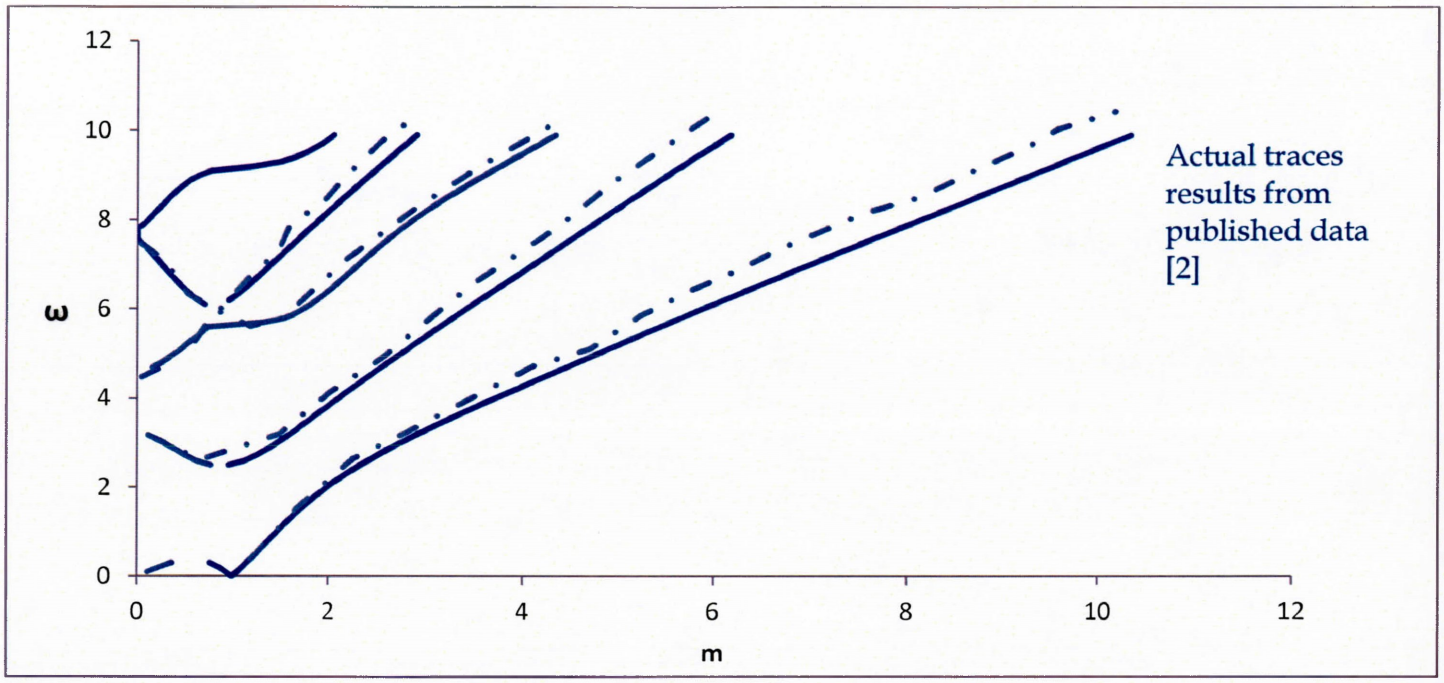

Figure 4: Comparison of actual results vs. simulated analytical solution results.

Figure 5 compared the actual results (dashed line) vs. the simulated results (solid line) using the FEM. The results show a good agreement.

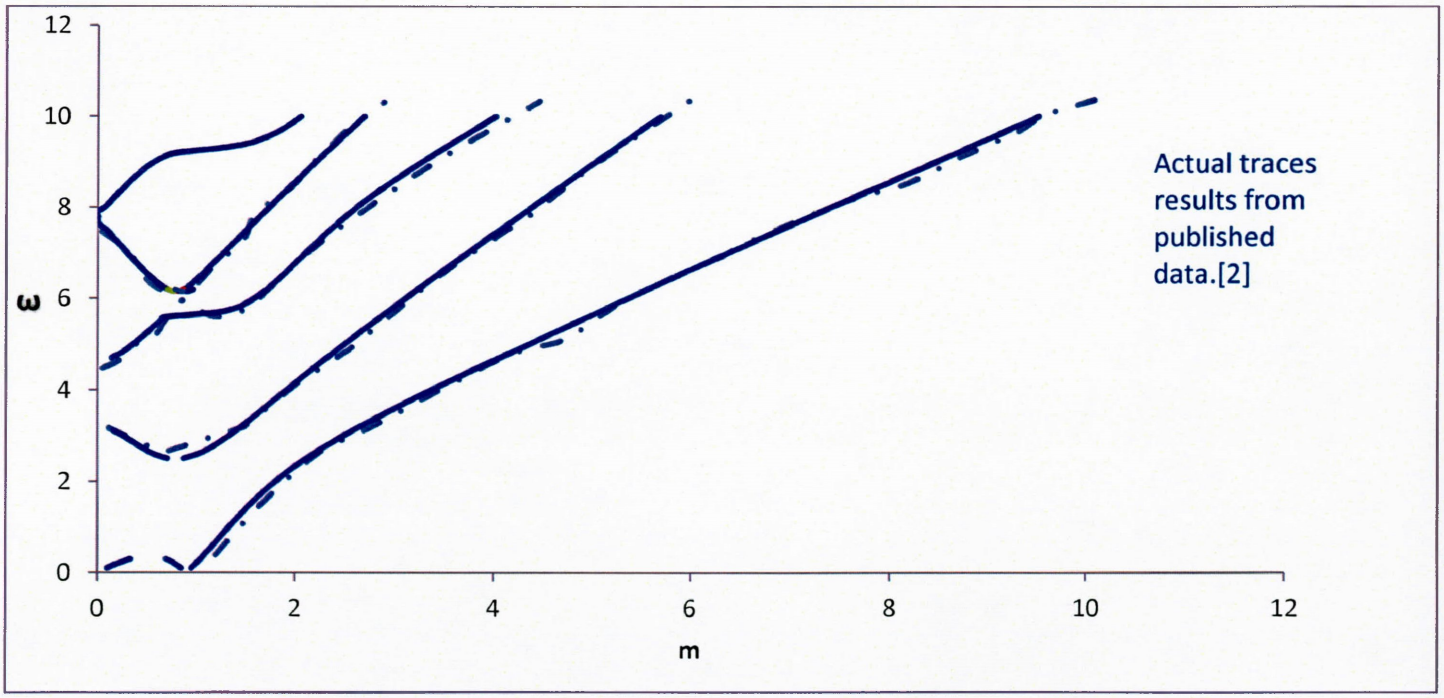

Figure 5: Comparison of actual results vs. simulated FEM solution results.

2.5.2 Numerical Examples

Two numerical examples are presented here. Two piezoelectric hollow homogenous cylinders are considered. One has inner and outer radii of r_i=0.5 and r_o=1.5 (thick cylinder), the other one has an inner and outer radii of r_i=6.9074 and r_o=7.9074 (thin cylinder). Both cylinders are subjected to traction free boundary conditions and closed or open circuit boundary conditions. Both are composed of PZT-4 material whose properties are taken from [40]. The normalized material constants are given by:

$$[\boldsymbol{c}] = \begin{bmatrix} 5.42969 & 3.03906 & 0 \\ 3.03906 & 5.42969 & 0 \\ 0 & 0 & 1.19531 \end{bmatrix} \tag{2.74}$$

$$[\boldsymbol{\varepsilon}] = \begin{bmatrix} 1.46628 & 0 \\ 0 & 1.46628 \end{bmatrix} \tag{2.75}$$

Four reference parameters are required for the normalization, and are chosen to be:

1) h=1
2) $c^0 = c_{44} = 25.6\ GPA$
3) $\rho^0 = 7500\ kg/m^3$
4) $\varepsilon^0 = 8.90664 \times 10^{-9} F/m$

ε^0 is calculated using Equation (2.22).

Based on these four parameters, the normalized frequency can be calculated by the following Equations:

$$\omega = \frac{\omega^*}{\omega_0}\ \omega_0 = \frac{1}{H}\sqrt{\frac{c^0}{\rho^0}} = 1847.52\ rad/s \tag{2.76}$$

2.5.3 Convergence Check

The next step is to perform a convergence check for the FEM results. Since, the accuracy of FEM solution depends on finite element discretization. Three different settings were tested, 20 element, 35 elements and 40 elements models. Based on previous research the 20 element model was chosen as a starting point. Figure 6 plots ω-m relationships for 20 elements, 35 elements and 40 elements models. As it can be observed from figure 6, the results do not vary greatly as the number of elements increases. When comparing the 35 elements model and the 40 elements

model, the results of the ω-m relationship were essentially identical. Then the 35 element model was compared to the 20 elements model, it was found that the results do not change up to 3 significant. Therefore, convergence occurred at 20 elements and the 20 element model was chosen for all the wave spectra study in this research. The colors are hard to see in Figure 6 due to the fact that the results are very close when the element number is increased.

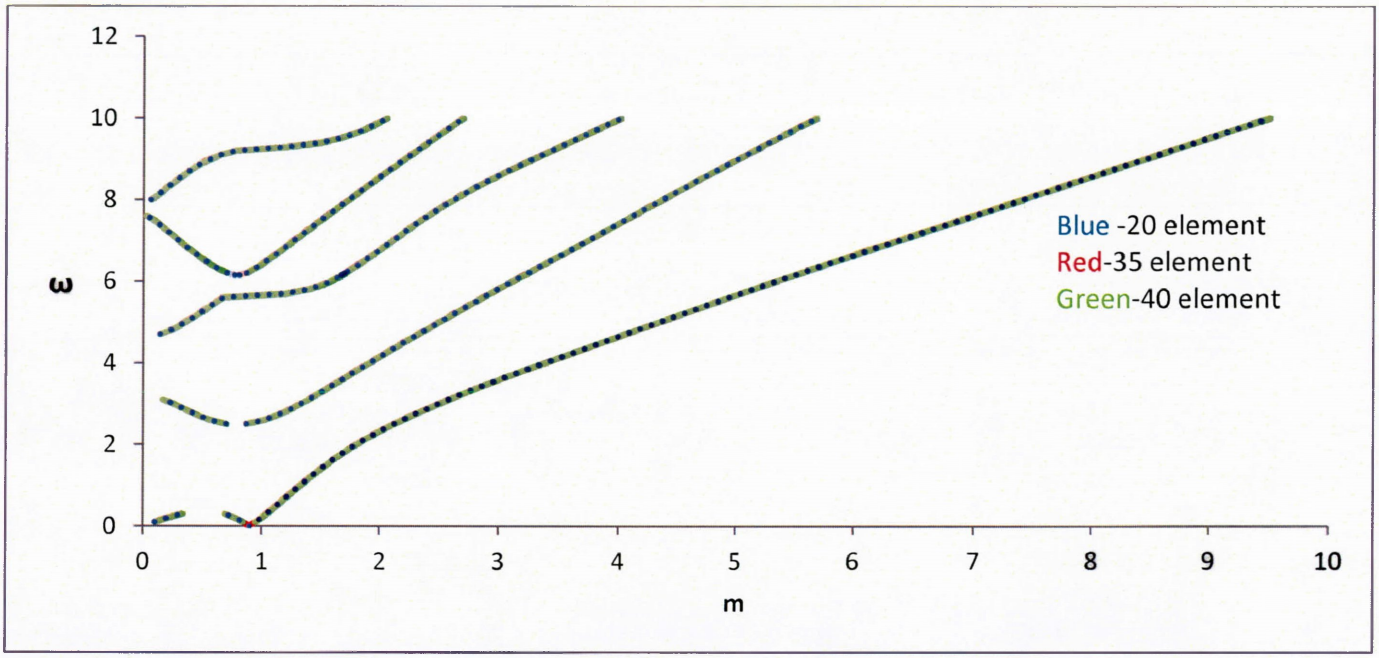

Figure 6: Convergence results of the FEM solution.

For a given value of the non-dimensional frequency ω, the eigenvalue problem of Equation (2.72) is solved numerically using the developed computer FORTRAN code. To obtain the analytical solution, one must solve the dispersion equation by finding the roots of the determinant of the Q (6x6) matrix.

The upcoming sections will present the dispersion curves according to geometry and electric boundary conditions. The FEM solution is presented for real, imaginary and complex non-dimensional circumferential wave number m. The analytical solution is presented only for the real non-dimensional circumferential wave number m, because the program for the analytical solution for imaginary and complex order of the Bessel function is not available.

2.5.4 The Case of a Thick Cylinder with Open-Circuit and Closed-Circuit Boundary Conditions

A hollow homogeneous PZT-4 cylinder with r_i=0.5 and r_o=1.5 is subjected to traction free and open-circuit and closed-circuit boundary conditions both at the inner and outer surface.

Figures 7 and 8 present the FEM and the analytical method results (Figure 7 open and Figure 8 closed). It is clearly seen that there exists a difference between the FEM and the analytical solution for each figure. This is expected due to the fact that the FEM is an approximation solution.

First, the results obtained from the open and the closed boundary conditions given in Figures 7 and 8 respectively, are compared. The same results indicated that the wave spectra are independent of the electric boundary conditions. Equations (2.37-2.39) show that potentials B and C are uncoupled from the electrical potential $\emptyset$. The mechanical stresses and the electrical displacements are uncoupled as well; therefore, in the case of the wave propagation in an annulus, the piezoelectricity and elasticity are decoupled.

One key feature of this curve is that at higher frequencies and especially at higher wave number, the first and second modes are almost a straight line, illustrating that those modes become almost non-dispersive at high frequencies.

Figure 7 and 8 shows that there exists a local minimum value at the first, second and the fourth branches. The second branch clearly illustrates this behavior, when looking at this branch we can see there exists a local minimum at about ω=2, to the right of the cut-off frequency. Any point after this local minimum point the slope of the ω-m relationship is positive corresponding to positive kinetic energy velocity. The fact that energy flow is positive means that the wave propagation is in the same direction as the energy flow. It is observed that any point to the left of this local minimum point (slope is negative), which in turn means negative kinetic energy flow (wave propagation is opposite of kinetic energy flow). The behavior also exists at the first branch at k=1. This branch is different since there exists a local maximum also. This means energy flow goes from positive at m=0 and ω=0 to negative at m=0.5 and ω=0.1, then the slope changes from positive to negative. This change of slope changes the energy flow from negative to positive all the way to the local minimum. After this point, the energy flow is positive which coincides with the wave propagation direction.

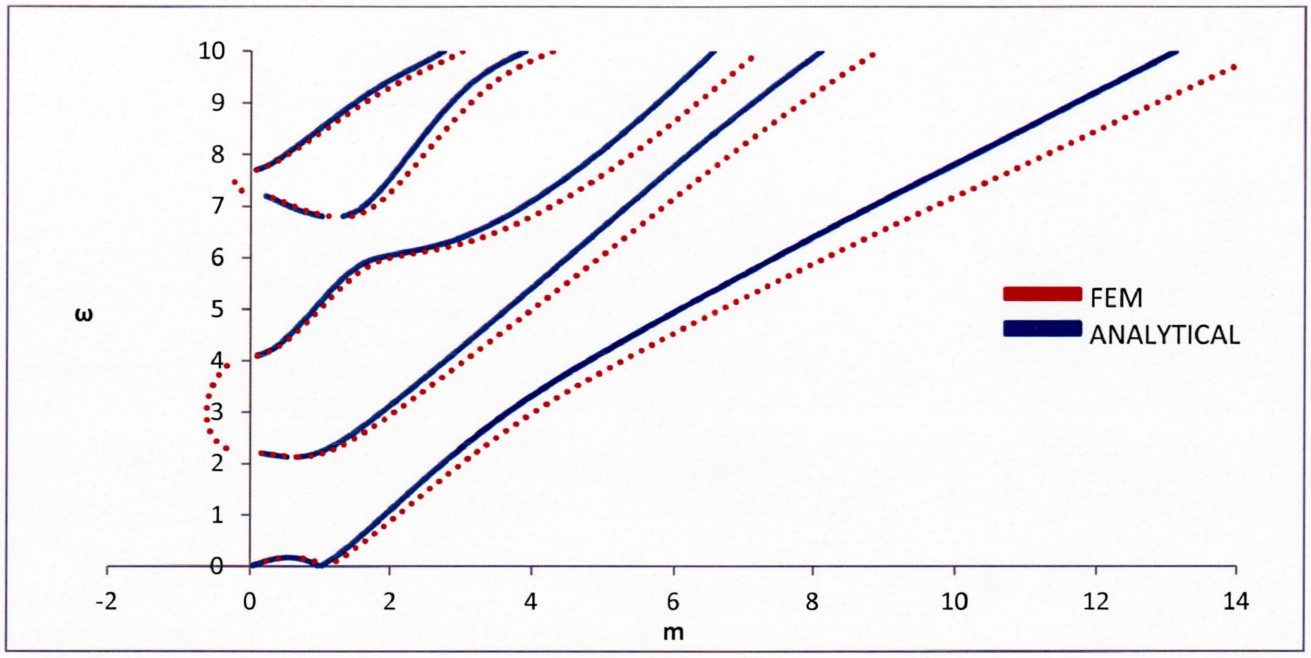

Figure 7: The results of the case of FEM and analytical solution for the open circuit thick cylinder.

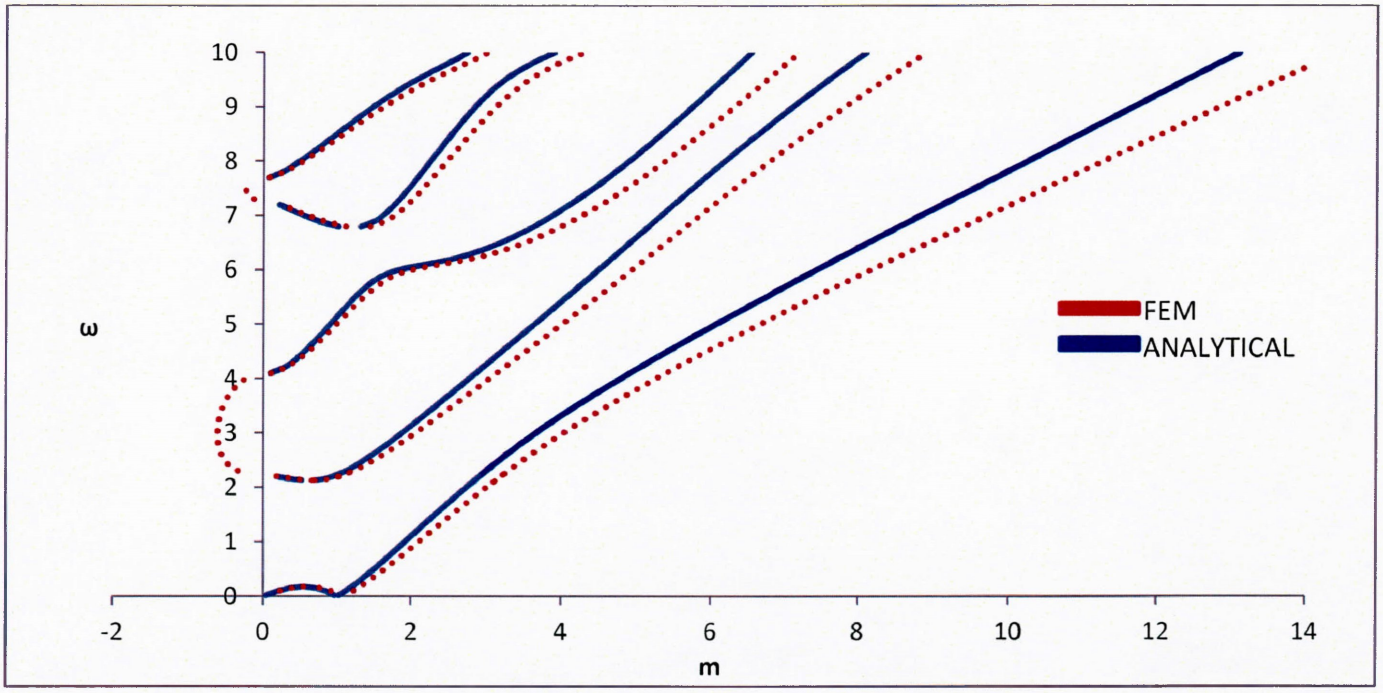

Figure 8: The results of the case of FEM and analytical solution for the closed circuit thick cylinder.

Figure 9 presents the wave spectra for real, complex and imaginary wave numbers for open boundary conditions (real is the green series, imaginary is the red series and complex is the blue series). The first two complex branches connect two real branches each, the third complex

branch starts from the complex plane and ends at a local minima of a real branch (the fourth mode), and the other complex branches start from the complex plane. The complex and imaginary results can be used for further studied in wave scattering.

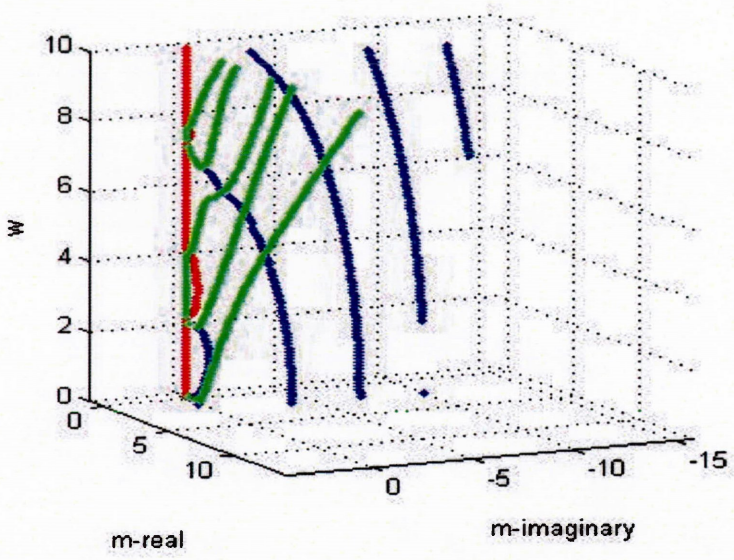

Figure 9: Results of complex wave number for the open circuit thick cylinder.

2.5.5 The Case of a Thin Cylinder with Open-Circuit and Closed-Circuit Boundary Conditions.

A hollow homogeneous PZT-4 cylinder with r_i=6.9074 and r_o=7.9074 is considered here. The cylinder is subjected to traction free, open-circuit or closed-circuit boundary conditions both at the inner and outer surface. This numerical example illustrates open and close circuit boundary condition for the thin cylinder geometry.

The five propagating modes are presented here and it can be seen that all the modes are dispersive. However, at higher frequencies and circumferential wave numbers, the curves are almost a straight line. The first and second mode show straight lines at much lower frequencies, which means they are almost non-dispersive.

It can also be seen from Figure 10 and 11 that there exist a local minimum at branch number 4 only. But all the other branches have positive slopes.

Once the dispersion curves are presented, one can calculate the linear wave velocity presented in reference [2] given by the following equation:

$$c(r) = \frac{\omega}{m}\frac{r}{r_i}c_T \tag{2.77}$$

Where, c_T is the shear wave velocity.

The propagating wave (phase) velocity can be calculated from Equation (2.78) by using the specific ω and m at a distant r from the inner surface of the hollow cylinder. The wave velocity can be measured experimentally at the outer surface and this can be used as a tool to determine the dispersion curve experimentally.

From the presented ω-m relationship, the group velocity can also be computed using the following formula taken from reference [2].

$$c_g = \frac{\partial\omega}{\partial m} \tag{2.78}$$

Which is simply the slope of the dispersion curve. This group velocity is also called the kinetic energy velocity (a representation of the kinetic energy).

In conclusion, it was found that when applying the open or closed circuit boundary conditions when axial wave number k=0, the mechanical potentials are decoupled from the electrical potential φ, which means that the electrical boundary conditions have no effect on the dispersion curves. It was also found that all the given branches are dispersive but are almost non-dispersive at higher frequencies and large cirumferential wave numbers.

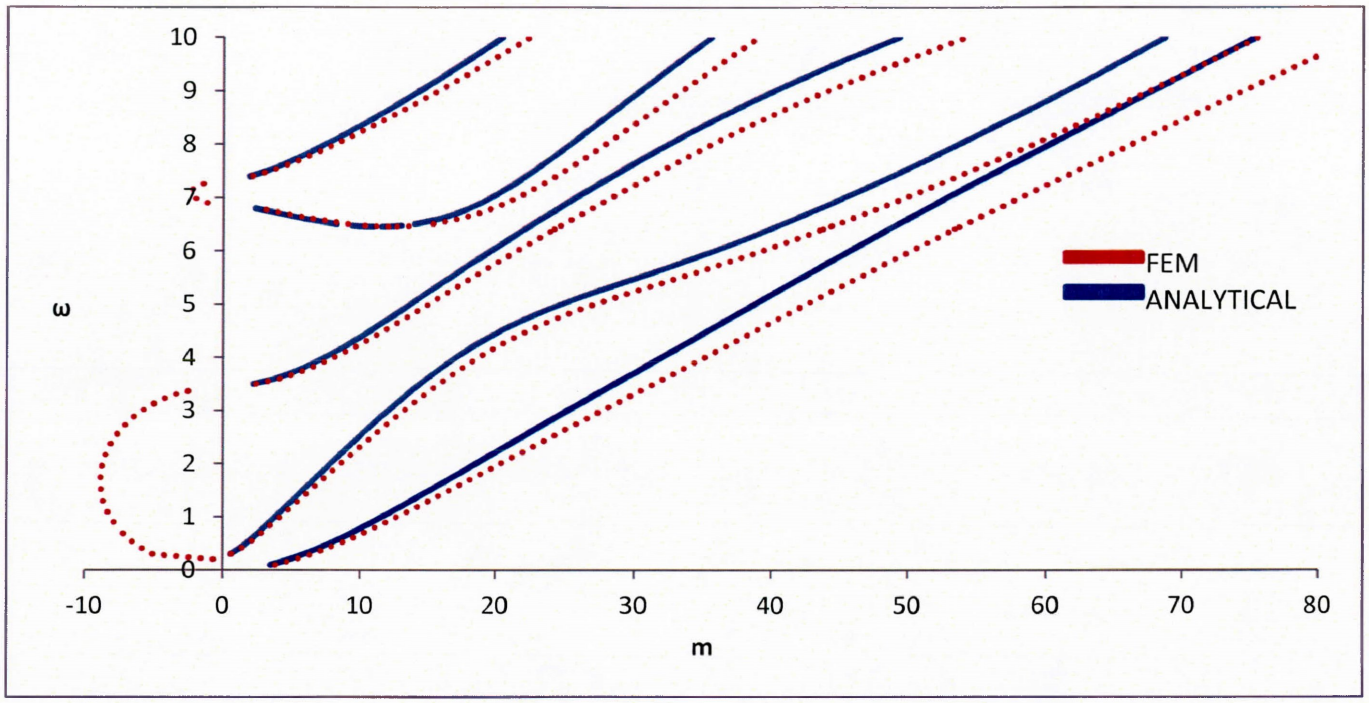

Figure 10: The results of the case of FEM and analytical for open circuit thin cylinder.

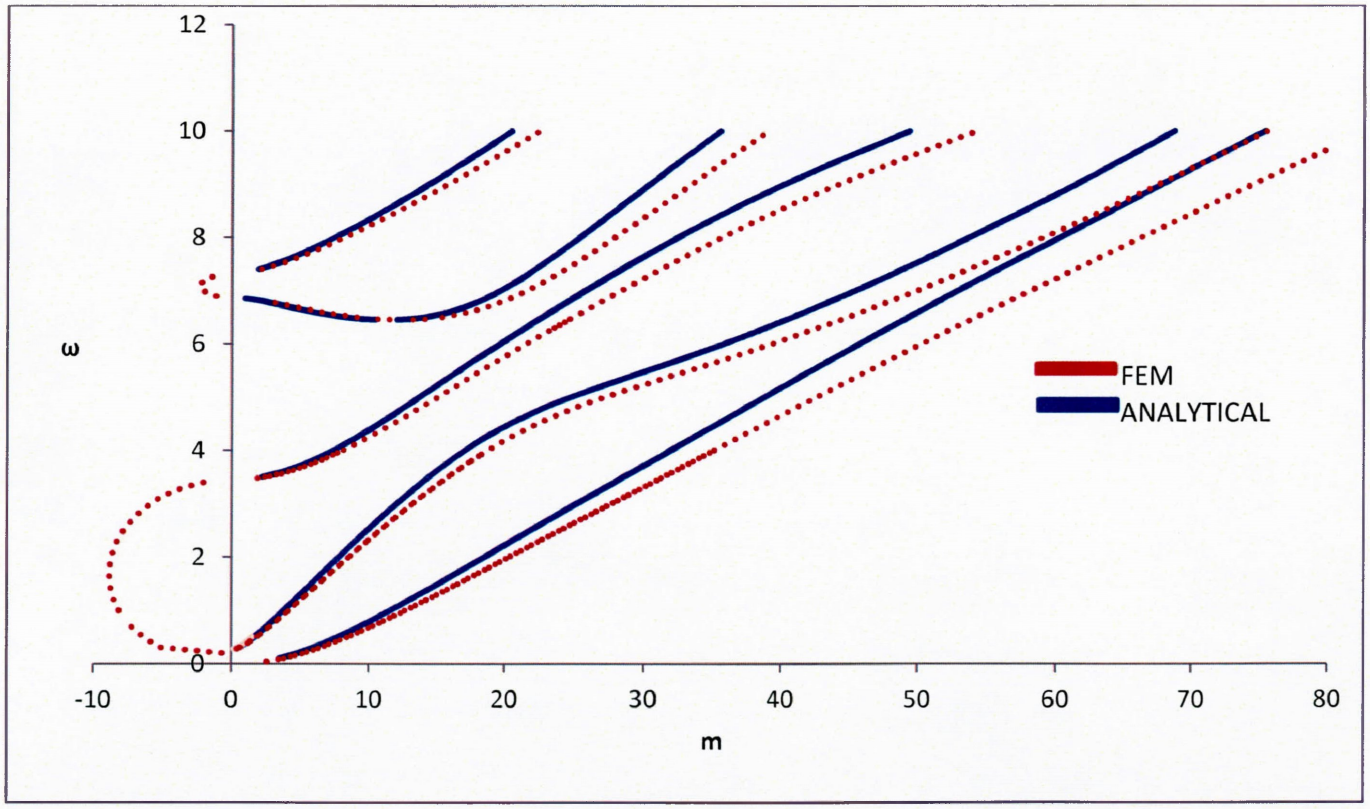

Figure 11: The results of the case of FEM and analytic solution for closed circuit thin cylinder.

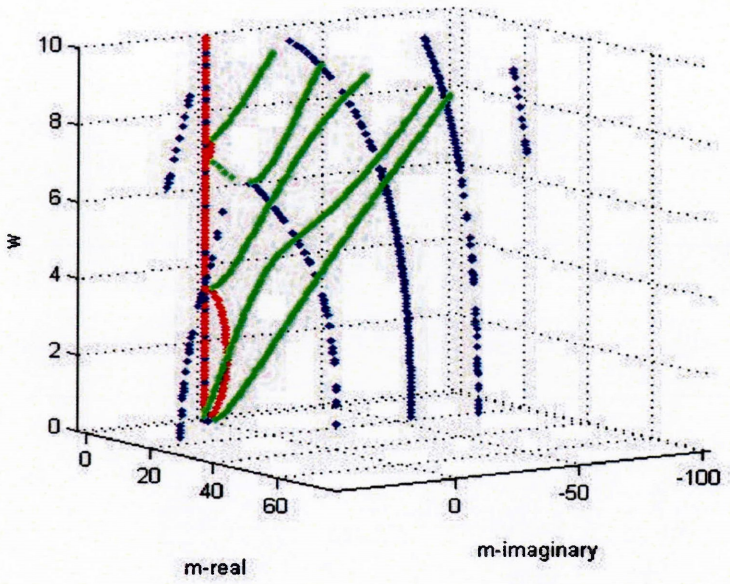

Figure 12: The case of complex wave number for open circuit thin cylinder.

Similar observations can be deduced from Figure 12 as with Figure 9. Two complex branches connect the second and third real branches, and the fourth and fifth real branches, respectively, another complex branch starts from the complex plane and ends at a local minima of the fourth real branch, and the other complex branches start from the complex plane. The complex branches will play an important role in studying the wave reflection and scattering problems.

Chapter 3: Spiral Wave in a Cylinder

A more general care for wave propagation in a hollow piezoelectric cylinder will be studied in this chapter. The previous chapter presented the mathematical formulation and results for a pure circumferential wave. This is achieved by setting the axial wave number, $k=0$. This chapter will present the results for a spiral wave. A spiral wave is propagating in both the circumferential direction and the axial direction (k . The mathematical formulation will be presented for both the finite element method and the analytical solution. Two piezoelectric cylinders will be studied, namely, the thin and thick cylinders. The piezoelectric cylinders made out of PZT4 material. The wave spectra will be presented as surfaces in the three-dimensional space. The wave spectra will also be presented by assigning k or m values and this will produce (two-dimensional) the ω-k relationship or ω-m relationship. Both relationships will be presented for k=0, 1, 2... 5 and m=0, 1, 2... 5

3.1 Equations of Motion

Consider an infinitely long cylinder. The cylindrical coordinates (r, θ, z) with origin located at the centre of the cross section, are employed here as shown in Figure 13. The independent variables are the mechanical displacement , stress , strain , electric displacements and electric fields . They are defined as follows;

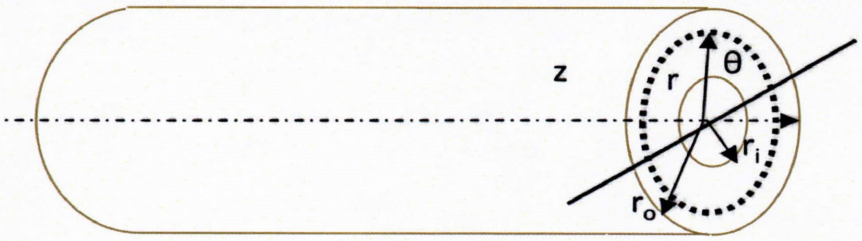

Figure 13: Infinite piezoelectric hollow cylinder.

(3.1)

(3.2)

(3.3)

= (3.4)

$$\{\boldsymbol{D}\} = \{D_r, D_\theta, D_z\}^T = \{D_1, D_2, D_3\}^T \tag{3.5}$$

Where, $u = u(\mathrm{r}, \theta, \mathrm{z}, \mathrm{t})$, $v = v(\mathrm{r}, \theta, \mathrm{z}, \mathrm{t})$ and $w = w(\mathrm{r}, \theta, \mathrm{z}, \mathrm{t})$ are the mechanical displacement components, and t is the time.

The strain displacement relations are [49]:

$$\{\boldsymbol{S}\} = ([\boldsymbol{L_r}] + [\boldsymbol{L_\theta}] + [\boldsymbol{L_z}])\{\boldsymbol{u}\} \tag{3.6}$$

The definitions of $[\boldsymbol{L_r}], [\boldsymbol{L_\theta}]$ *and* $[\boldsymbol{L_z}]$ are given in Appendix B.

The electric field components are;

$$\{\boldsymbol{E}\} = \{E_r, E_\theta, E_z\}^T \tag{3.7}$$

Where,

$$E = -\nabla\varphi \tag{3.8}$$

The coupled constitutive equations are given by [48]:

$$\{\boldsymbol{T}\} = [\boldsymbol{C^*}]\{\boldsymbol{S}\} - [\boldsymbol{e}]^{\boldsymbol{T}}\{\boldsymbol{E}\} \tag{3.9}$$

$$\{\boldsymbol{D}\} = [\boldsymbol{e}]\{\boldsymbol{S}\} + [\boldsymbol{\varepsilon}]\{\boldsymbol{E}\} \tag{3.10}$$

Where

$$[\boldsymbol{C^*}] = \begin{bmatrix} C_{11} & C_{12} & C_{13} & 0 & 0 & 0 \\ C_{12} & C_{11} & C_{13} & 0 & 0 & 0 \\ C_{13} & C_{13} & C_{33} & 0 & 0 & 0 \\ 0 & 0 & 0 & C_{44} & 0 & 0 \\ 0 & 0 & 0 & 0 & C_{44} & 0 \\ 0 & 0 & 0 & 0 & 0 & C_{66} \end{bmatrix} \tag{3.11}$$

$$[\boldsymbol{e}] = \begin{bmatrix} 0 & 0 & 0 & 0 & e_{15} & 0 \\ 0 & 0 & 0 & e_{15} & 0 & 0 \\ e_{31} & e_{32} & e_{33} & 0 & 0 & 0 \end{bmatrix} \tag{3.12}$$

$$[\boldsymbol{\varepsilon}] = \begin{bmatrix} \varepsilon_{11} & 0 & 0 \\ 0 & \varepsilon_{11} & 0 \\ 0 & 0 & \varepsilon_{33} \end{bmatrix} \tag{3.13}$$

$[C^*]$ is the elastic stiffness constant matrix at constant electric field, $[e]$ is the piezoelectric constant matrix or also known as the electro-mechanical coupling factors, and $[\varepsilon]$ is the clamped dielectric constant matrix at constant strain.

The equations of motion are given by [49]:

$$\frac{\partial T_1}{\partial r} + \frac{1}{r}\frac{\partial T_6}{\partial \theta} + \frac{\partial T_5}{\partial z} + \frac{T_1 - T_2}{r} = \rho \ddot{u} \tag{3.14}$$

$$\frac{\partial T_6}{\partial r} + \frac{1}{r}\frac{\partial T_2}{\partial \theta} + \frac{\partial T_4}{\partial z} + 2\frac{T_6}{r} = \rho \ddot{v} \tag{3.15}$$

$$\frac{\partial T_5}{\partial r} + \frac{1}{r}\frac{\partial T_4}{\partial \theta} + \frac{\partial T_3}{\partial z} + \frac{T_5}{r} = \rho \ddot{w} \tag{3.16}$$

The double dot notation is the second time derivative. The charge equation of electrostatics is given by [48]:

$$\frac{\partial D_1}{\partial r} + \frac{1}{r}\frac{\partial D_2}{\partial \theta} + \frac{\partial D_3}{\partial z} + \frac{D_1}{r} = 0 \tag{3.17}$$

The traction free mechanical boundary conditions and the open and closed electrical boundary conditions are:

Traction free boundary conditions

$$T_1 = T_6 = T_5 = 0 \ @ \ r = r_i, r_o \tag{3.18}$$

Open circuit boundary conditions

$$D_1 = 0 \ @ \ r = r_i, r_o \tag{3.19}$$

Closed circuit boundary conditions

$$\emptyset = 0 \ @ \ r = r_i, r_o \tag{3.20}$$

3.2 Finite Element Formulation

The Hamilton principle is first applied and followed by the finite element discretization to the cylinder in the radial direction and integration over the axial and circumferential direction.

One may introduce Hamilton's principle [40], to include piezoelectric effects in a body of volume B which has the form:

$$\delta \int_{t_0}^{t_1} (KE - H)dt = 0 \tag{3.21}$$

Where, KE and H are the kinetic energy and the electric enthalpy

$$KE = \frac{1}{2} \iiint \{\dot{v}\}^T [\rho] \{\dot{v}\} dB \tag{3.22}$$

$$H = \frac{1}{2} \iiint \{q\}^T [C] \{q\} dB \tag{3.23}$$

Where,

$$[C] = \begin{bmatrix} [c] & -[e]^T \\ [e] & -[\epsilon] \end{bmatrix} \tag{3.24}$$

$$\{v\} = \begin{Bmatrix} u \\ \varphi \end{Bmatrix} \tag{3.25}$$

$$\{q\} = \begin{Bmatrix} S \\ E \end{Bmatrix} \tag{3.26}$$

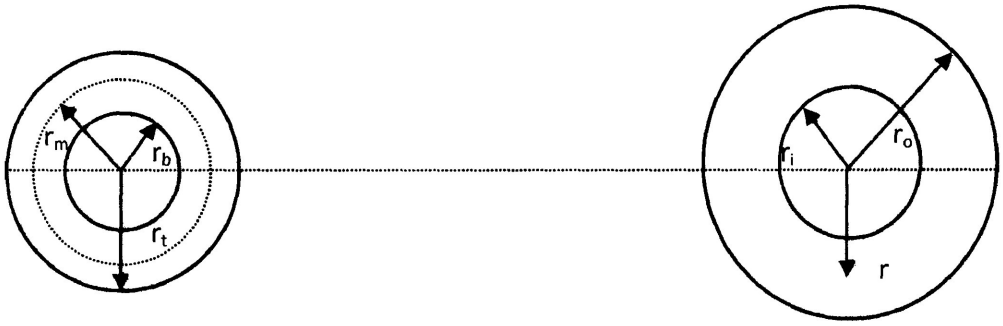

Figure 14: A Finite element lamina.

Figure 14 shows a typical 3-node (r_b, r_m and r_t) finite-element lamina (left cylinder). Isoperimetric finite-element methodology and numerical integration are used to discretize the cylinder in the radial direction.

The displacements and electric potential in a typical element can be expressed as:

$$\{v_e(r, \theta, z, t)\} = [N_e]\{V_e(\theta, z, t)\} \tag{3.27}$$

$$\{V_e(\theta, z, t)\} = \{u_1, u_2, u_3, v_1, v_2, v_3, w_1, w_2, w_3, \varphi_1, \varphi_2, \varphi_3\}^T \tag{3.28}$$

Where, $\{\boldsymbol{V_e}\}$ is the nodal value vector containing the displacement *u*, *v*, *w* and electric potential φ at the three nodes.

$$[\boldsymbol{N_e}] = \begin{bmatrix} n_1(\zeta) & n_2(\zeta) & n_3(\zeta) & 0 & 0 & 0 & 0 & 0 & 0 & 0 & 0 & 0 \\ 0 & 0 & 0 & n_1(\zeta) & n_2(\zeta) & n_3(\zeta) & 0 & 0 & 0 & 0 & 0 & 0 \\ 0 & 0 & 0 & 0 & 0 & 0 & n_1(\zeta) & n_2(\zeta) & n_3(\zeta) & 0 & 0 & 0 \\ 0 & 0 & 0 & 0 & 0 & 0 & 0 & 0 & 0 & n_1(\zeta) & n_2(\zeta) & n_3(\zeta) \end{bmatrix} \quad (3.29)$$

Here, $[\boldsymbol{N_e}]$ means the finite element interpolation matrix.

$$n_1(\zeta) = \frac{1}{2}\zeta(\zeta - 1), n_2(\zeta) = 1 - \zeta^2, n_3(\zeta) = \frac{1}{2}\zeta(\zeta + 1) \quad (3.30)$$

The displacement vector defined by Equation (3.26) has the form

$$\{\boldsymbol{q}\} = [\boldsymbol{B_1}]\{\boldsymbol{V}\} + [\boldsymbol{B_2}]\{\boldsymbol{V_{,\theta}}\} + [\boldsymbol{B_3}]\{\boldsymbol{V_{,z}}\} \quad (3.31)$$

Where,

$$[\boldsymbol{B_1}] = [\boldsymbol{L_r}][\boldsymbol{N_e}] \quad (3.32)$$

$$[\boldsymbol{B_2}] = [\boldsymbol{L_\theta}][\boldsymbol{N_e}] \quad (3.33)$$

$$[\boldsymbol{B_3}] = [\boldsymbol{L_z}][\boldsymbol{N_e}] \quad (3.34)$$

By taking the time derivative of (3.27) and substituting in (3.22) leads to the following:

$$KE = \frac{1}{2}\iint \{\dot{\boldsymbol{V}}\}^{\boldsymbol{T}} [\boldsymbol{M}]\{\boldsymbol{V}\}\, d\theta\, dz \quad (3.35)$$

Substitution of Equation (3.32) into Equation (3.23) yields the following;

$$H = \frac{1}{2}\iiint \left[[\boldsymbol{B_1}^{\boldsymbol{T}}]\{\boldsymbol{V^T}\} + [\boldsymbol{B_2}^{\boldsymbol{T}}]\{\boldsymbol{V_\theta}^{\boldsymbol{T}}\} + [\boldsymbol{B_3}^{\boldsymbol{T}}]\{\boldsymbol{V_z}^{\boldsymbol{T}}\}\right][\boldsymbol{C}][[\boldsymbol{B_1}]\{\boldsymbol{V}\} + [\boldsymbol{B_2}]\{\boldsymbol{V_\theta}\} + [\boldsymbol{B_3}]\{\boldsymbol{V_z}\}]dB \quad (3.36)$$

Equation (3.37) can be rewritten as:

$$H = \frac{1}{2}\iint[\{V^T\}K_{11}\{V\} + \{V^T\}K_{12}\{V_{,\theta}\} + \{V^T\}K_{13}\{V_{,z}\} + \{V_{,\theta}{}^T\}K_{21}\{V\} + \{V_{,\theta}{}^T\}K_{22}\{V_{,\theta}\} + \{V_{,\theta}{}^T\}K_{23}\{V_{,z}\} + \{V_{,z}{}^T\}K_{31}\{V\} + \{V_{,z}{}^T\}K_{31}\{V\} + \{V_{,z}{}^T\}K_{32}\{V_{\theta}\} + \{V_{,z}{}^T\}K_{33}\{V_{,z}\}]d\theta dz \quad (3.37)$$

Substitution of Equation (3.36) and Equation (3.38) into (3.21) yields the following equation:

$$\delta\int_{t_0}^{t_1} dt\frac{1}{2}\iint\left[\{\dot{V}\}^T[M]\{V\} - \{V\}^T[K_{11}]\{V\} - \{V\}^T[K_{12}]\{V_{,\theta}\} - \{V\}^T[K_{13}][V_{,z}] - \{V_{,\theta}\}^T[K_{21}]\{V\} - \{V_{,\theta}\}^T[K_{22}]\{V_{,\theta}\} - \{V_{,\theta}\}^T[K_{23}]\{V_{,z}\} - \{V_{,z}\}^T[K_{31}]\{V\} - \{V_{,z}\}^T[K_{32}]\{V_{,\theta}\} - \{V_{,z}\}^T[K_{33}]\{V_{,z}\}\right]d\theta dz = 0 \quad (3.38)$$

This will yield the system of partial differential equations of motion given by:

$$[M]\{\ddot{V}\} + [K_1]\{V\} + [K_2]\{V_{,\theta}\} + [K_3]\{V_{,z}\} - [K_4]\{V_{,\theta\theta}\} - [K_5]\{V_{,\theta z}\} - [K_6]\{V_{,zz}\} = \mathbf{0} \quad (3.39)$$

Where,

$$[K_1] = [K_{11}] \quad (3.40)$$

$$[K_2] = [K_{12}] - [K_{21}] \quad (3.41)$$

$$[K_3] = [K_{13}] - [K_{31}] \quad (3.42)$$

$$[K_4] = [K_{22}] \quad (3.43)$$

$$[K_5] = [K_{23}] - [K_{32}] \quad (3.44)$$

$$[K_6] = [K_{33}] \quad (3.45)$$

The definitions of $[K_{11}]$ to $[K_{33}]$ and $[M]$ can be found in their explicit form in Appendix C.

The solution to Equation (3.40) is given by the following wave form solution [49]:

$$\{V\} = \{V_0\}e^{i(kz+m\theta-\omega t)} \quad (3.46)$$

Where $\{V_0\}$, is the vector of the radial nodal distribution of the displacement and electric potential.

Substitution of Equation (3.47) into equation (3.40) will yield the following equation:

$$([\boldsymbol{K_1}] + im[\boldsymbol{K_2}] + ik[\boldsymbol{K_3}] + m^2[\boldsymbol{K_4}] + mk[\boldsymbol{K_5}] + k^2[\boldsymbol{K_6}] - \omega^2[\boldsymbol{M}])\{\boldsymbol{V_0}\} = 0 \quad (3.47)$$

Here, we have a generalized eigenvalue problem having three parameters ω, m and k. Any of the three parameters can be chosen as the eigenvalue as long as the other two are assigned values.

When ω is given and m is assigned an integer, the conventional ω-k relationship is found. Given ω and k, eigenvalue problem in terms of m is given. It is clear that m could be a real non-integer number, or complex number. In other words, the periodicity in the circumference does not hold. When both m and k are assigned, one will have wave spectra as ω=ω (m, k), for the piezoelectric cylinder.

3.3 Analytical Solution Formulation

The mechanical displacements are represented by three scalar potentials given by [41]:

$$u = \frac{\partial B}{\partial r} + \frac{1}{r}\frac{\partial C}{\partial \theta} \quad (3.48)$$

$$v = \frac{1}{r}\frac{\partial B}{\partial \theta} - \frac{\partial C}{\partial r} \quad (3.49)$$

$$w = \frac{\partial A}{\partial z} \quad (3.50)$$

The strains are then derived using the above three potentials and are given by the following:

$$S_1 = \frac{\partial^2 B}{\partial r^2} - \frac{1}{r^2}\frac{\partial C}{\partial \theta} + \frac{1}{r}\frac{\partial^2 C}{\partial \theta \partial r} \quad (3.51)$$

$$S_2 = \frac{1}{r}\left[\frac{1}{r}\frac{\partial^2 B}{\partial \theta^2} - \frac{\partial^2 C}{\partial \theta \partial r} + \frac{\partial B}{\partial r} + \frac{1}{r}\frac{\partial C}{\partial \theta}\right] \quad (3.52)$$

$$S_3 = \frac{\partial^2 A}{\partial z^2} \quad (3.53)$$

$$S_4 = \frac{1}{r}\frac{\partial^2 B}{\partial \theta \partial z} - \frac{\partial^2 C}{\partial r \partial z} + \frac{1}{r}\frac{\partial^2 A}{\partial z^2} \quad (3.54)$$

$$S_5 = \frac{\partial^2 A}{\partial z \partial r} + \frac{\partial^2 B}{\partial r \partial z} + \frac{1}{r}\frac{\partial^2 C}{\partial \theta \partial z} \quad (3.55)$$

$$S_6 = \frac{2}{r}\frac{\partial^2 B}{\partial \theta \partial r} - \frac{2}{r^2}\frac{\partial B}{\partial \theta} + \frac{1}{r^2}\frac{\partial^2 C}{\partial \theta^2} - \frac{\partial^2 C}{\partial r^2} + \frac{1}{r}\frac{\partial C}{\partial r} \quad (3.56)$$

The stresses are also derived by applying the definitions of the strain displacement and electric potential in the above Equations (3.52-3.57).

$$T_1 = C_{11}\left[\frac{\partial^2 B}{\partial r^2} - \frac{1}{r^2}\frac{\partial C}{\partial \theta} + \frac{1}{r}\frac{\partial^2 C}{\partial \theta \partial r}\right] + C_{12}\frac{1}{r}\left[\frac{1}{r}\frac{\partial^2 B}{\partial \theta^2} - \frac{\partial^2 C}{\partial \theta \partial r} + \frac{\partial B}{\partial r} + \frac{1}{r}\frac{\partial C}{\partial \theta}\right] + C_{13}\left[\frac{\partial^2 A}{\partial z^2}\right] + e_{31}\left[\frac{\partial^2 \varphi}{\partial z^2}\right] \tag{3.57}$$

$$T_2 = C_{12}\left[\frac{\partial^2 B}{\partial r^2} - \frac{1}{r^2}\frac{\partial C}{\partial \theta} + \frac{\partial^2 C}{\partial \theta \partial r}\right] + C_{11}\frac{1}{r}\left[\frac{1}{r}\frac{\partial^2 B}{\partial \theta^2} - \frac{\partial^2 C}{\partial \theta \partial r} + \frac{\partial B}{\partial r} + \frac{1}{r}\frac{\partial C}{\partial \theta}\right] + C_{13}\left[\frac{\partial^2 A}{\partial z^2}\right] + e_{31}\left[\frac{\partial^2 \varphi}{\partial z^2}\right] \tag{3.58}$$

$$T_3 = C_{13}\left[\frac{\partial^2 B}{\partial r^2} - \frac{1}{r^2}\frac{\partial C}{\partial \theta} + \frac{\partial^2 C}{\partial \theta \partial r} + \frac{1}{r^2}\frac{\partial^2 B}{\partial \theta^2} - \frac{1}{r}\frac{\partial^2 C}{\partial \theta \partial r} + \frac{1}{r}\frac{\partial B}{\partial r} + \frac{1}{r^2}\frac{\partial C}{\partial \theta} + \frac{\partial^2 A}{\partial z^2}\right] + e_{33}\left[\frac{\partial^2 \varphi}{\partial z^2}\right] \tag{3.59}$$

$$T_4 = C_{44}\left[\frac{1}{r}\frac{\partial^2 B}{\partial \theta \partial z} - \frac{\partial^2 C}{\partial r \partial z} + \frac{1}{r}\frac{\partial^2 A}{\partial z^2}\right] + \frac{e_{15}}{r}\left[\frac{\partial^2 \varphi}{\partial z \partial \theta}\right] \tag{3.60}$$

$$T_5 = C_{44}\left[\frac{\partial^2 A}{\partial z \partial r} - \frac{\partial^2 B}{\partial r \partial z} + \frac{1}{r}\frac{\partial^2 C}{\partial \theta \partial z}\right] + e_{15}\left[\frac{\partial^2 \varphi}{\partial z \partial r}\right] \tag{3.61}$$

$$T_6 = C_{66}\left[\frac{2}{r}\frac{\partial^2 B}{\partial \theta \partial r} - \frac{2}{r^2}\frac{\partial B}{\partial \theta} + \frac{1}{r^2}\frac{\partial^2 C}{\partial \theta^2} - \frac{\partial^2 C}{\partial r^2} + \frac{1}{r}\frac{\partial C}{\partial r}\right] \tag{3.62}$$

The electric displacements in terms of the four scalar potentials A, B, C and φ are;

$$D_1 = -\varepsilon_{11}\left[\frac{\partial^2 \varphi}{\partial z^2}\right] + e_{31}\left[\frac{\partial^2 B}{\partial r^2} + \frac{1}{r^2}\frac{\partial^2 B}{\partial \theta^2} + \frac{1}{r}\frac{\partial B}{\partial r}\right] + e_{33}\left[\frac{\partial^2 A}{\partial z^2}\right] \tag{3.63}$$

$$D_2 = -\varepsilon_{11}\left[\frac{1}{r}\frac{\partial \varphi}{\partial \theta}\right] + e_{31}\left[\frac{1}{r}\frac{\partial^2 B}{\partial \theta \partial z} - \frac{\partial^2 C}{\partial r \partial z} + \frac{1}{r}\frac{\partial^2 A}{\partial z^2}\right] \tag{3.64}$$

$$D_3 = -\varepsilon_{33}\left[\frac{\partial^2 \varphi}{\partial z^2}\right] + e_{31}\left[\frac{\partial^2 B}{\partial r^2} - \frac{1}{r^2}\frac{\partial C}{\partial \theta} + \frac{\partial^2 C}{\partial \theta \partial r} + \frac{1}{r^2}\frac{\partial^2 B}{\partial \theta^2} - \frac{1}{r}\frac{\partial^2 C}{\partial \theta \partial r} + \frac{1}{r}\frac{\partial B}{\partial r} + \frac{1}{r^2}\frac{\partial C}{\partial \theta}\right] + e_{33}\left[\frac{\partial^2 A}{\partial z^2}\right] \tag{3.65}$$

Equations (3.14-3.17) can be simplified by substituting the stress and electric displacements terms given in Equations (3.58-3.66) into the Equations (3.49-3.51) to yield:

$$c_{66}\nabla_{\perp}^2 C + c_{44}\frac{\partial^2 C}{\partial z^2} = \rho\frac{\partial^2 C}{\partial t^2} \tag{3.66}$$

$$(c_{13}+c_{44})\frac{\partial^2 A}{\partial z^2}+c_{11}\nabla_{\perp}^2 B+c_{44}\frac{\partial^2 B}{\partial z^2}+(e_{15}+e_{31})\frac{\partial^2 \phi}{\partial z^2}=\rho\frac{\partial^2 B}{\partial t^2} \tag{3.67}$$

$$c_{44}\nabla_{\perp}^2 A+c_{33}\frac{\partial^2 A}{\partial z^2}+(c_{13}+c_{44})\nabla_{\perp}^2 B+e_{15}\nabla_{\perp}^2\phi+e_{33}\frac{\partial^2 \phi}{\partial z^2}=\rho\frac{\partial^2 A}{\partial t^2} \tag{3.68}$$

$$e_{15}\nabla_{\perp}^2 A+e_{33}\frac{\partial^2 A}{\partial z^2}+(e_{15}+e_{31})\nabla_{\perp}^2 B-\varepsilon_{11}\nabla_{\perp}^2\phi-\varepsilon_{33}\frac{\partial^2 \phi}{\partial z^2}=0 \tag{3.69}$$

Where,

$$\nabla_{\perp}^2=[\,]_{,rr}+\frac{1}{r}[\,]_{,r}+\frac{1}{r^2}[\,]_{,\theta\theta} \tag{3.70}$$

One may assume the following wave form solutions [49]:

$$A=A_0(r)e^{i(kz+m\theta-\omega t)} \tag{3.71}$$

$$B=B_0(r)e^{i(kz+m\theta-\omega t)} \tag{3.72}$$

$$C=C_0(r)e^{i(kz+m\theta-\omega t)} \tag{3.73}$$

$$\emptyset=\emptyset_0(r)e^{i(kz+m\theta-\omega t)} \tag{3.74}$$

Equation (3.67) becomes:

$$c_{66}\nabla_0^2 C_0+(\rho\omega^2-c_{44}k_m^2)C_0=0 \tag{3.75}$$

Equations of (3.68-3.70) are rewritten as:

$$\begin{bmatrix}1 & 1+\frac{c_{13}}{c_{44}} & \frac{e_{15}}{c_{44}}\\ 0 & 1 & 0\\ \frac{e_{15}}{\varepsilon_{11}} & \frac{e_{31}+e_{15}}{\varepsilon_{11}} & 1\end{bmatrix}\nabla_0^2\begin{Bmatrix}A_0\\B_0\\\phi_0\end{Bmatrix}+\begin{bmatrix}\frac{\rho\omega^2-c_{33}k^2}{c_{44}} & 0 & -\frac{e_{33}k^2}{c_{44}}\\ -\frac{(c_{13}+c_{44})k^2}{c_{11}} & \frac{\rho\omega^2-c_{44}k^2}{c_{11}} & -\frac{(e_{15}+e_{31})k^2}{c_{11}}\\ -\frac{e_{33}k^2}{\varepsilon_{11}} & 0 & \frac{\varepsilon_{33}k^2}{\varepsilon_{11}}\end{bmatrix}\begin{Bmatrix}A_0\\B_0\\\phi_0\end{Bmatrix}=0 \tag{3.76}$$

Where,

$$\nabla_0^2=\frac{d^2[\,]}{dr^2}+\frac{1}{r}\frac{d^2[\,]}{dr^2}-\frac{m^2[\,]}{r^2} \tag{3.77}$$

To solve equation (3.77), first consider a generalized eigenvalue problem defined below by:

$$\left\{\begin{bmatrix} \frac{\rho\omega^2-c_{33}k^2}{c_{44}} & 0 & -\frac{e_{33}k^2}{c_{44}} \\ -\frac{c_{13}+c_{44}}{c_{11}}k^2 & \frac{\rho\omega^2-c_{44}k^2}{c_{11}} & -\frac{e_{15}+e_{31}}{c_{11}}k^2 \\ -\frac{e_{33}k^2}{\varepsilon_{11}} & 0 & \frac{\varepsilon_{33}k^2}{\varepsilon_{11}} \end{bmatrix} - \alpha^2 \begin{bmatrix} 1 & 1+\frac{c_{13}}{c_{44}} & \frac{e_{15}}{c_{44}} \\ 0 & 1 & 0 \\ \frac{e_{15}}{\varepsilon_{11}} & \frac{e_{31}+e_{15}}{\varepsilon_{11}} & 1 \end{bmatrix}\right\} \begin{Bmatrix} A_1 \\ B_1 \\ \phi_1 \end{Bmatrix} = 0 \quad (3.78)$$

The eigenvalues and corresponding eigenvectors are $\alpha_j, \varphi_j = \begin{Bmatrix} \varphi_{1j} \\ \varphi_{2j} \\ \varphi_{3j} \end{Bmatrix}, j = 1,2,3$, respectively.

Then the solutions [49] of equation (3.77) will be given by :

$$\begin{Bmatrix} A_0 \\ B_0 \\ \phi_0 \end{Bmatrix} = \sum_{j=1}^{3}\left(p_j J_m(\alpha_j r) + p_{j+4} Y_m(\alpha_j r)\right) \begin{Bmatrix} \varphi_{1j} \\ \varphi_{2j} \\ \varphi_{3j} \end{Bmatrix} \quad (3.79)$$

The solution of Equation (3.76) is given by [50]:

$$C_0 = p_4 J_m(\alpha_4 r) + p_8 Y_m(\alpha_4 r) \quad (3.80)$$

Here

$$\alpha_4 = \sqrt{\frac{\rho\omega^2-c_{44}k^2}{c_{66}}} \quad (3.81)$$

And $p_1, \ldots, p_8$ are unknown constants to be determined by the mechanical and electrical boundary conditions, which are the traction free boundary conditions and the open and closed circuit boundary conditions.

By substituting solutions into the stress and electric displacement or electric potential boundary conditions, the linear homogeneous equations are derived as:

$$[Q]_{8\times 8} \begin{Bmatrix} p_1 \\ p_2 \\ p_3 \\ p_4 \\ p_5 \\ p_6 \\ p_7 \\ p_8 \end{Bmatrix} = 0 \quad (3.82)$$

Here, the elements of the Q matrix are given in Appendix D. The frequency spectra can be obtained by find the non-zero solution of the above equation which is given by:

$$|Q| = 0 \tag{3.83}$$

3.4 Computer Programming

Computer programs are developed in order to obtain the numerical results of the finite element method. The FEM program was obtained from previous research work and modified for the purpose of this research. For the analytical method computer codes could not be developed to obtain the numerical results due to the fact that computer codes are not available for solving Bessel's function of complex order.

Figure 15, shows the flow chart of the developed FEM flow chart. The program starts out by reading the input provided by the user. The material properties, geometry, load, boundary conditions, assigned ω/m, ω/k and m/k and the FEM parameters such as number of elements, Gauss approximation points etc. Then the program will assemble the global matrix by first evaluating the element matrix. The eigenvalue problem is then solved and the results can be obtained to draw the wave spectra.

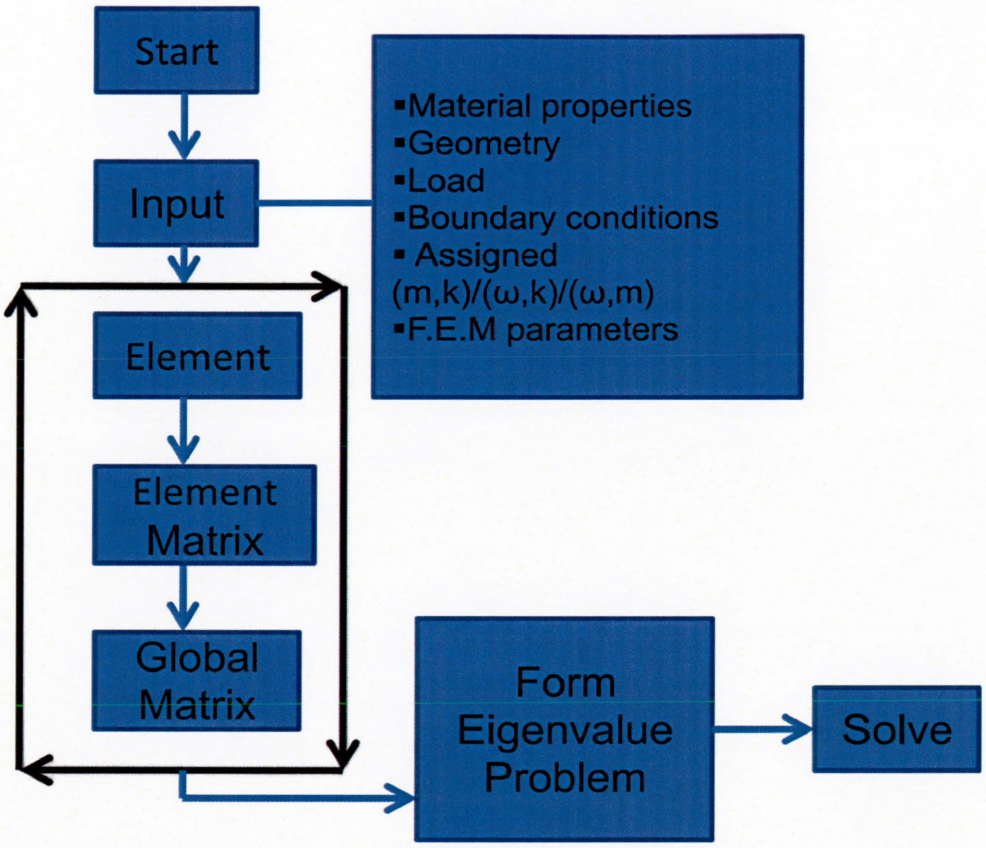

Figure 15: FEM program flow chart.

3.5 Numerical Results

Numerical examples will be studied in this section. Different cylinders with different electric boundary conditions will be studied here. The material properties were presented in chapter 2.

The first example is comparison study. In this example, the axial wave number, k, is assigned to be zero, and the electric potential and axial displacement are set to be zero for all the nodes. For such a setup, one should be able to retrieve the results presented in the previous chapter. It is noted that only the thick cylinder is considered in the study. This can be justified by observing the results of Figure 16 given in the next example.

3.5.1 Comparison Study

Thick open boundary condition case is compared to the thick open boundary condition case for the circular annulus (plain strain, Chapter 2).

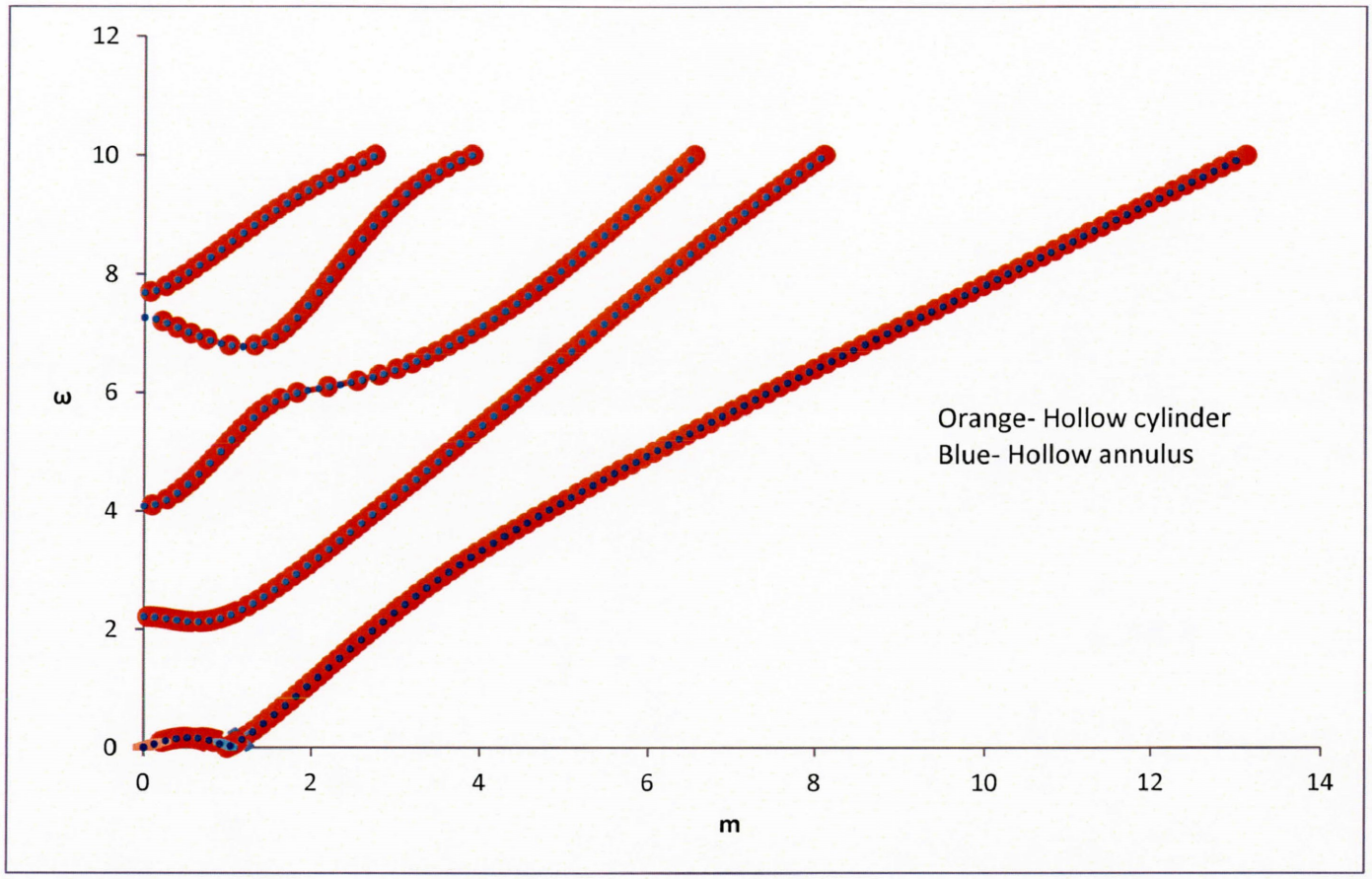

Figure 16: Data comparison.

It can be clearly seen from Figure 16 that they have a very good agreement.

3.5.2 A Thick Cylinder with Open-Circuit Electric Boundary Conditions

A hollow homogeneous PZT-4 cylinder with r_i=0.5 and r_o=1.5 subjected to traction free and open circuit boundary conditions both at the inner and outer surfaces is studied here.

The wave spectra surfaces for the cylinder are shown in below from Figure 17 to Figure 20. They are representing the first four propagating modes in the cylinder. A notable feature of the wave spectra is that the lower order modes are almost non-dispersive. For example, in Figure 17 the wave spectra display a smooth surface for different k and m. In Figure 18, it is almost non-dispersive for higher values of k and m, say, for example, at about k=4 and m=2. At higher propagating modes (modes three and four) the non-dispersive behavior starts to develop at much higher k and m values (k=8 and m=7).

To help better understand the wave spectra, a 2-D representation will be presented next. First, the ω-k relationships will be presented by making cuts at m=0, 1, 2, 3, 4 and 5. Then the ω-m relationships will be presented by making cuts at k=0, 1, 2, 3, 4 and 5.

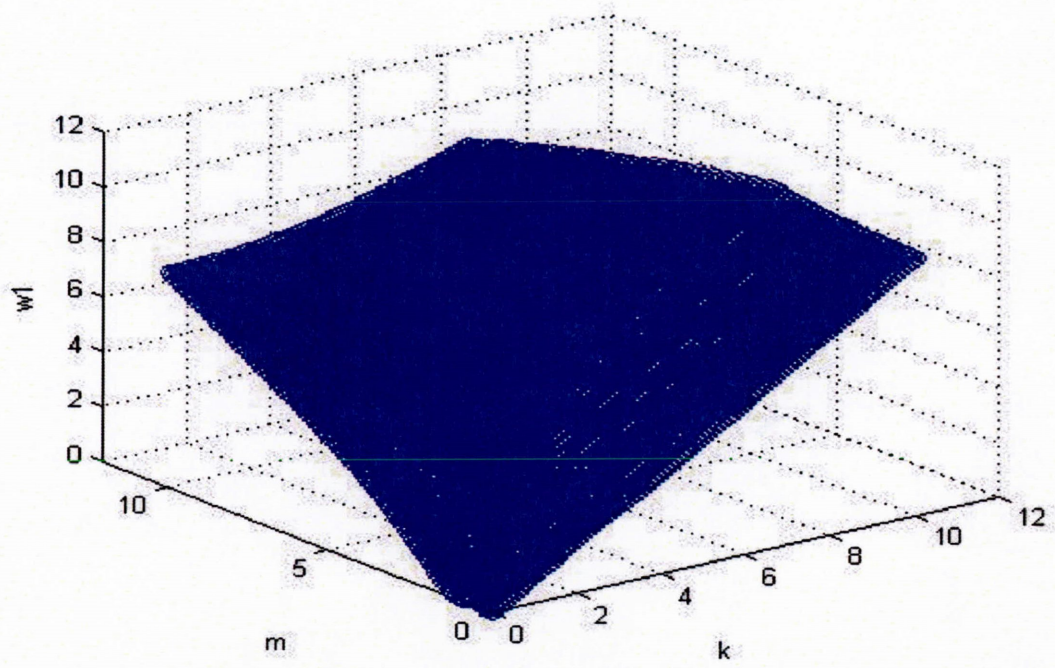

Figure 17: Thick cylinder with open-circuit boundary condition. (3-D surface first propagating mode).

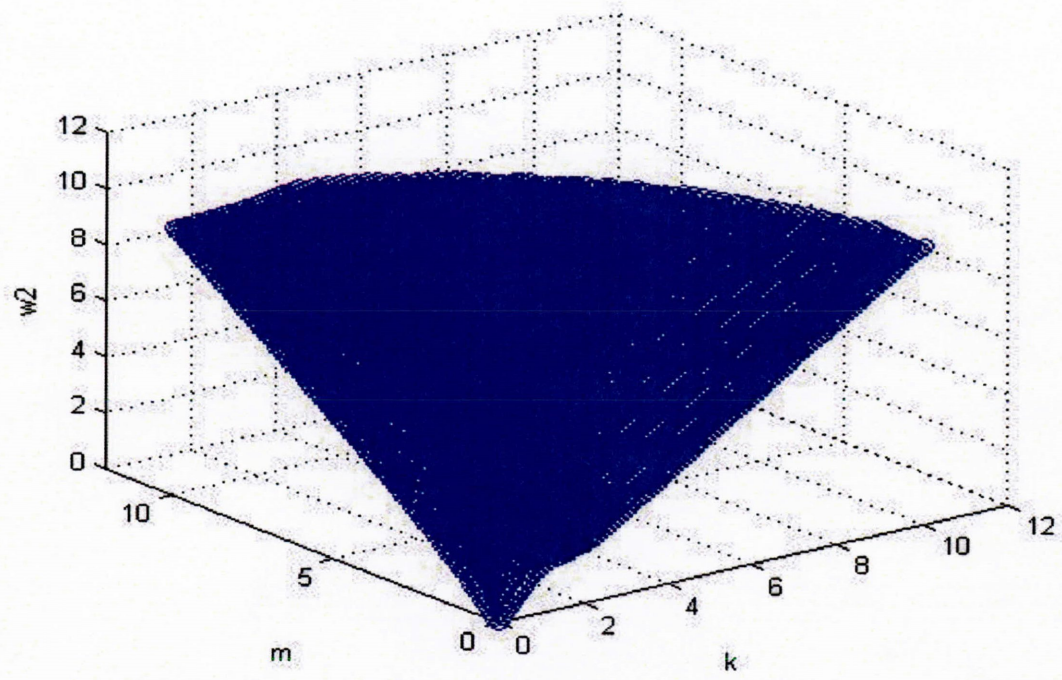

Figure 18: Thick cylinder with open-circuit boundary condition. (3-D surface second propagating mode).

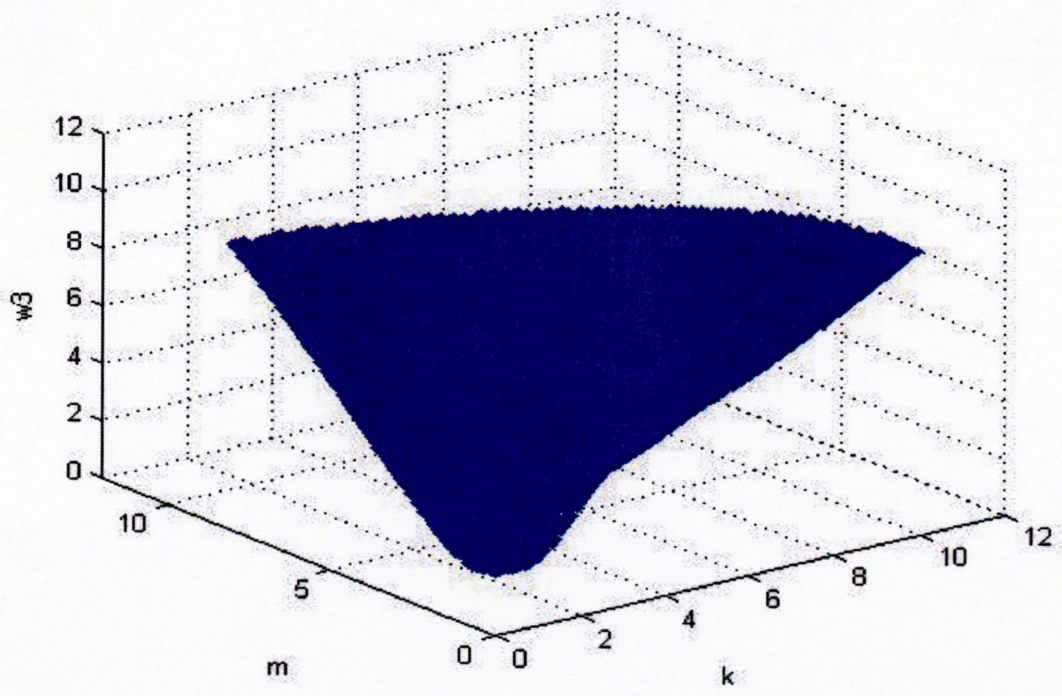

Figure 19: Thick cylinder with open-circuit boundary condition. (3-D surface second propagating mode).

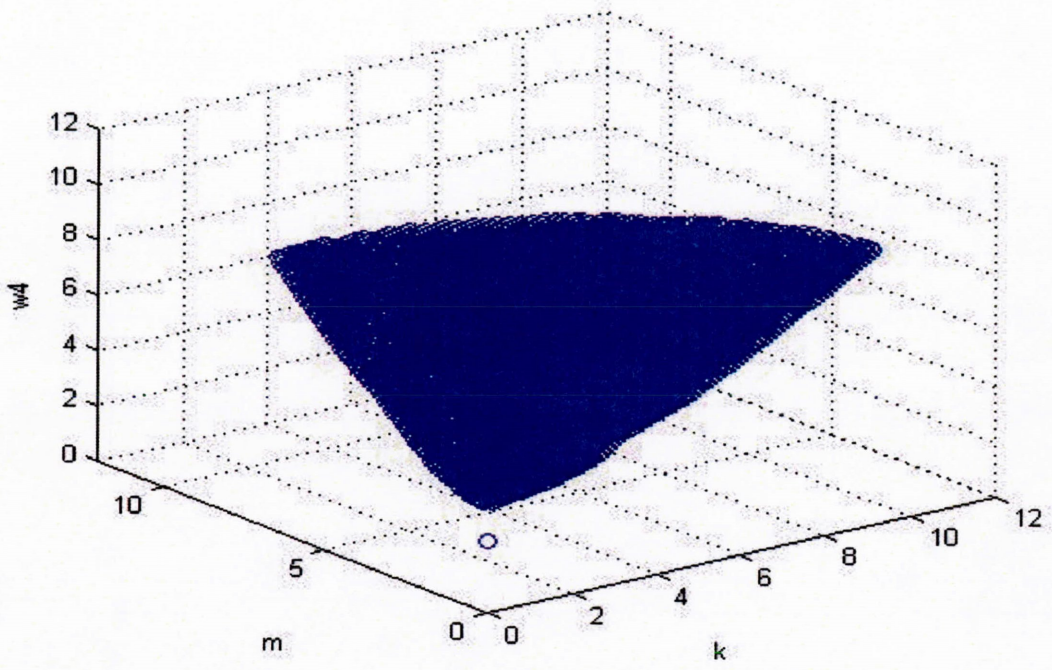

Figure 20: Thick cylinder with open-circuit boundary condition. (3-D surface third propagating mode).

In order to better understand the wave spectra surfaces, the variation of frequency with each individual m and k are presented in below. Figures 21(a)-21(f) shows the frequency as a function of axial wave number when the circumferential wave number is given. For each m, the lowest wave mode always shows an almost non-dispersive property, especially for the large value of k. The first cut-off frequency for different circumferential wave number increases with the increase of the circumferential wave number.

As one observes Figures 21(a)-21(f), it can be seen from the ω-k relationship that as m (circumferential wave number) raises the modes cut-off frequency shifts upward on the ω axis. For example, at m=0, the cut-off frequency of the second mode is at ω=0. At m=1 the cut-off frequency increases to about ω=1.8. This can also be seen for the fourth and fifth propagating mode at m=1. This carries on for m=2, 3, 4 and 5. For example, at m=0 the cut-off frequency is at ω=0 and keeps rising to ω=4 at m=5. Therefore, when m increases the cut-off frequencies for all propagating modes increase.

At m=0 (Figure 21(a)), the first modes is almost non-dispersive (linear) for all k values. As m increases, the first propagating mode is almost non-dispersive at higher values of k. For example,

at m=2, the first mode is almost non-dispersive at values of higher then about k=2. This range of almost non-dispersive behavior seems to decrease as m increases and this can be seen in Figures 21(c-f). Mode 2 at m=0, is almost non-dispersive starting at k=2 and as m increases to higher values the starting values seems to decrease. For example, at m=4 (second propagating mode), all values of k are almost non-dispersive. Mode 2 at low $k<2$ (m=1 and 2) is not linear but as m rises the mode seems to be more linear, exhibiting an almost non-dispersive behavior. This behavior is observed on modes 3, 4 and 5. Higher order modes are almost non-dispersive at higher values of k and ω. For example, mode 3 (m=0), is only almost non-dispersive for values of k higher than 4.2. At m=5 (mode 3), the mode is almost non-dispersive at values of k higher than 2. Therefore, the range of k where modes are non-dispersive increases as m is increased.

***Note series 1, series 2, series 3, series 4 and series 5 represent first propagating mode, second propagating mode, third propagating mode, fourth propagating mode and fifth propagating mode respectively.**

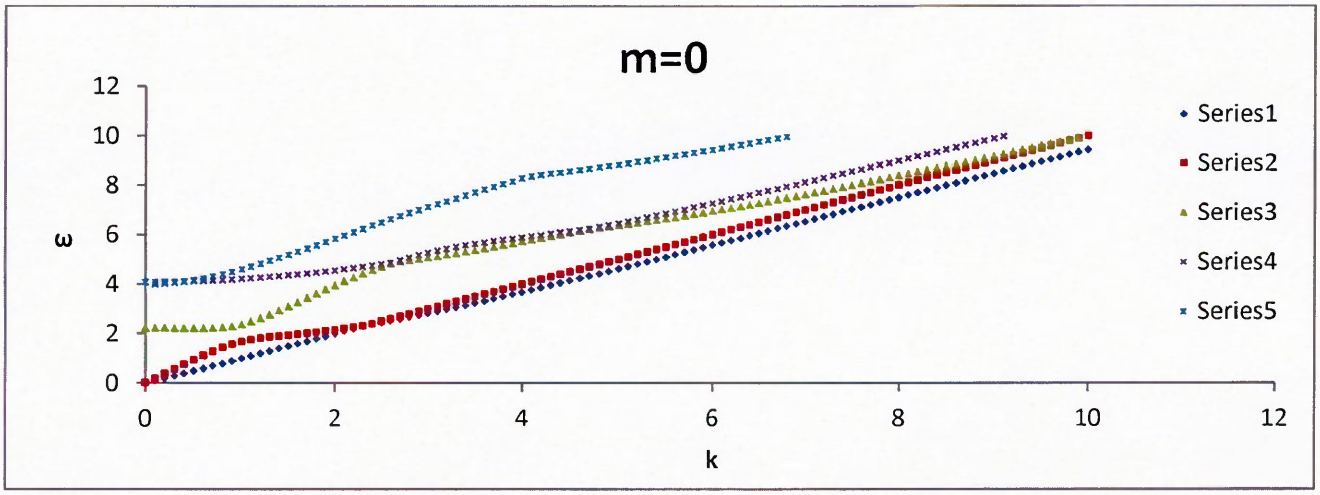

Figure 21(a): ω-k Relationship for m=0 (Thick cylinder with open-circuit case).

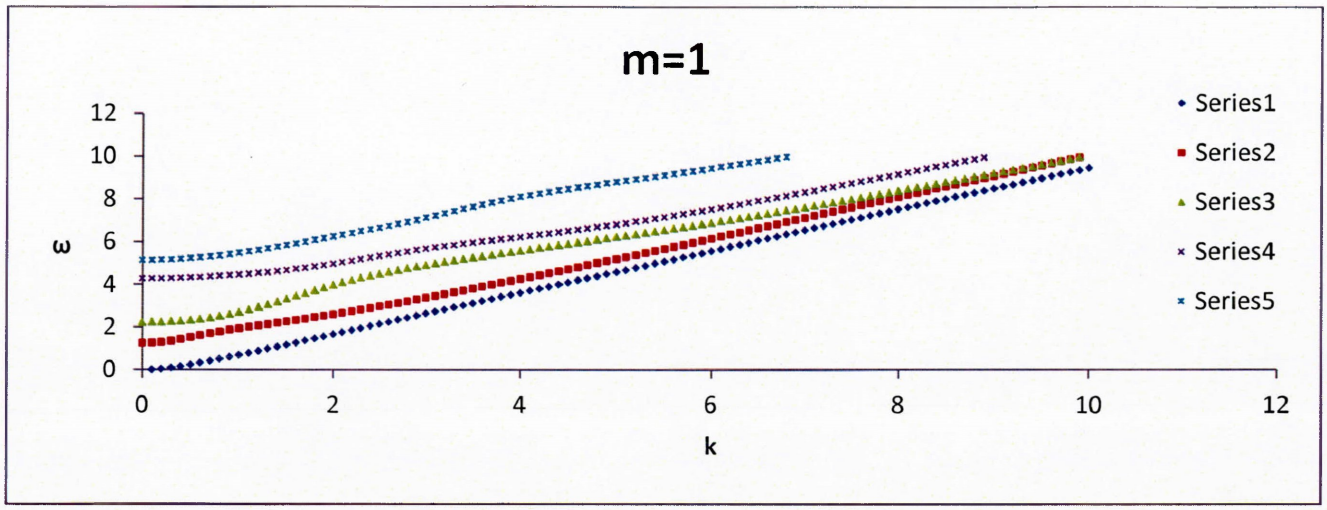

Figure 21(b): ω-k Relationship for m=1 (Thick cylinder with open-circuit case).

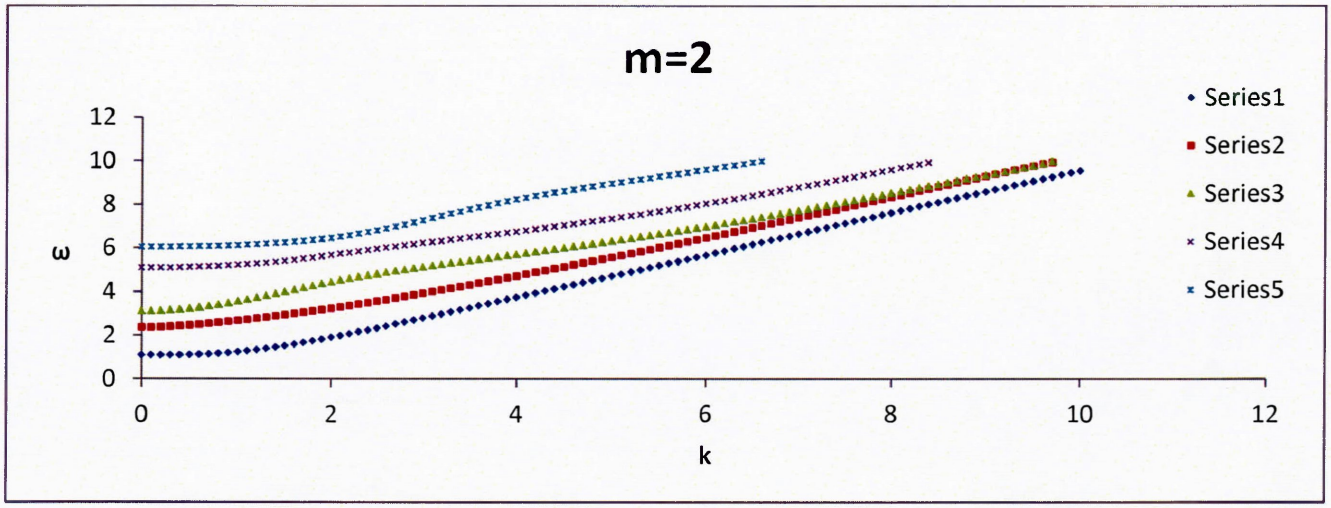

Figure 21(c): ω-k Relationship for m=2 (Thick cylinder with open-circuit case).

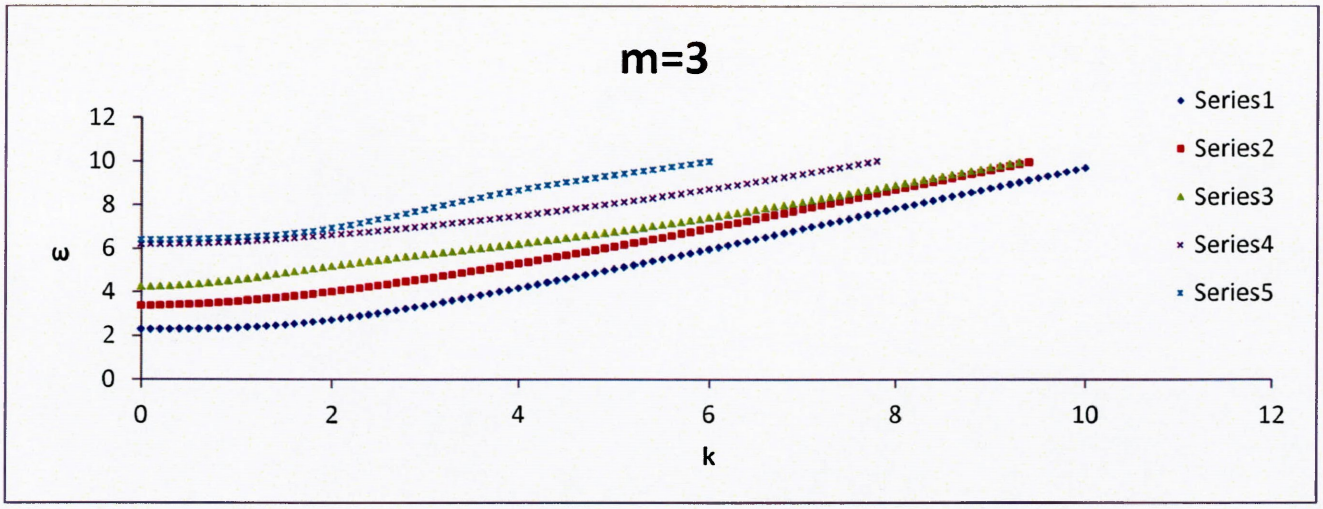

Figure 21(d): ω-k Relationship for m=3 (Thick cylinder with open-circuit case).

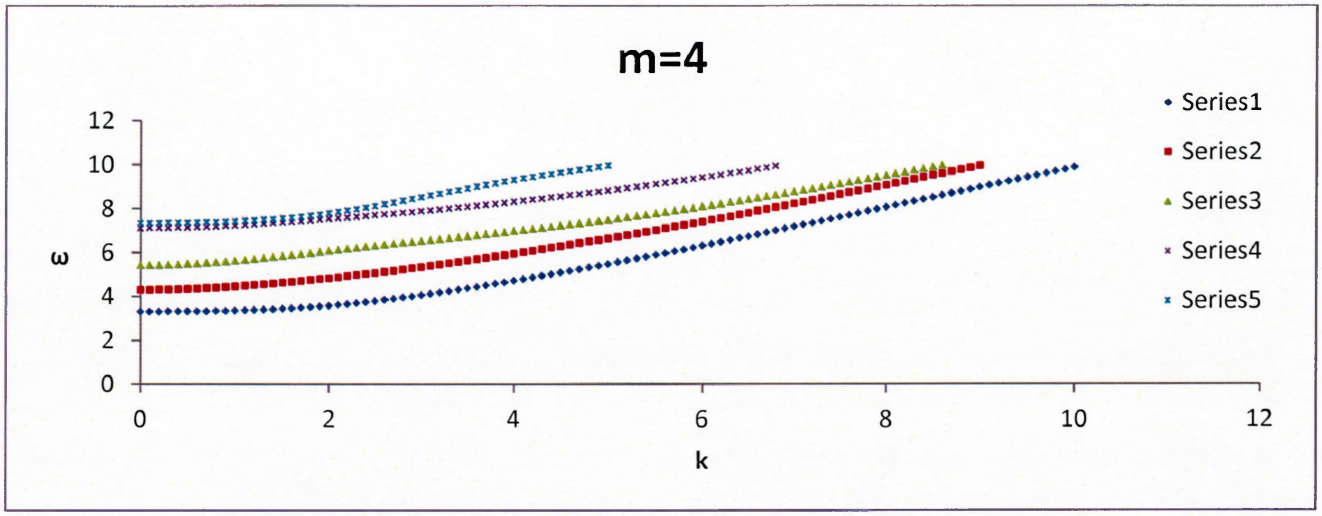

Figure 21(e): ω-k Relationship for m=4 (Thick cylinder with open-circuit case).

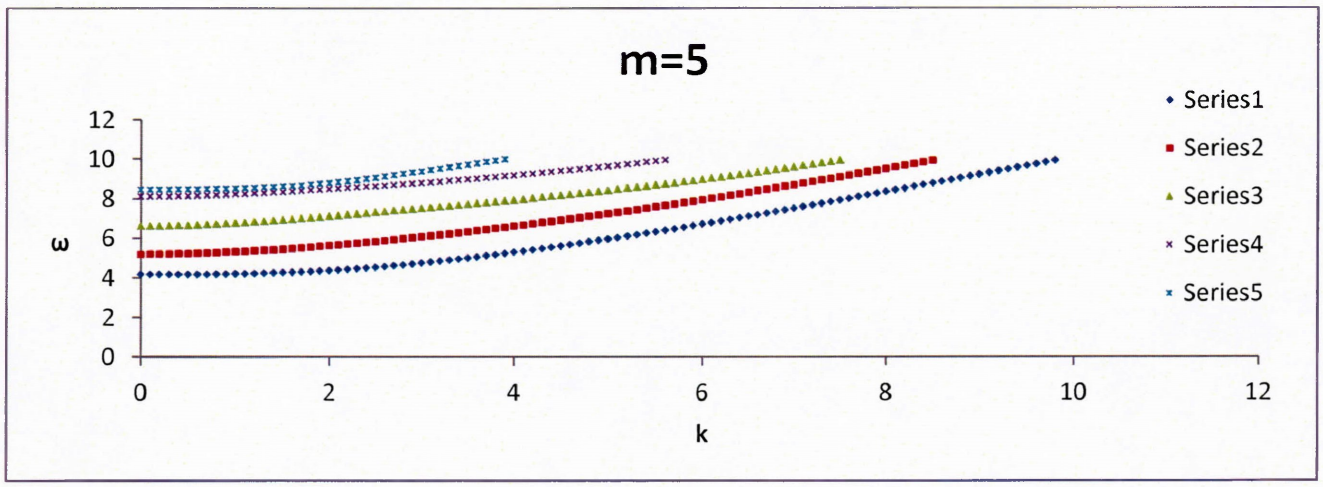

Figure 21(f): ω-k Relationship for m=5 (Thick cylinder with open-circuit case).

Figures 22(a)-22(f), show the frequency as a function of circumferential wave number when the axial wave number is given. The cut-off frequency for different circumferential wave number increases with the increase of the circumferential wave number. At k=0 (mode one and two), the cut-off frequency is at ω=0 and as k increases to 1 the cut-off frequency raises to ω=1 and ω=1.8 for mode 1 and mode 2, respectively. This trend is seen as throughout different k values. Finally, at k=5 the cut-off frequency is at value of ω=4.5 and 5 for mode 1 and 2, respectively. The other remaining modes seem to follow a similar trend. For example, mode 5, the cut-off frequency starts at ω=4 (k=0) and rises all the way to ω=9 (k=5). In conclusion, the cut-off frequency of each propagating mode increases with the increase of k.

All the propagating modes have certain ranges that are almost non-dispersive. But the lower order modes have higher ranges of being almost non-dispersive. For example, mode 1 at k=0, is almost non-dispersive for values of k>2. Then, as k is increases to 2, the almost non-dispersive range changes to values of k>1.8. As k increases the almost non-dispersive range of mode 1 seems to stay around values of k>2. The major of effect of increasing k for mode 1, is seen at lower k values (k<2) where the wave spectra becomes more of straight line. This means that the phase velocity is almost zero at values of k<2. All the modes have a similar behavior to mode number 1. The major effect of increasing k is seen at lower values of k for different modes. For example, mode 5 at k=0, for values of k<3 is dispersive. But at k increases to 3, this non-dispersive area becomes more linear and then k=5 it is almost a straight line. Therefore, the almost non-dispersive range does not change as k increases. But the dispersive range changes to almost non-dispersive or a straight line for lower values of m.

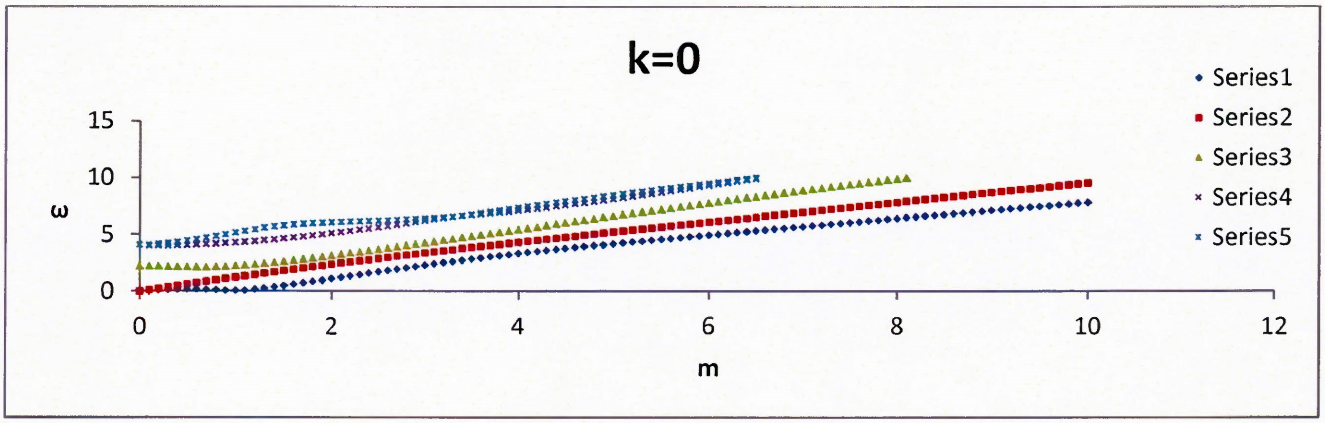

Figure 22(a): ω-m Relationship for k=0 (Thick cylinder with open-circuit case).

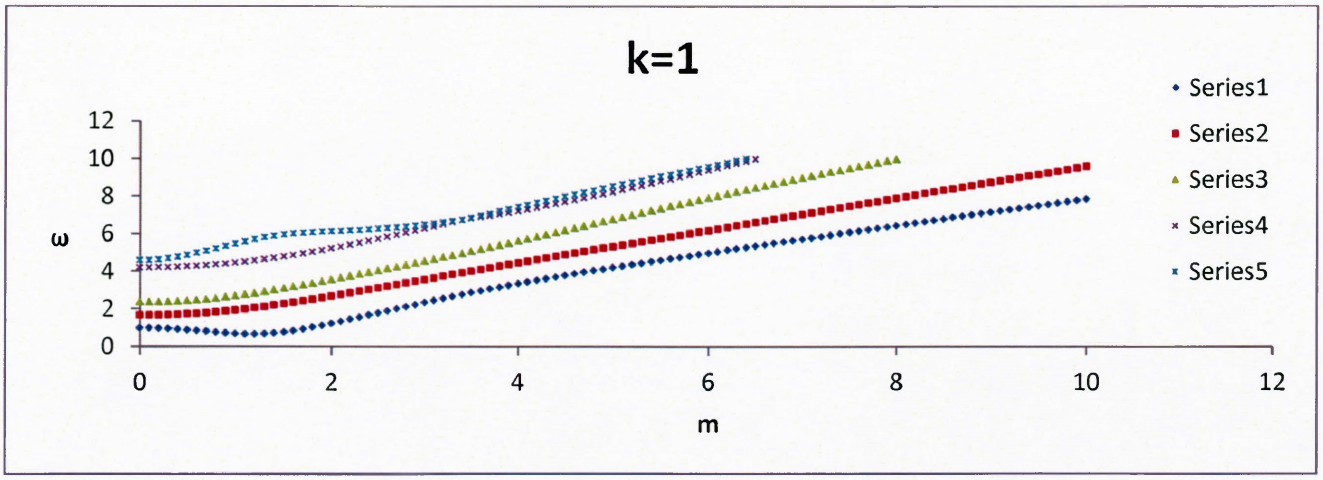

Figure 22(b): ω-m Relationship for k=1 (Thick cylinder with open-circuit case).

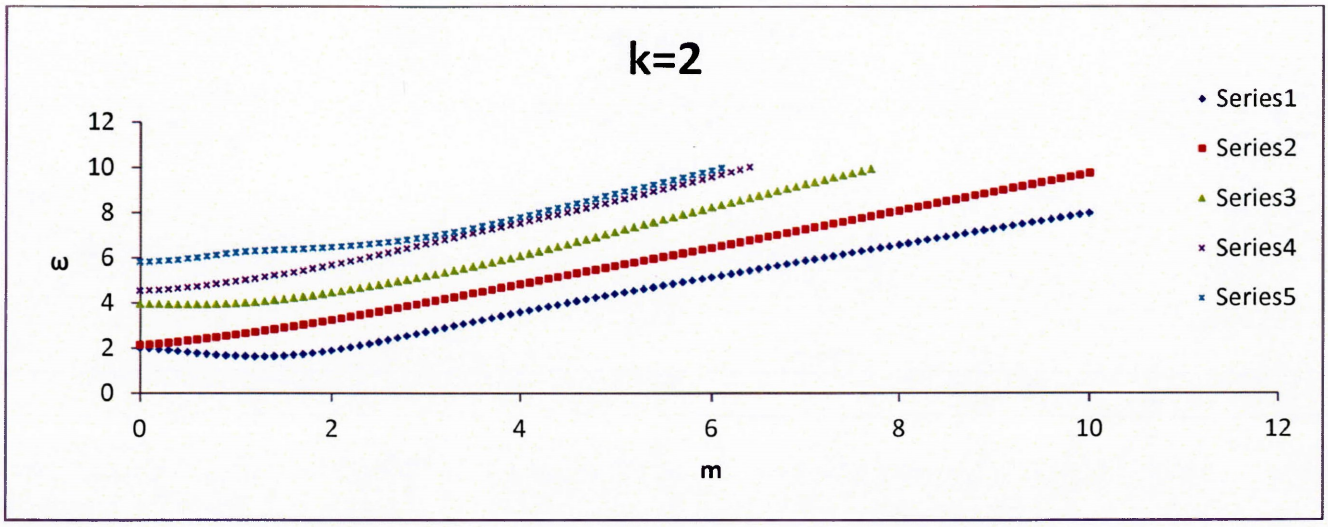

Figure 22(c): ω-m Relationship for k=2 (Thick cylinder with open-circuit case).

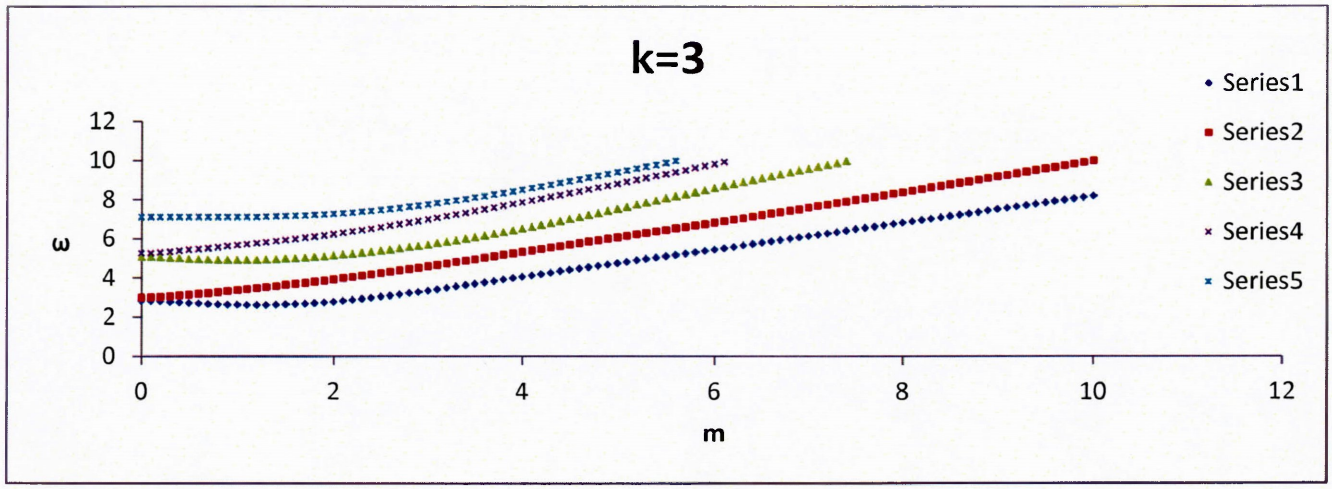

Figure 22(d): ω-m Relationship for k=3 (Thick cylinder with open-circuit case).

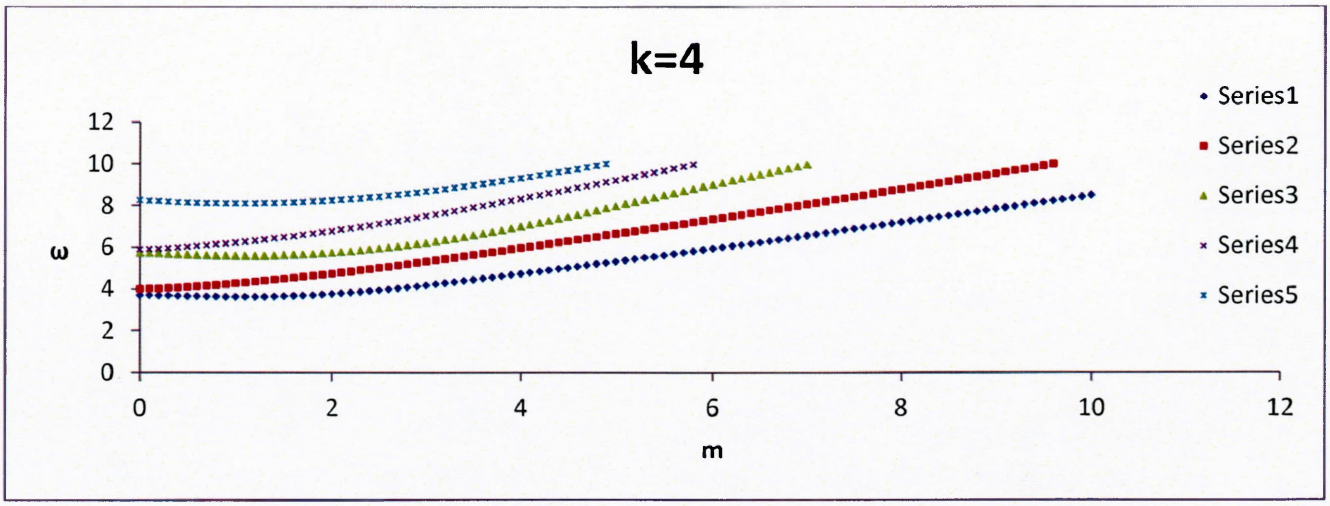

Figure 22(e): ω-m Relationship for k=4 (Thick cylinder with open-circuit case).

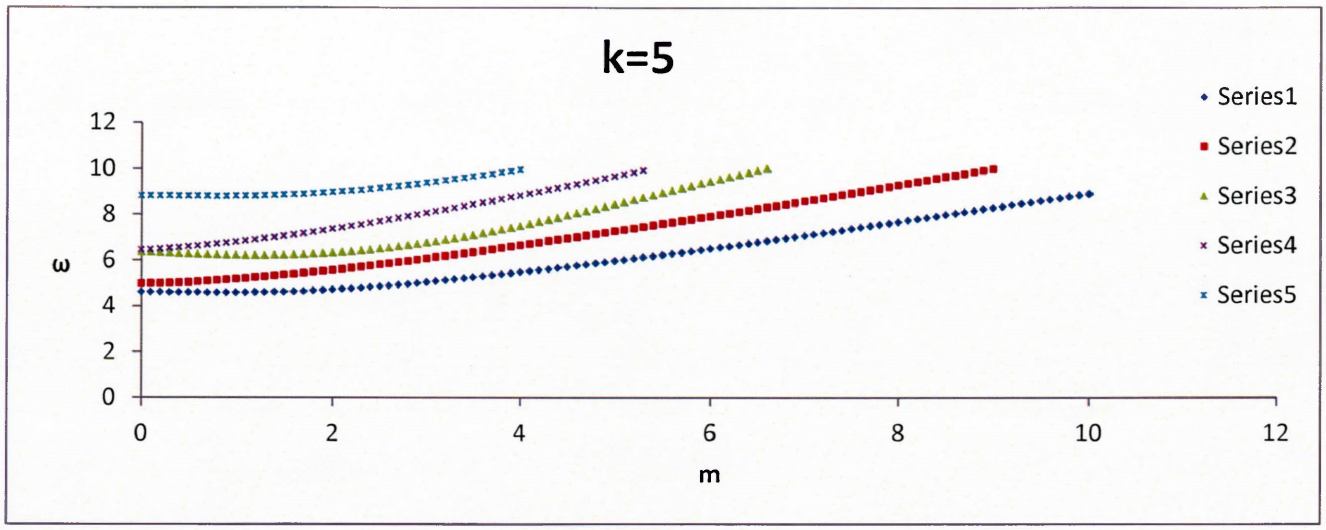

Figure 22(f): ω-m Relationship for k=5 (Thick cylinder with open-circuit case).

3.5.3 A Thick Cylinder with Closed-Circuit Electric Boundary Conditions

A hollow homogeneous PZT-4 cylinder with r_i=0.5 and r_o=1.5 subjected to traction free and closed circuit boundary conditions both at the inner and outer surface is considered here.

The wave spectra surfaces for the cylinder are shown in below from Figure 23 to 26. They are representing the first four propagating modes in the cylinder. Figures 23 to 26 are similar to Figures 17 to 20. This is interesting because the electric boundary conditions have changed but the wave spectra have not changed even though the equations of motion are said to be coupled. This signifies the fact that the electrical boundary conditions have minimum effect on the wave spectra. Similar observations can be made in this example (closed circuit) to the previous example (open circuit).

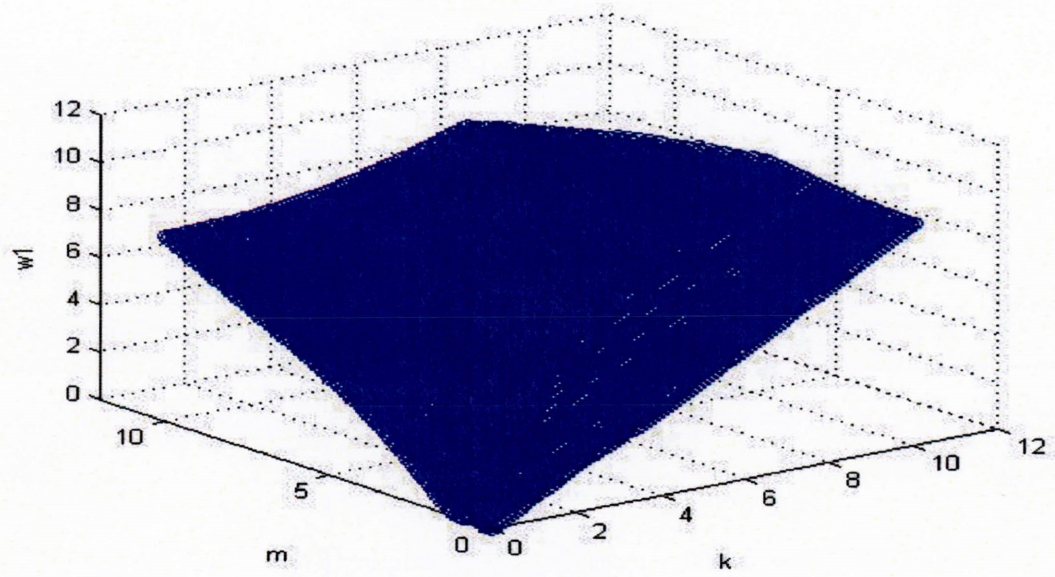

Figure 23: Thick cylinder with closed-circuit boundary condition. (3-D surface first propagating mode).

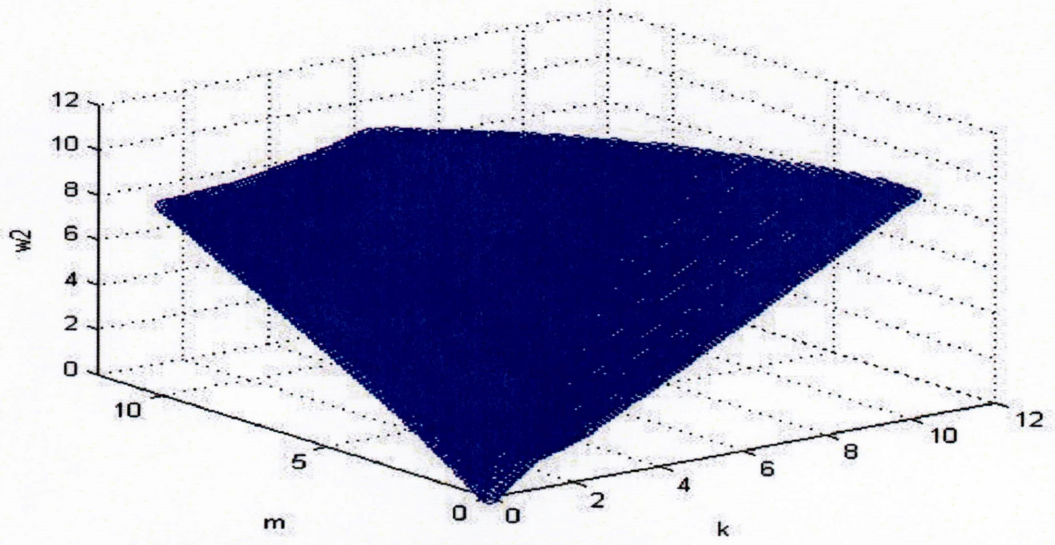

Figure 24: Thick cylinder with closed-circuit boundary condition. (3-D surface second propagating mode).

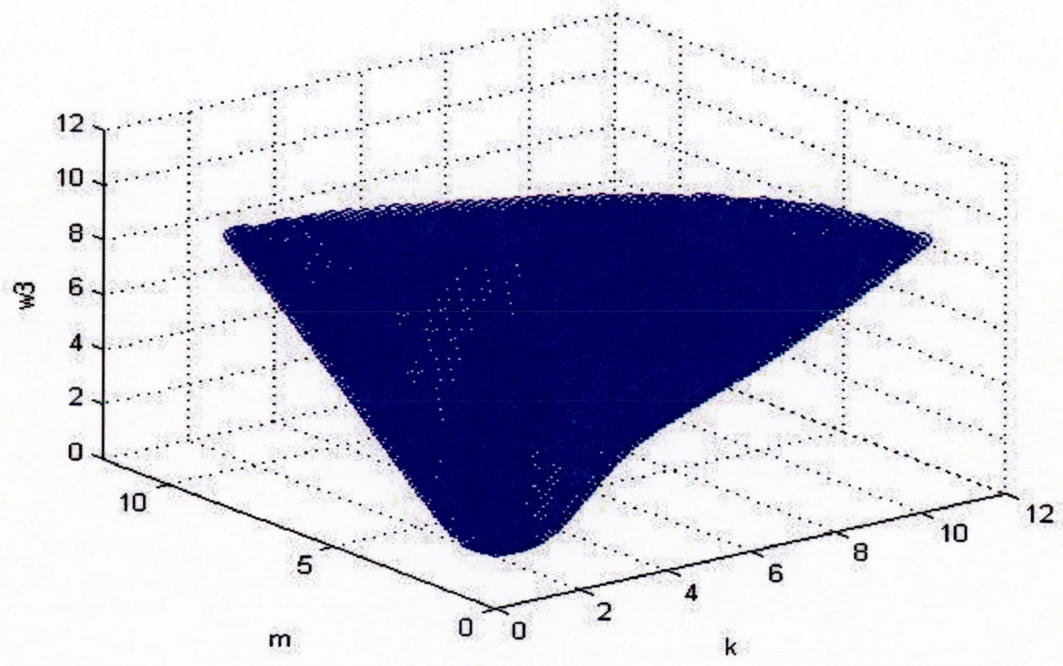

Figure 25: Thick cylinder with closed-circuit boundary condition. (3-D surface third propagating mode).

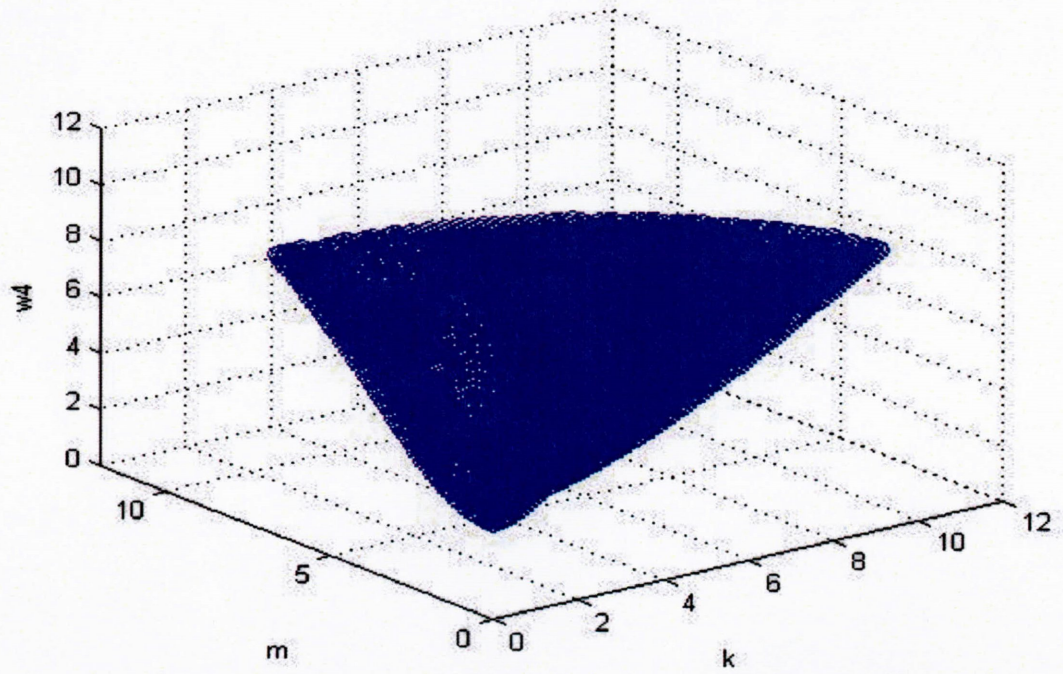

Figure 26: Thick cylinder with closed-circuit boundary condition. (3-D surface fourth propagating mode).

When observing the closed circuit case (Figures 27 (a)-27(f)) there exist some similarities with the open circuit case that is the starting point of all modes seems to shift on the ω axis. The same trend seems to exist between this case (close circuit) and the previous case (open circuit) is that the modes seem to separate away from each other. At m=0 the modes seem to interact with each other at different points on the graph, but as m increases the modes shift away from each other. This is very similar to the previous case (open circuit).

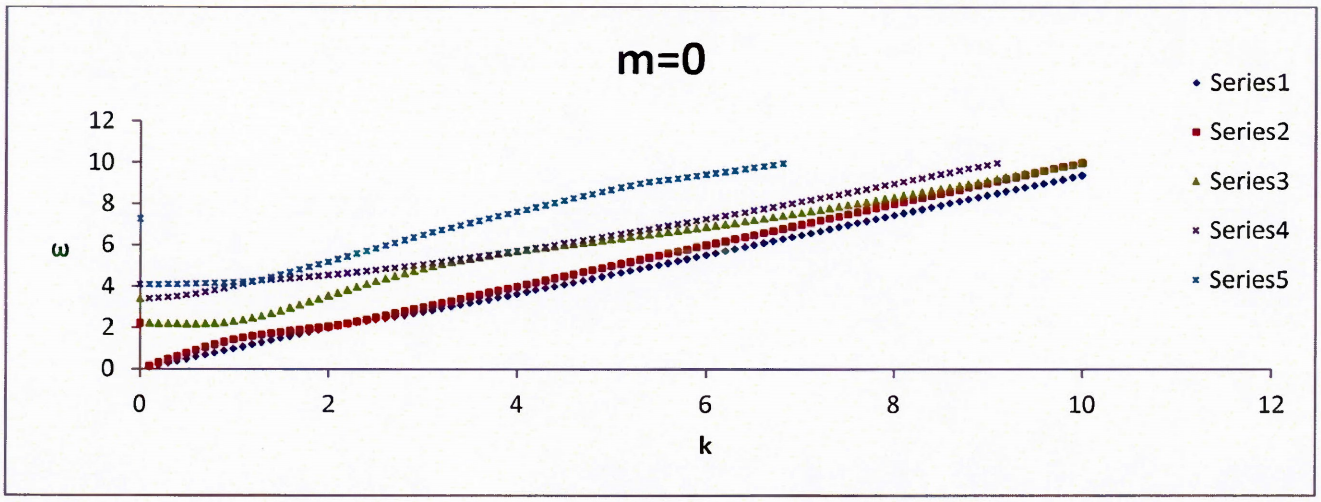

Figure 27(a): ω-k Relationship for m=0 (Thick cylinder with closed-circuit case).

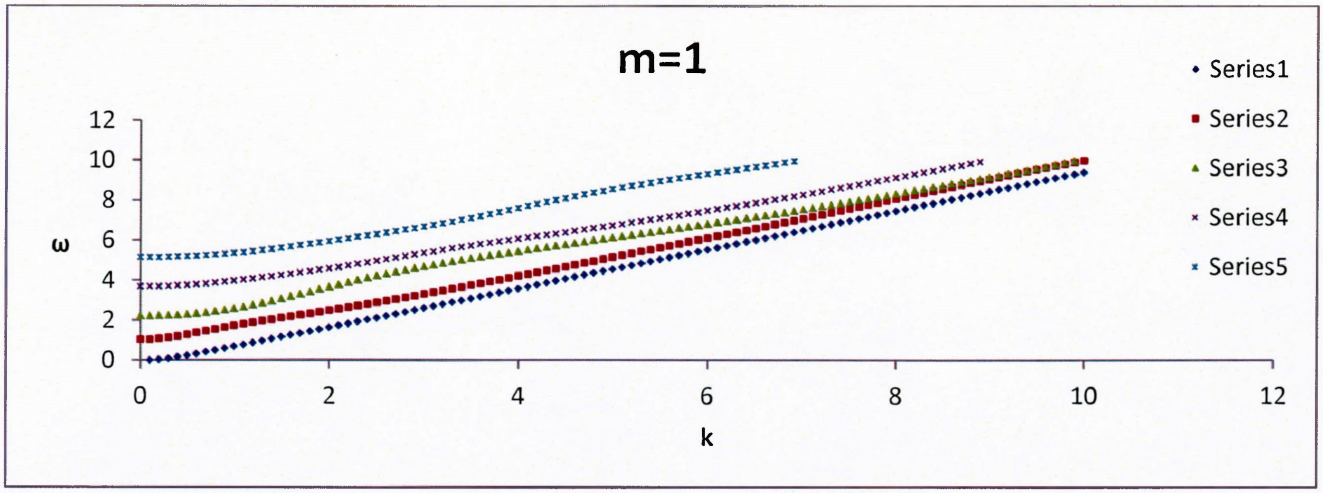

Figure 27(b): ω-k Relationship for m=1 (Thick cylinder with closed-circuit case).

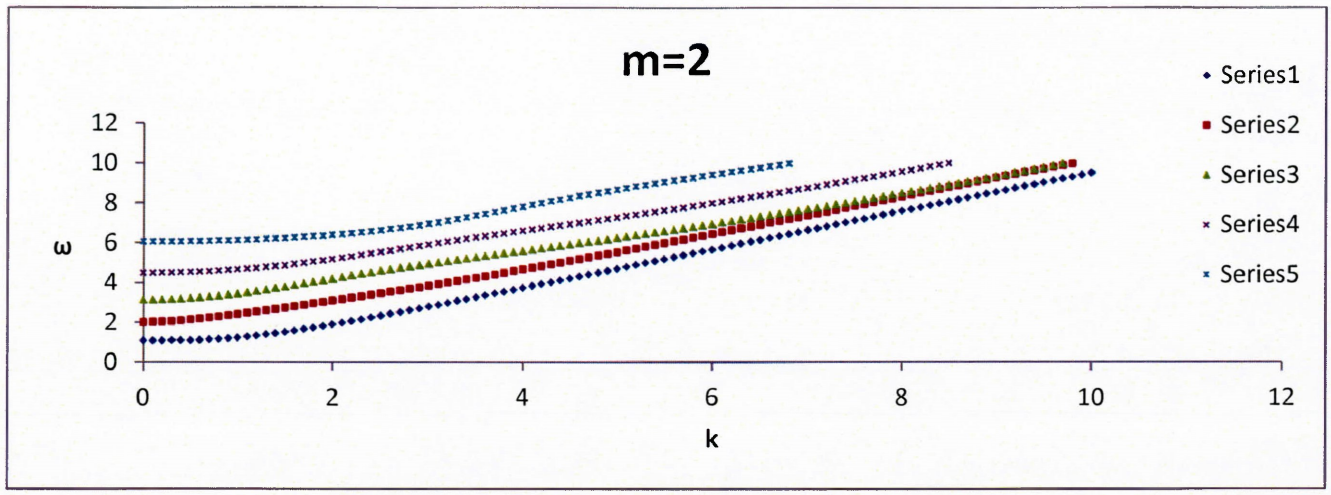

Figure 27(c): ω-k Relationship for m=2 (Thick cylinder with closed-circuit case).

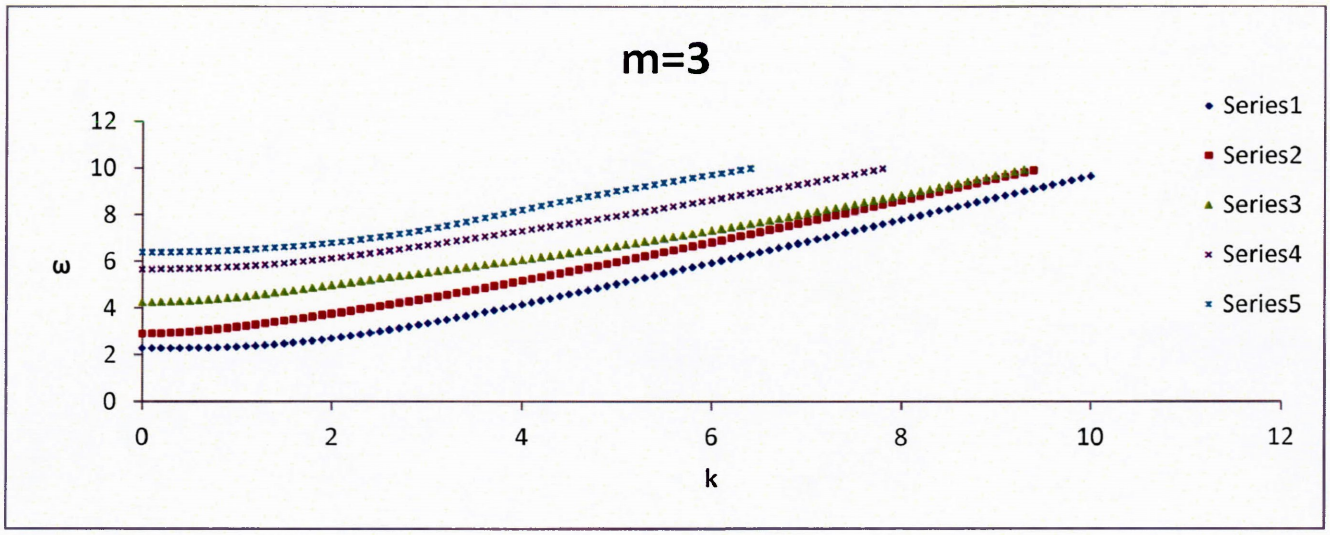

Figure 27(d): ω-k Relationship for m=3 (Thick cylinder with closed-circuit case).

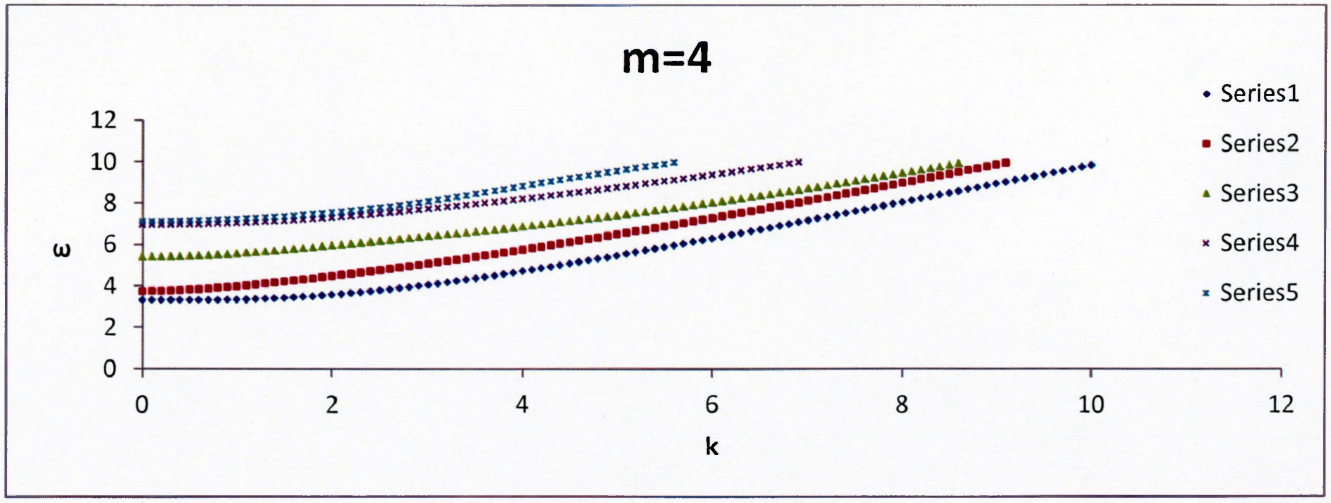

Figure 27(e): ω-k Relationship m=4 (Thick cylinder with closed-circuit case).

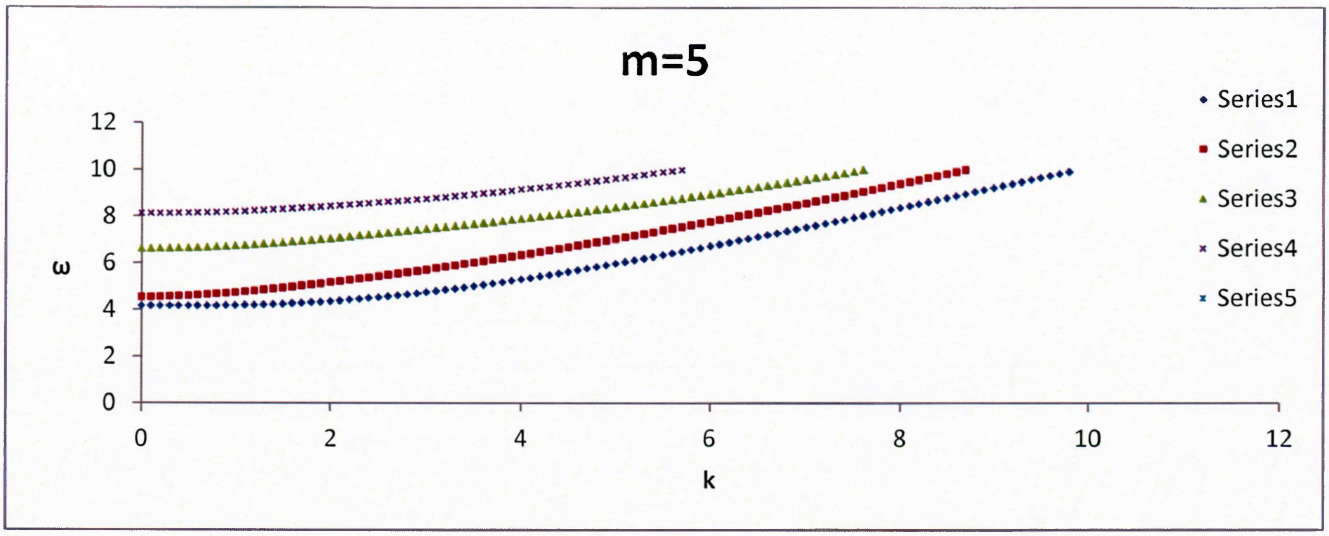

Figure 27(f): ω-k Relationship for m=5 (Thick cylinder with closed-circuit case).

First interesting detail here (Figures 28(a)-28(f)) is that the general shape of the modes changes in a similar fashion as the previous case of the open circuit case. As k increases the modes seem to shift to a more linear behavior. As with all the previous cases, the starting point of each mode seems to shift upward on the ω-axis. Modes 4 and 5 shift away from each other as k increases from k=0 to k=5.

The electric boundary conditions seem not to affect the wave properties greatly even though the mechanical and electric fields are coupled here. Physically the open-circuit and close-circuit are different but when observing the wave spectra they are essentially very similar. To fully understand all the effects of the electrical boundary conditions a closer observation is needed into the eigenvalues (modal shapes).

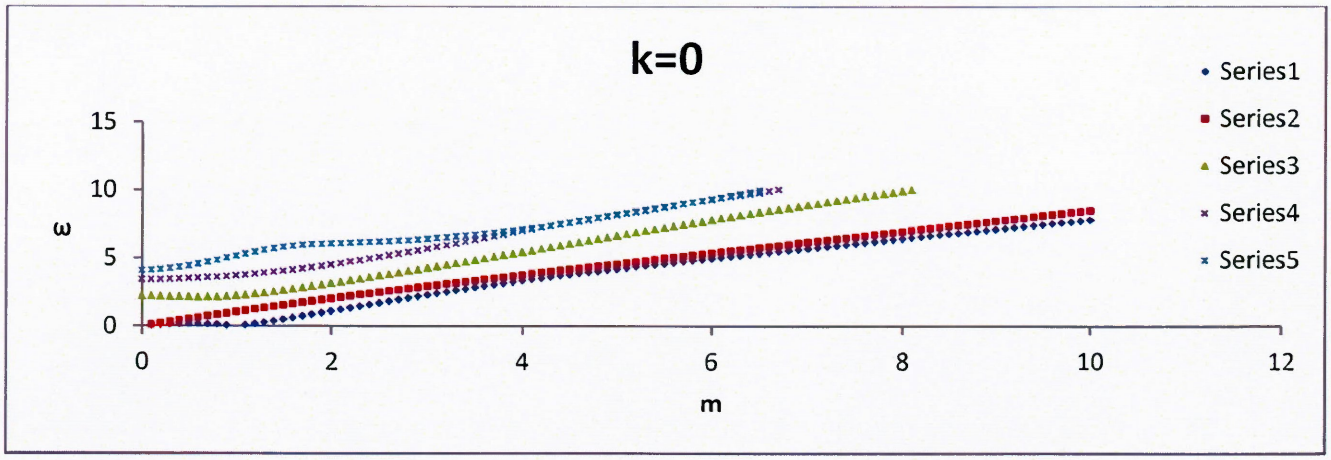

Figure 28(a): ω-m Relationship for k=0 (Thick cylinder with closed-circuit case).

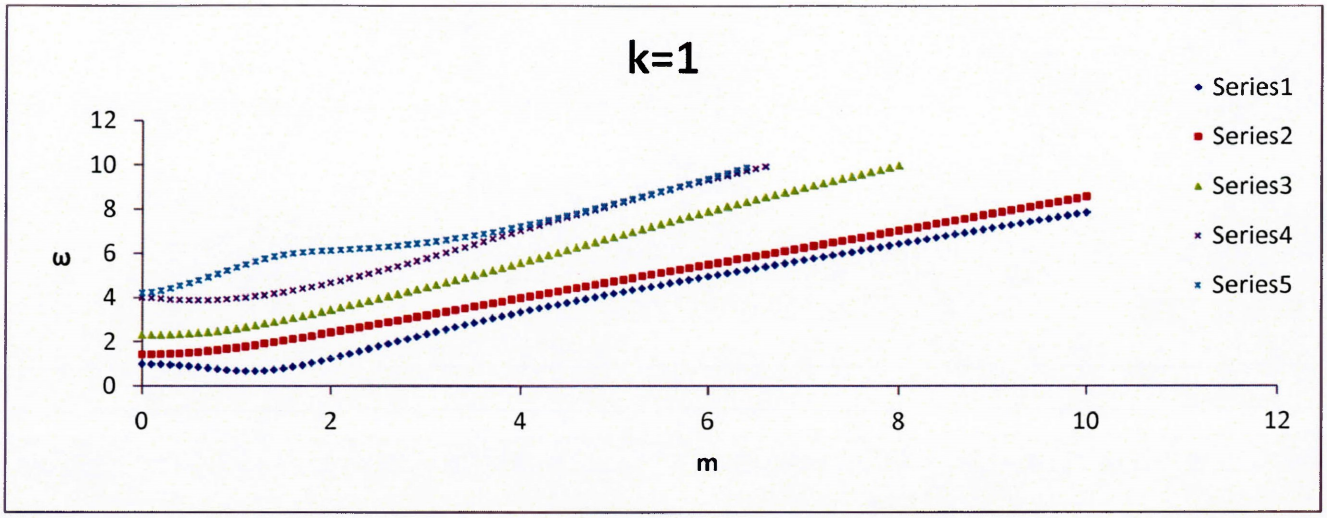

Figure 28(b): ω-m Relationship for *k=1* (Thick cylinder with closed-circuit case).

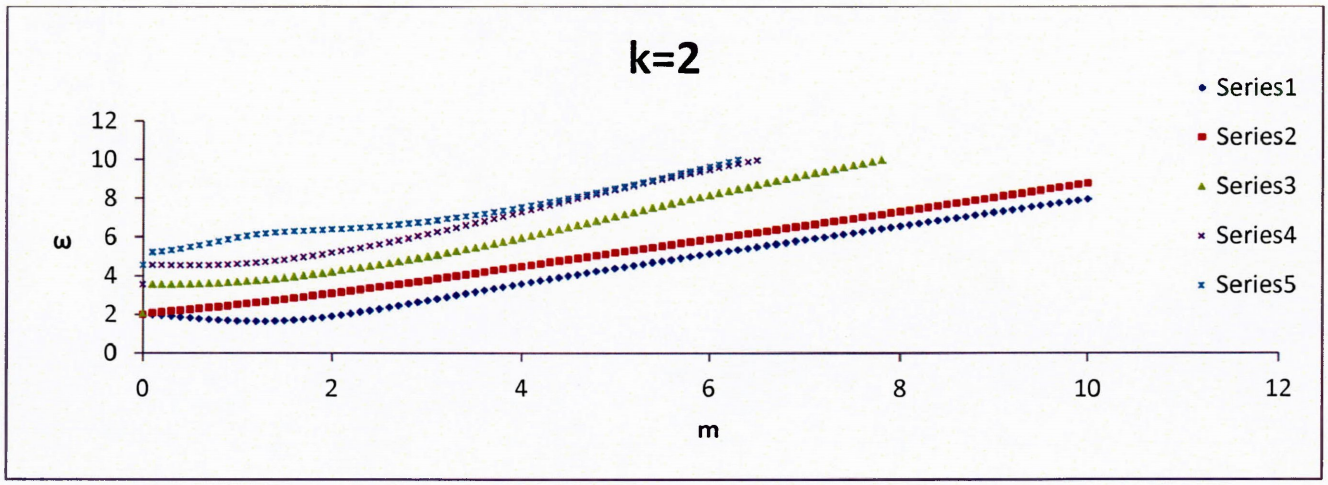

Figure 28(c): ω-m Relationship for *k=2* (Thick cylinder with closed-circuit case).

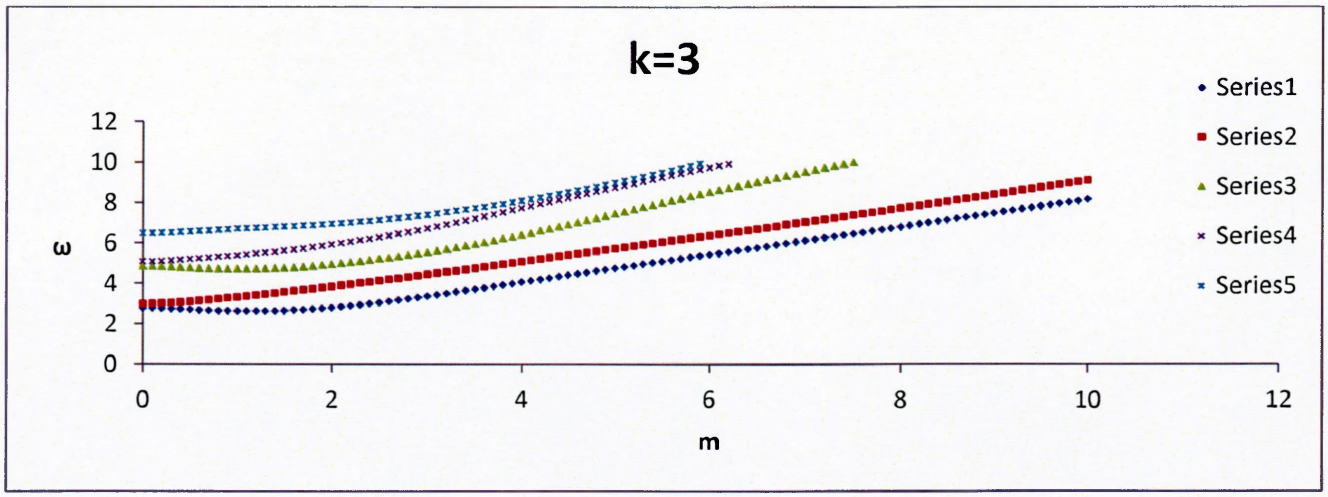

Figure 28(d): ω-m Relationship for *k=3* (Thick cylinder with closed-circuit case).

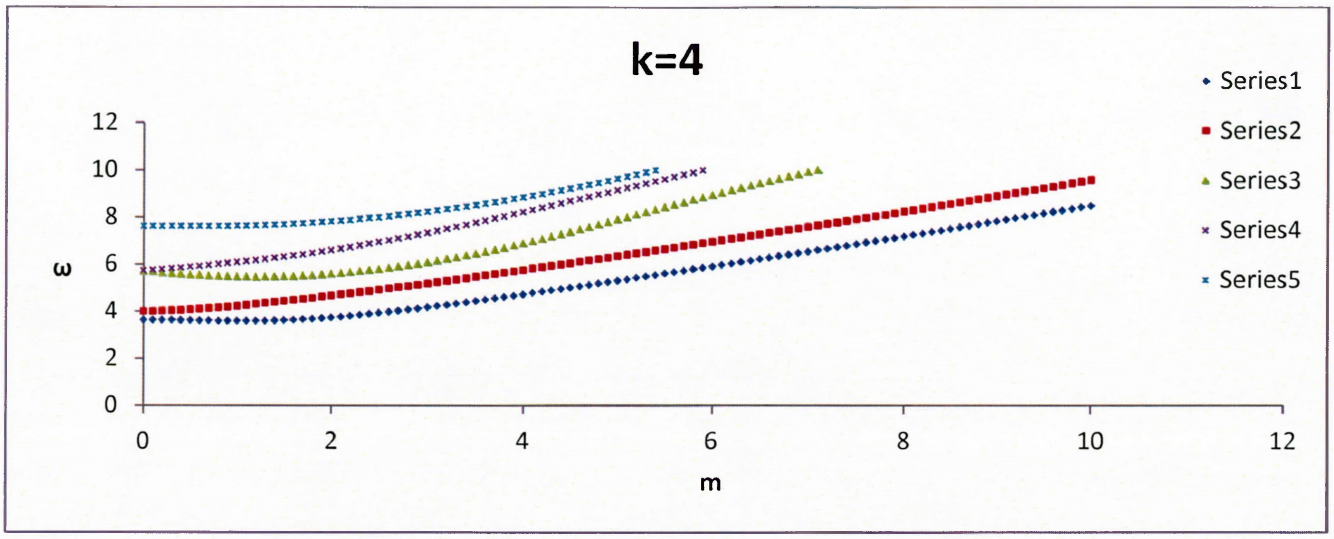

Figure 28(e): ω-m Relationship for *k=4* (Thick cylinder with closed-circuit case).

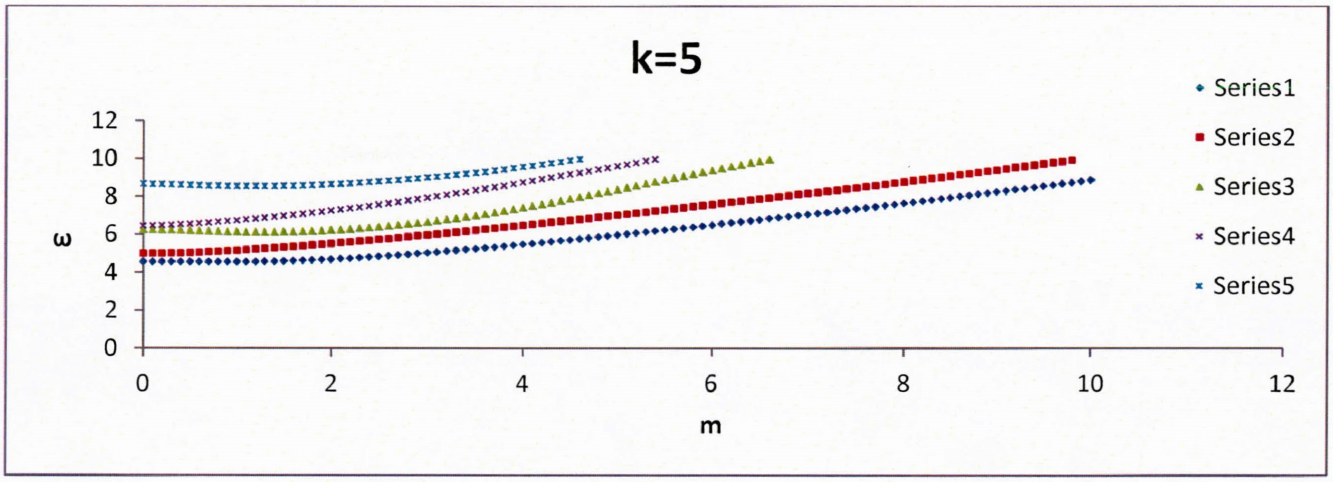

Figure 28(f): ω-m Relationship for *k=5* (Thick cylinder with closed-circuit case).

3.5.4 A Thin Cylinder with Open-Circuit Electric Boundary Conditions

A hollow and homogeneous PZT-4 cylinder with r_i=6.9704 and r_o=7.9704 subjected to traction free and open circuit boundary conditions both at the inner and outer surface is studied here.

The first surface corresponding to the first propagating modes in the cylinder is almost a plane in a large range of *m* and *k*. The first mode is almost non-dispersive in these ranges of *m* and *k*. For example, for k>2 the curve is almost non-dispersive. When observing the second propagating mode, the range of almost non-dispersive is higher especially at lower values of k and m. Higher propagating modes are only almost non-dispersive at higher values of k and m. For example, Figure 31, the mode is dispersive at values of k<4. This is also seen in mode 4 (Figure 32). This can be clearly observed when the 2-D figures are presented in the upcoming section.

One interesting point that can be made here is the fact that the 3-D wave spectra are very different from the previous 3-D wave spectra (thick cylinder). The geometry has changed here and this has a great effect on the wave spectra. Therefore, the geometry has an affect (dominant effect) on the wave spectra. This can be seen clearly when two dimensional curves are showed later on in this study.

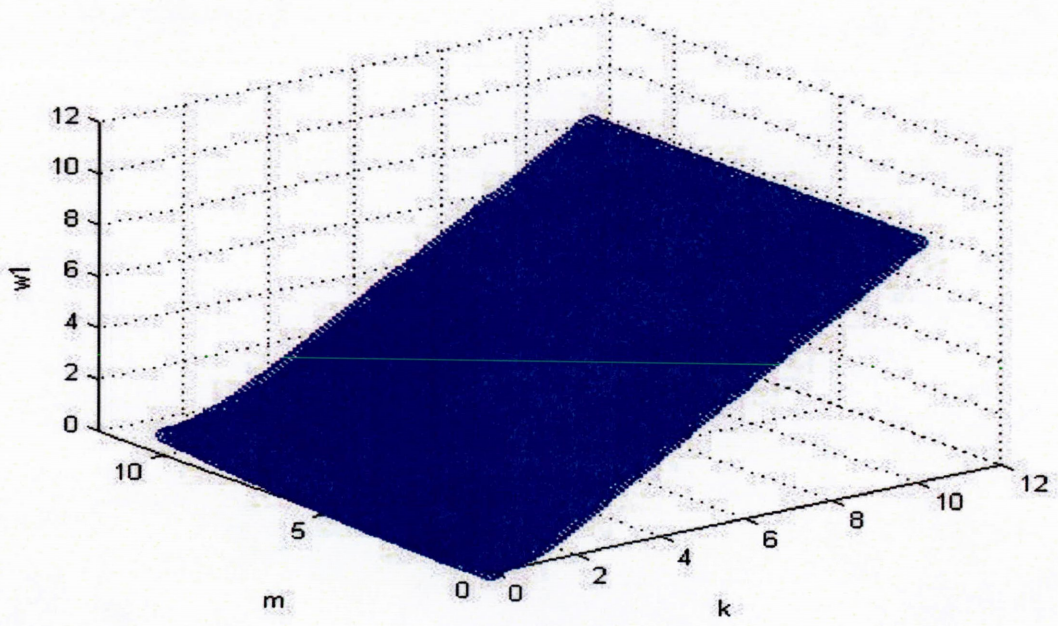

Figure 29: Thin cylinder with open-circuit boundary condition. (3-D surface first propagating mode).

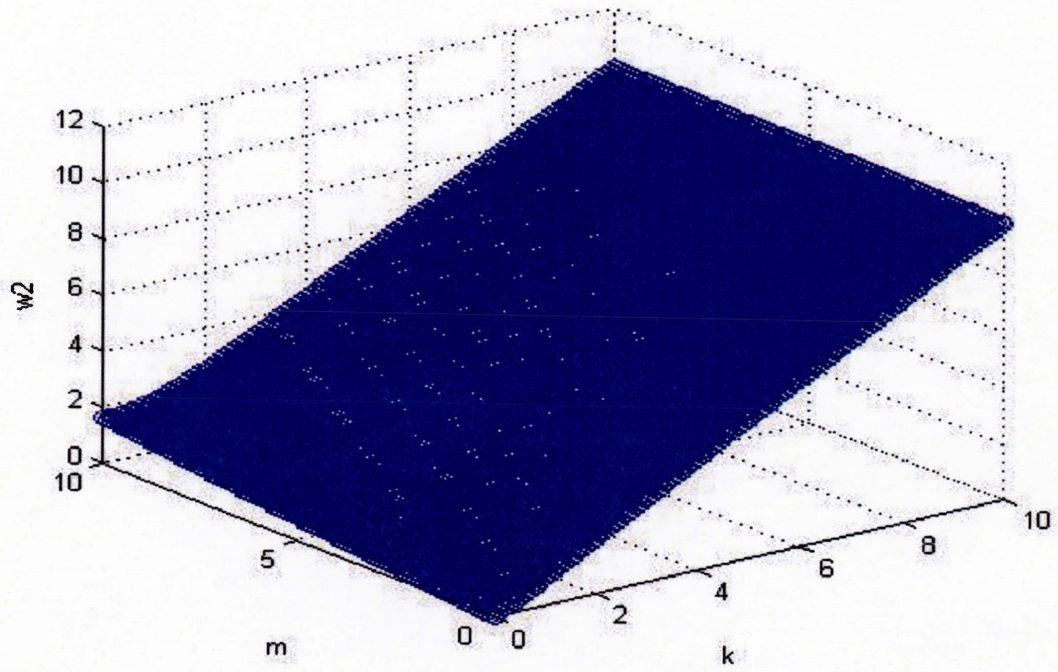

Figure 30: Thin cylinder with open-circuit boundary condition. (3-D surface second propagating mode).

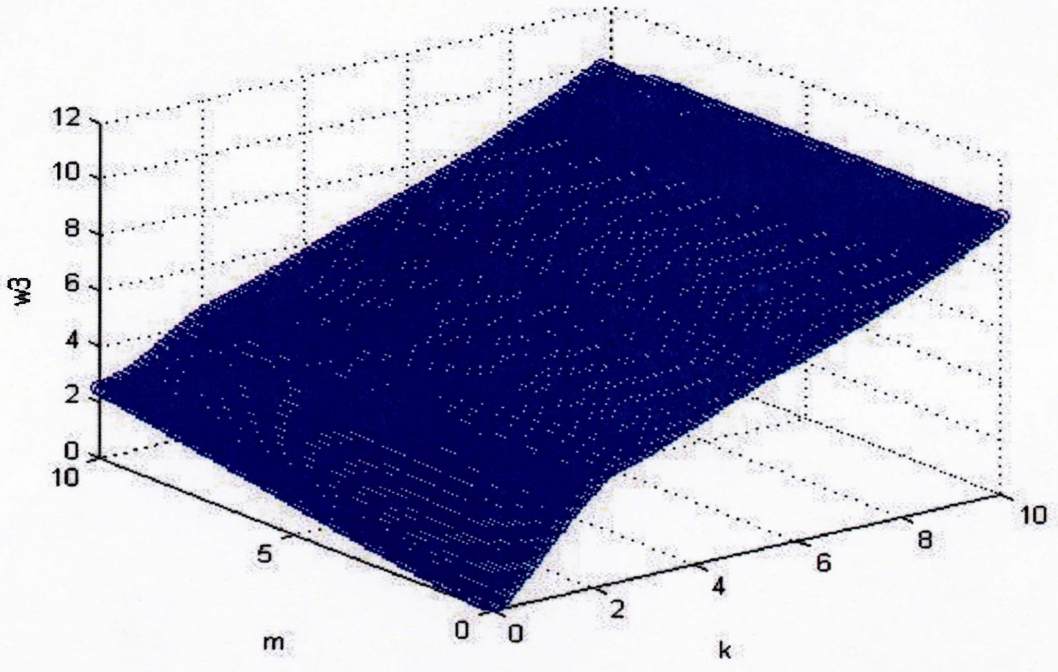

Figure 31: Thin cylinder with open-circuit boundary condition. (3-D surface third propagating mode).

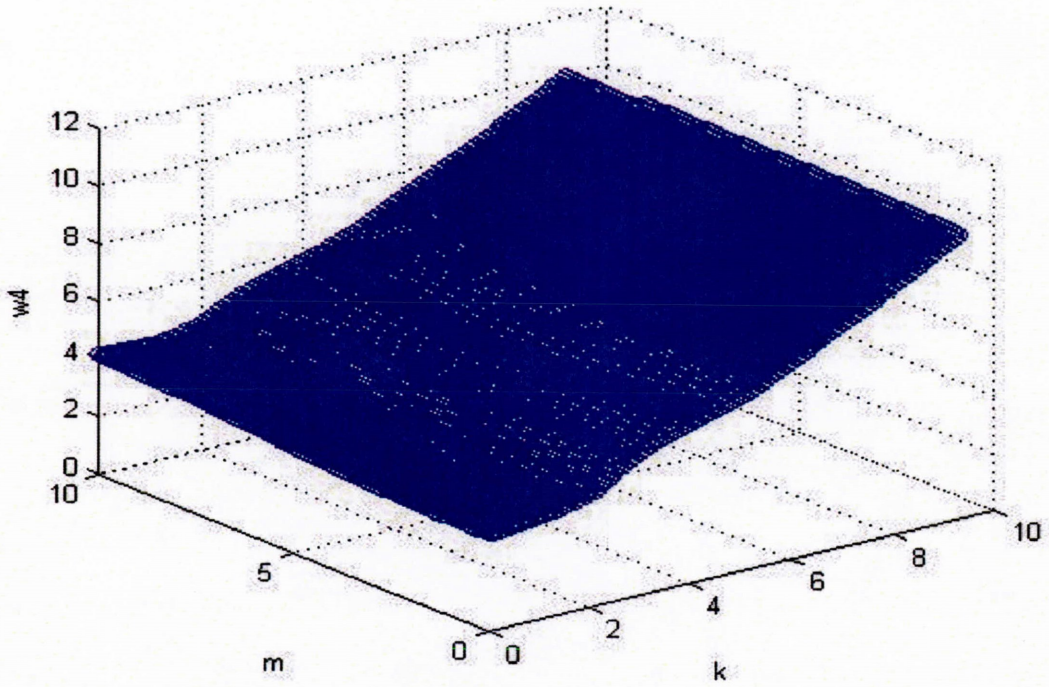

Figure 32: Thin cylinder with open-circuit boundary condition. (3-D surface fourth propagating mode).

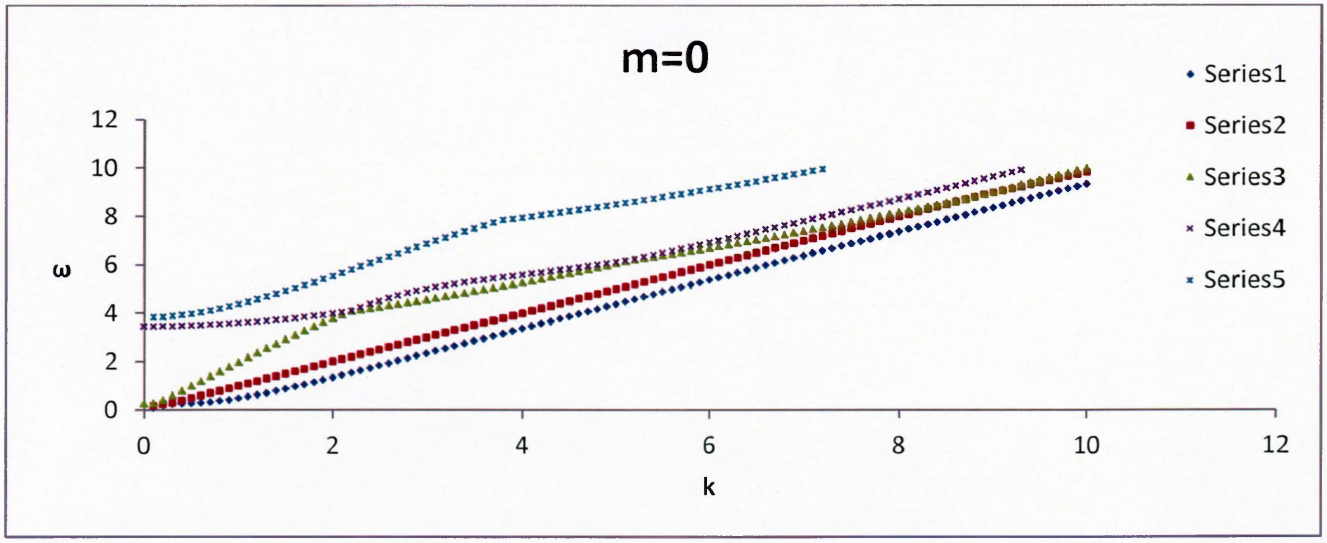

Figure 33(a): ω-k Relationship for *m=0* (Thin cylinder with open-circuit case).

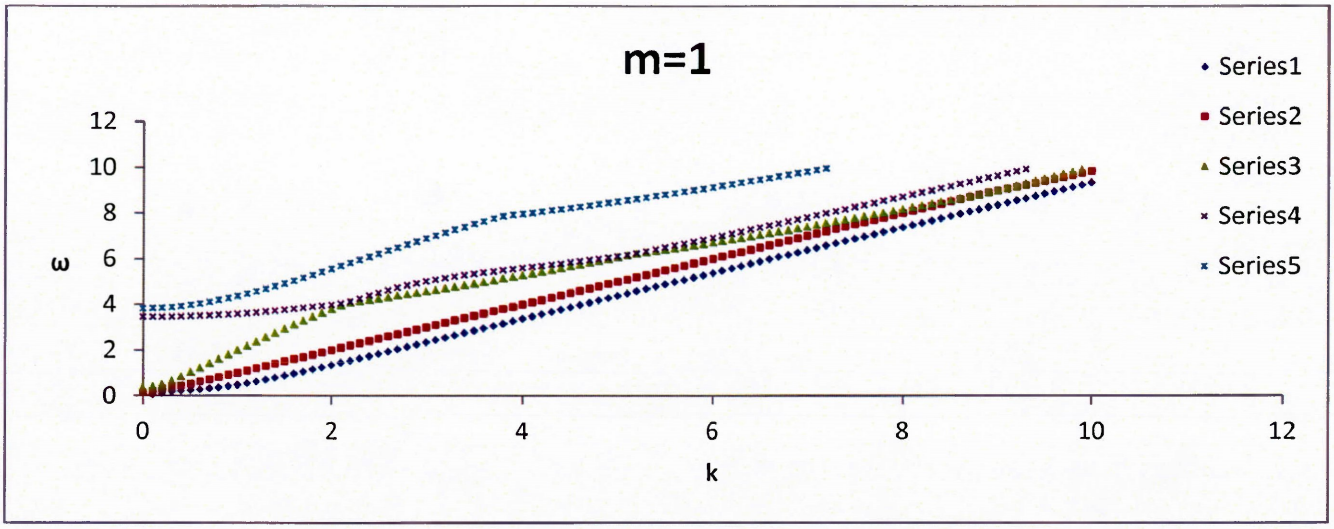

Figure 33(b): ω-k Relationship for *m=1* (Thin cylinder with open-circuit case).

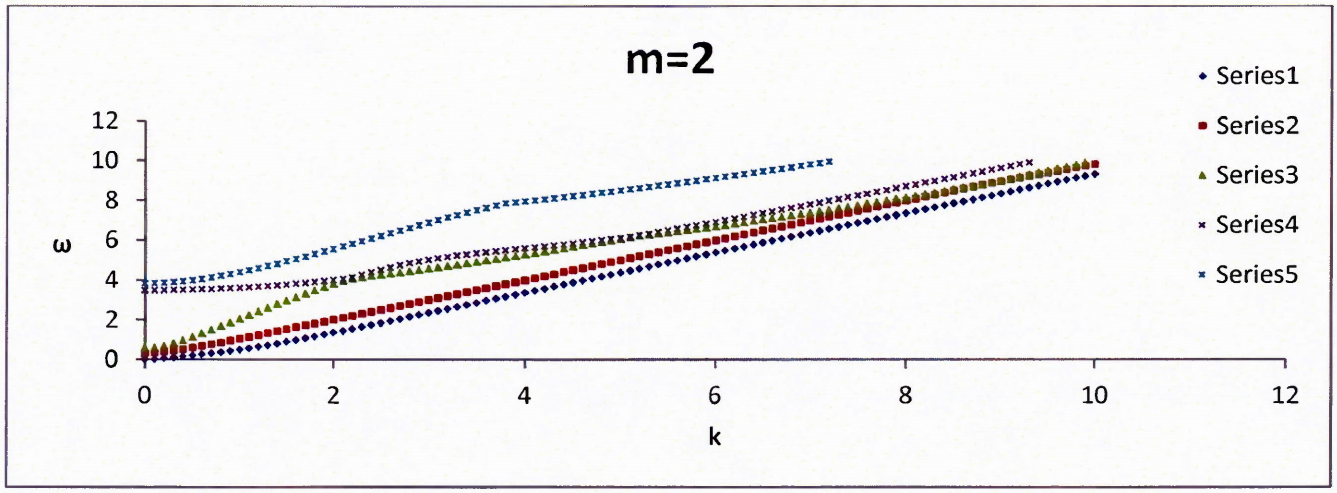

Figure 33(c): ω-k Relationship for *m=2* (Thin cylinder with open-circuit case).

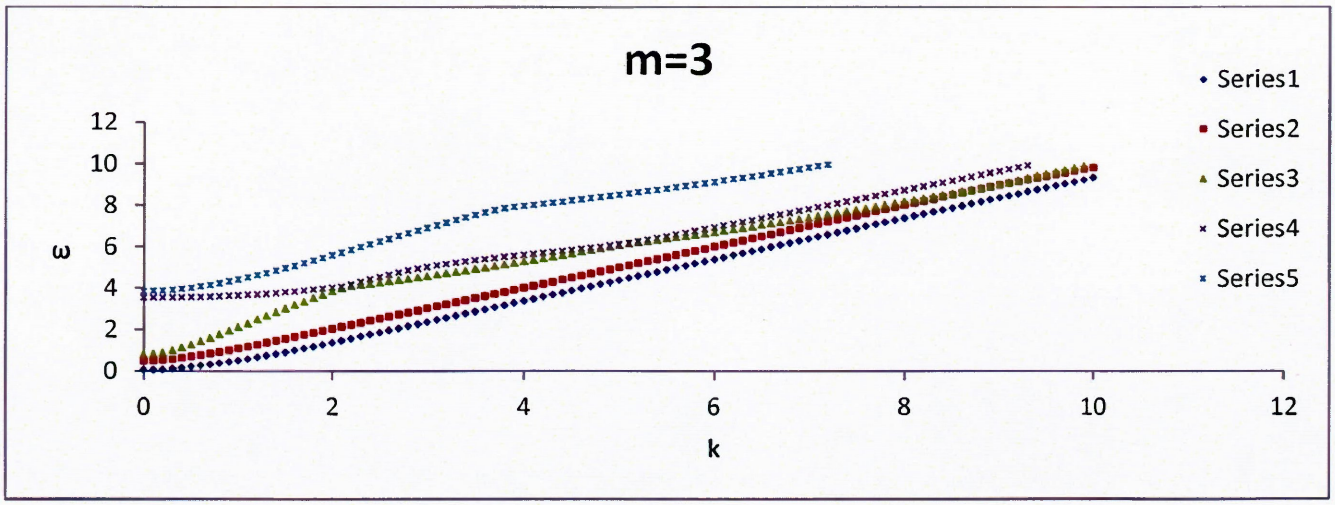

Figure 33(d): ω-k Relationship for *m=3* (Thin cylinder with open-circuit case).

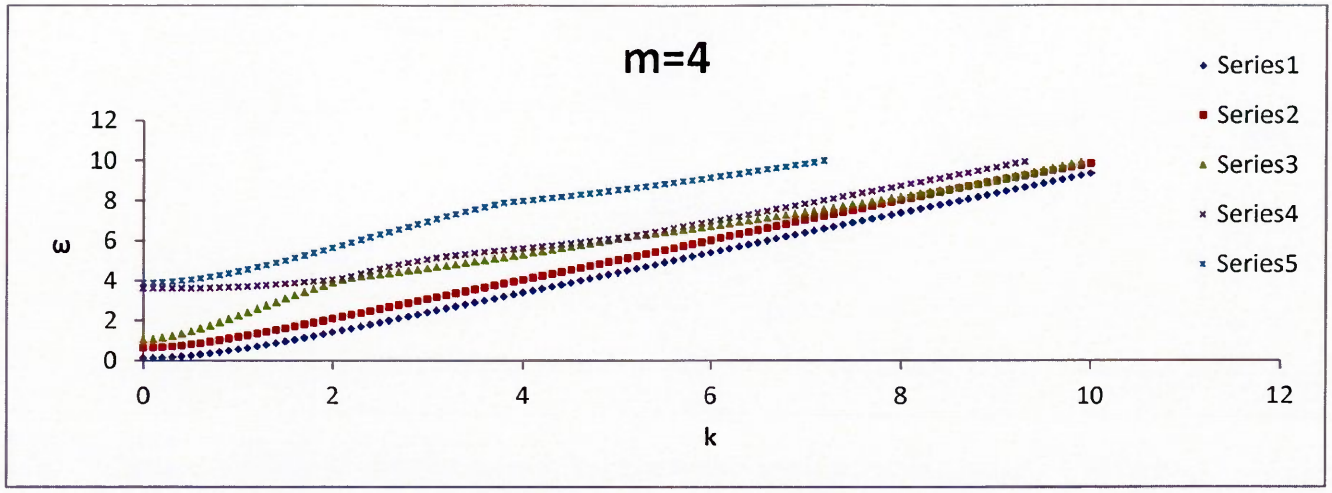

Figure 33(e): ω-k Relationship for *m=4* (Thin cylinder with open-circuit case).

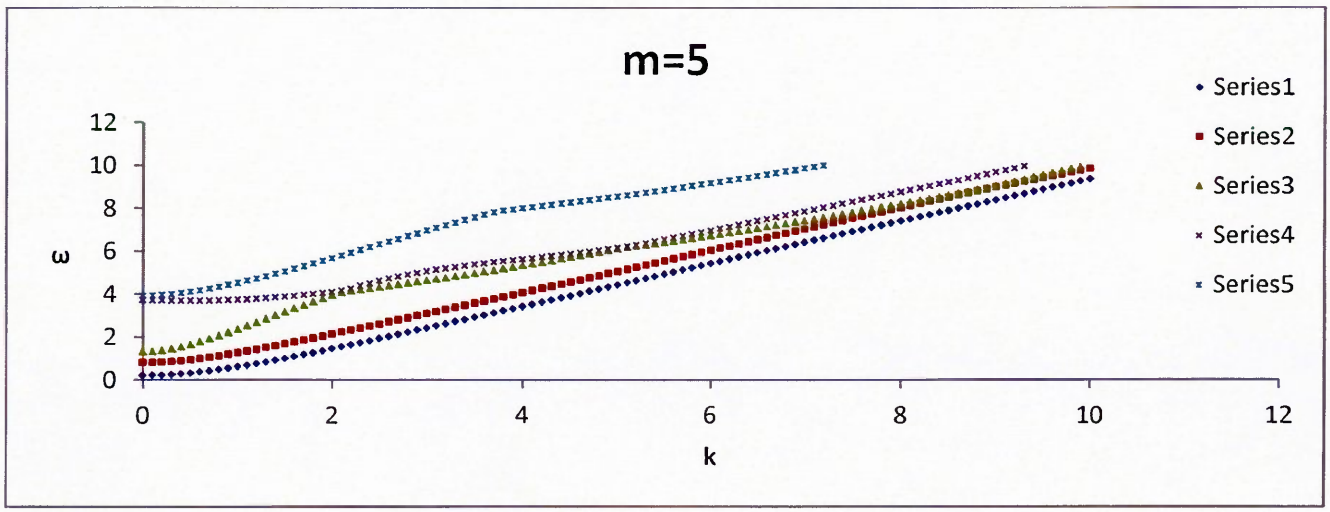

Figure 33(f): ω-k Relationship for *m=5* (Thin cylinder with open-circuit case).

Figures 33(a)-33(f) (thin cylinder open-circuit case) show that as *m* increases the modes seem not change drastically. Also, a very minimum change is observed for all the propagating modes. The scale and size of the graphs are identical to each other in order to be able to look at the difference from *m*=0 to *m*=5 it is more useful to observe the numbers presented in Table 1.

Modes one and two are almost non-dispersive for all values of $k>1.8$. Modes three, four and five are almost non-dispersive at values of $k>4$. The ranges of dispersive behavior do not change as *m* increases. Therefore, the dispersive behaviors of Figure 33(a-f) are essentially independent of the circumferential wave number *m*.

In the thin cylinder open-circuit case the effect of changing m is hardly observed on the wave spectra. This is different when compared to the previous case (thick cylinder open-circuit case) which the effect of changing m can clearly be observed on the wave spectra.

Table 1: Thin cylinder with open-circuit boundary condition. (Comparison m=0 to m=5)

	m=0	m=1	m=2	m=3	m=4	m=5
ω	k	k	k	k	k	k
3	2.348242	2.351590	2.361622	2.378303	2.401569	2.431332
3.1	2.450045	2.453299	2.463048	2.479258	2.501870	2.530800
3.2	2.551940	2.555103	2.564581	2.580343	2.602330	2.630465
3.3	2.653894	2.656971	2.666191	2.681524	2.702915	2.730291
3.4	2.755881	2.758876	2.767850	2.782773	2.803596	2.830247
3.5	2.857881	2.860797	2.869535	2.884068	2.904347	2.930307
3.6	2.959873	2.962714	2.971228	2.985387	3.005147	3.030446
3.7	3.061843	3.064612	3.072910	3.086713	3.105977	3.130644
3.8	3.163776	3.166477	3.174570	3.188031	3.206821	3.230884
3.9	3.265663	3.268297	3.276193	3.289329	3.307665	3.331150
4	3.367492	3.370064	3.377772	3.390595	3.408497	3.431429
4.1	3.469257	3.471768	3.479296	3.491820	3.509307	3.531708
4.2	3.570951	3.573405	3.580760	3.592998	3.610086	3.631979

The ω-m relationships presented in Figures 34(a)-34(f) have a very distinct behavior when compared with the previous ω-m relationships (thick open and thin open). In particular, Figure 34(a) shows wave spectra for k=0. The first five propagating wave modes are in two different groups: the first three modes have small cut-off frequency and the other two's cut-off frequencies are larger than 3.5. The gap between the mentioned modes appears to be getting smaller as k increases. The modes start out in a linear behavior (k=0) and shift toward an almost straight line (k=5).

As k increases, the frequency of each wave mode has lesser variation with the circumferential wave number as shown in the Figures 34(a)-34(f). This suggests that the wave modes show an almost non-dispersive nature in the circumferential direction. As k increases the ω-m relationship becomes non-dispersive and therefore independent of m.

Modes one, two and three are almost non-dispersive for all values of m for non-zero k. Also, when k increases these modes are still almost non-dispersive. Modes 4 and 5 are almost non-

dispersive for all values of m. As k increases modes 4 and 5 become almost a straight line indicating almost zero group velocity especially at very small values of m.

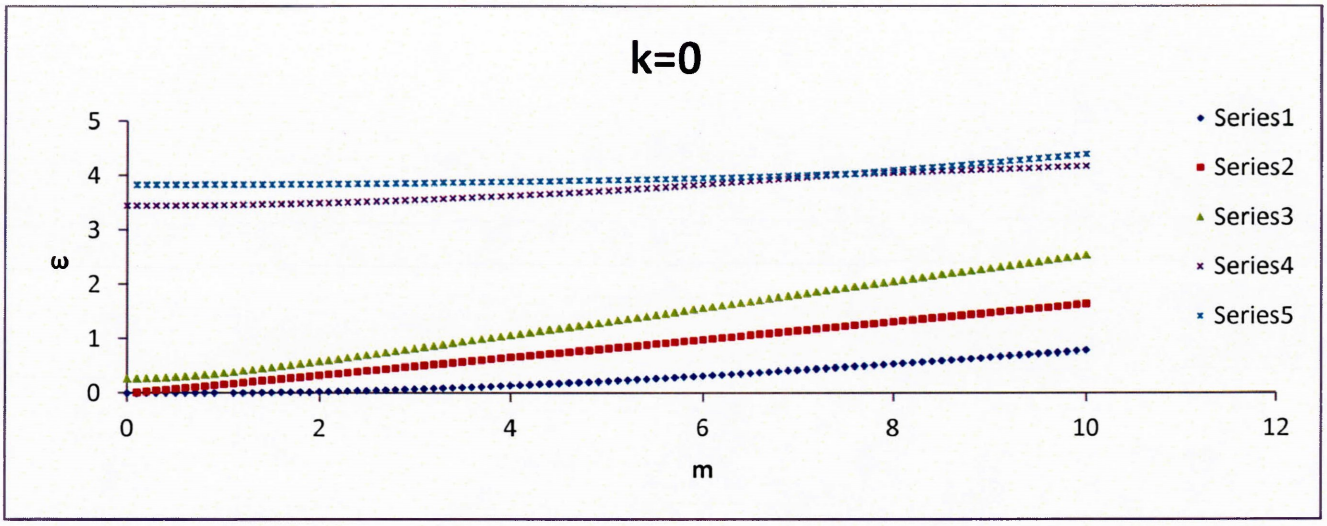

Figure 34(a): ω-m Relationship for *k=0* (Thin cylinder with open-circuit case).

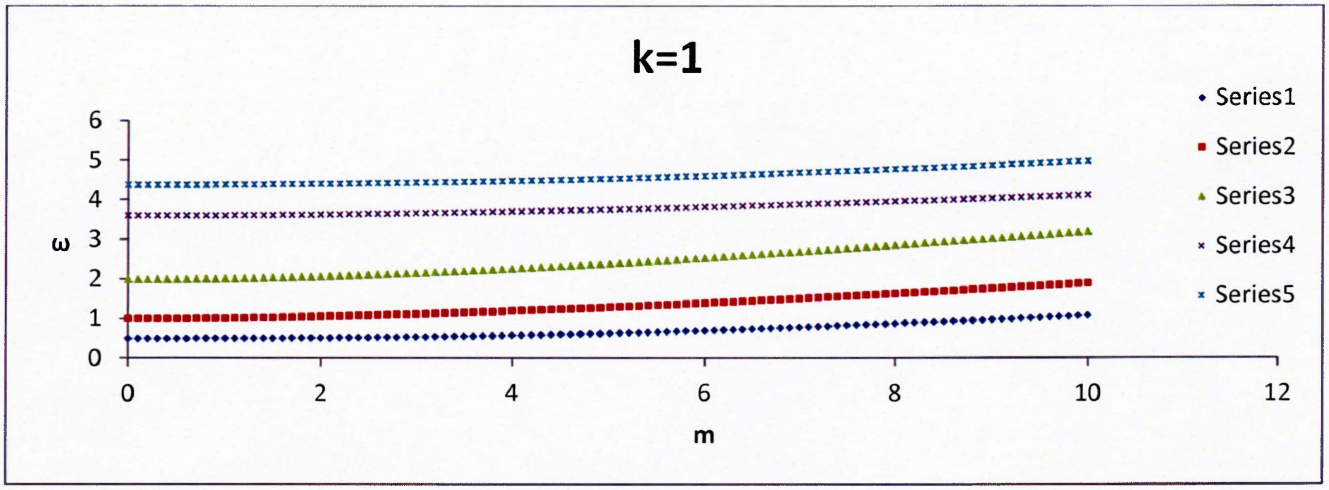

Figure 34(b): ω-m Relationship for *k=1* (Thin cylinder with open-circuit case).

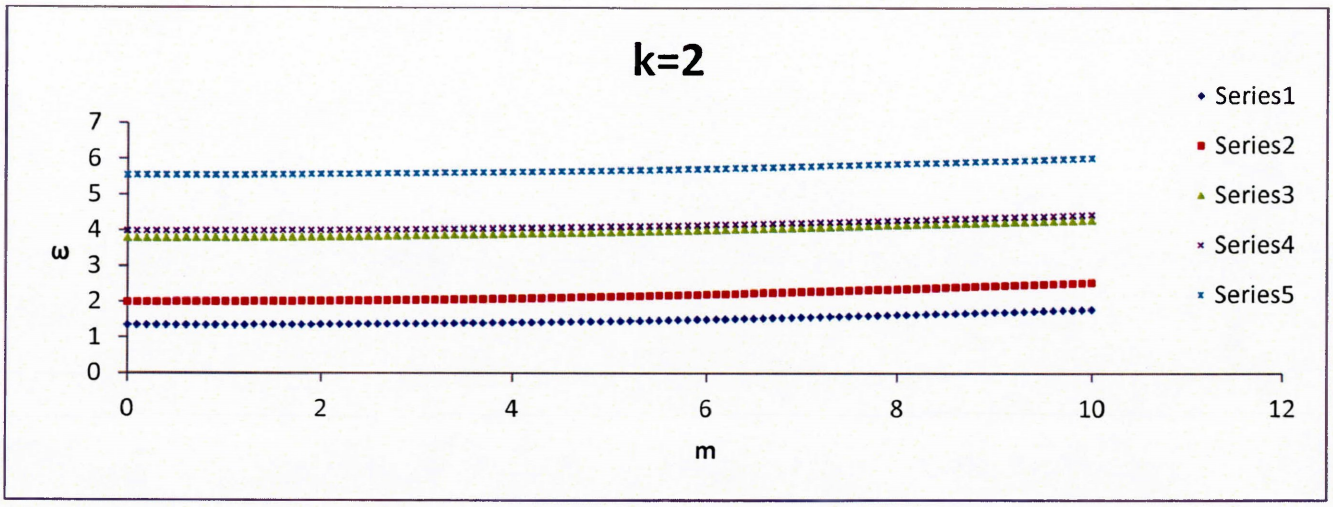

Figure 34(c): ω-m Relationship for *k=2* (Thin cylinder with open-circuit case).

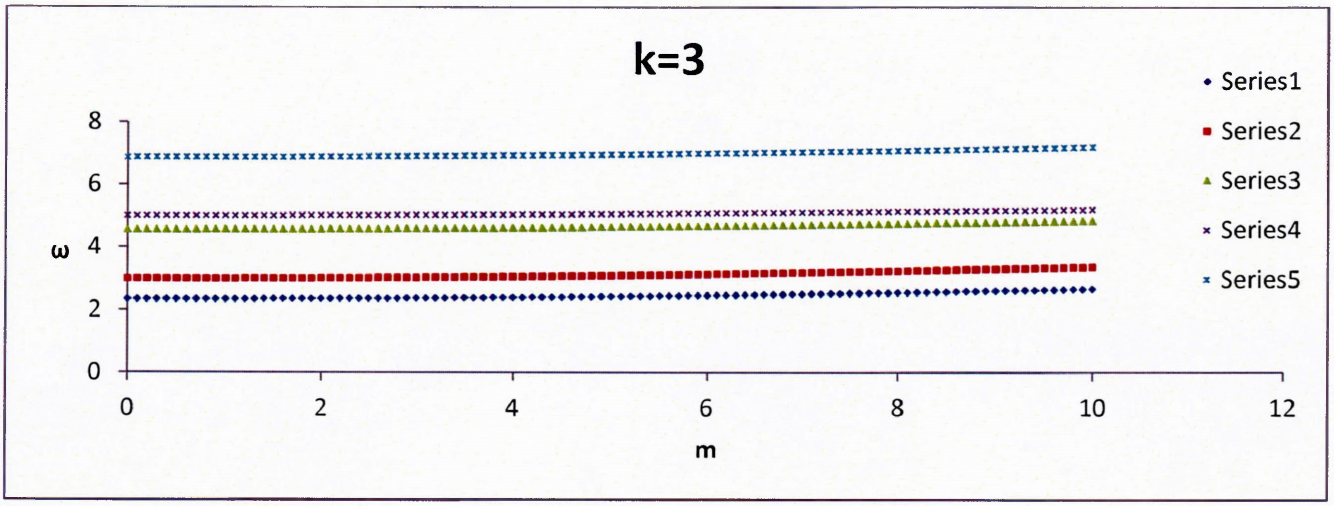

Figure 34(d): ω-m Relationship for *k=3* (Thin cylinder with open-circuit case).

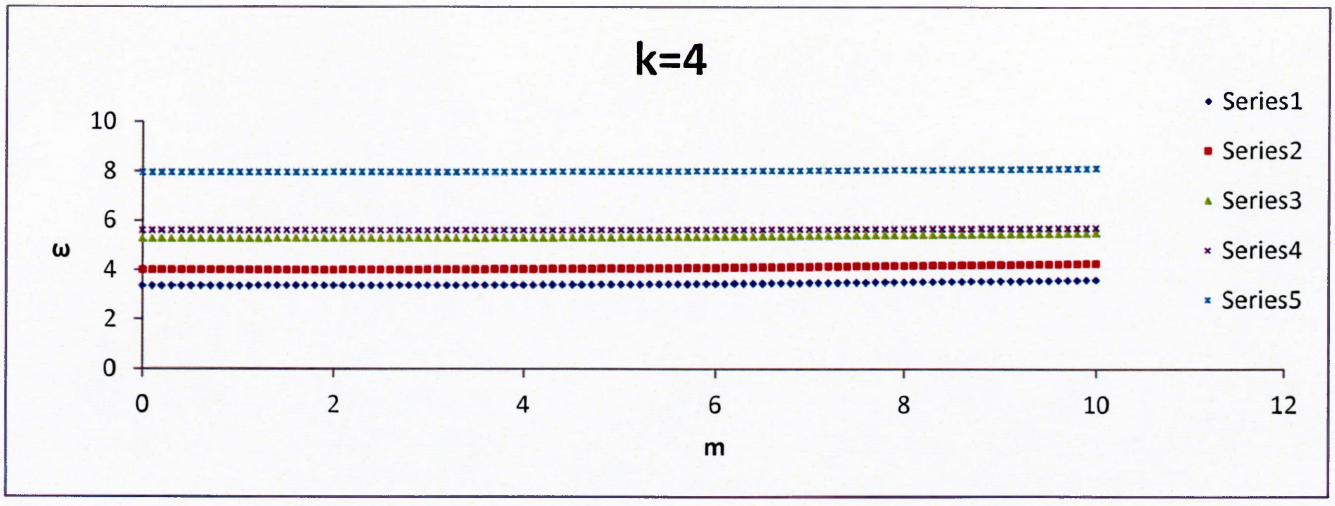

Figure 34(e): ω-m Relationship for *k=4* (Thin cylinder with open-circuit case).

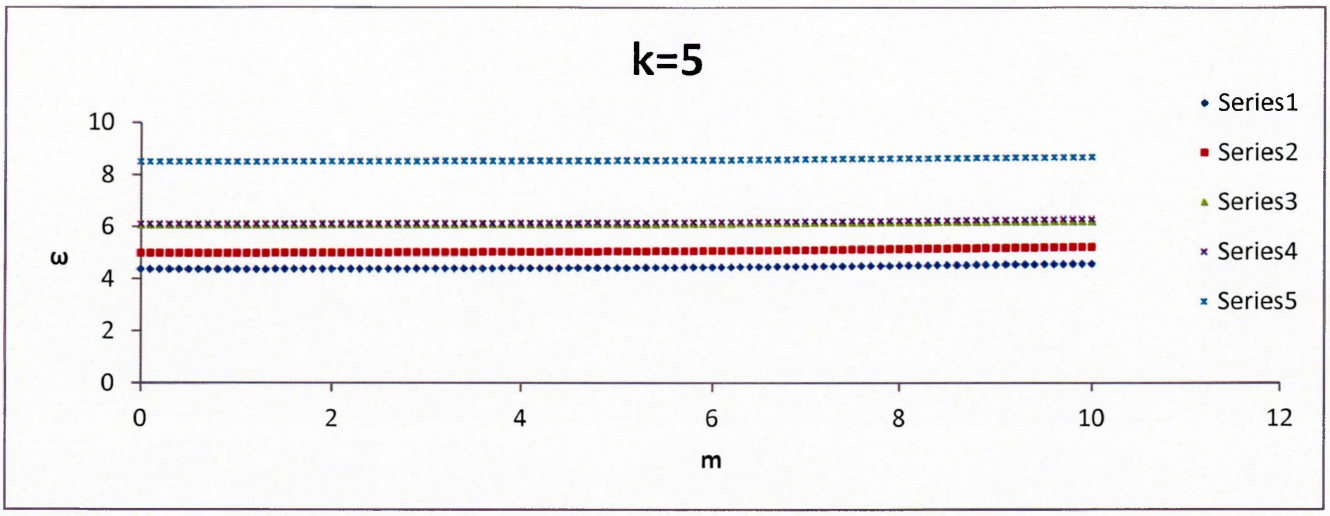

Figure 34(f): ω-m Relationship for *k=5* (Thin cylinder with open-circuit case).

3.5.5 A Thin Cylinder with Closed-Circuit Electric Boundary Conditions

A hollow homogeneous PZT-4 cylinder with r_i=6.9704 and r_o=7.9604 is subjected to traction free and closed circuit boundary conditions both at the inner and outer surface.

When comparing this case (closed-circuit case) to the previous case (open-circuit case) they are almost identical especially at lower order modes. The cut-off frequency of modes three and four (Figures 37 and 38) change slightly when compared with the previous example. Here, the electrical boundary conditions have a very minimum effect on the wave spectra. All previous observations that were made can be applied to these figures (Figures 35-38).

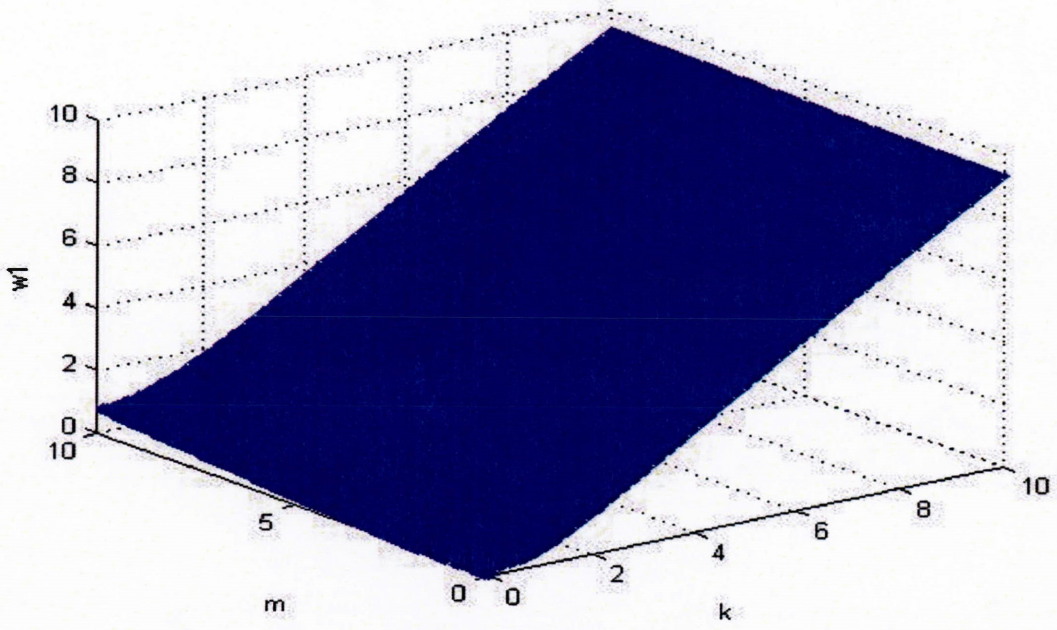

Figure 35: Thin cylinder with closed-circuit boundary condition. (3-D surface first propagating mode).

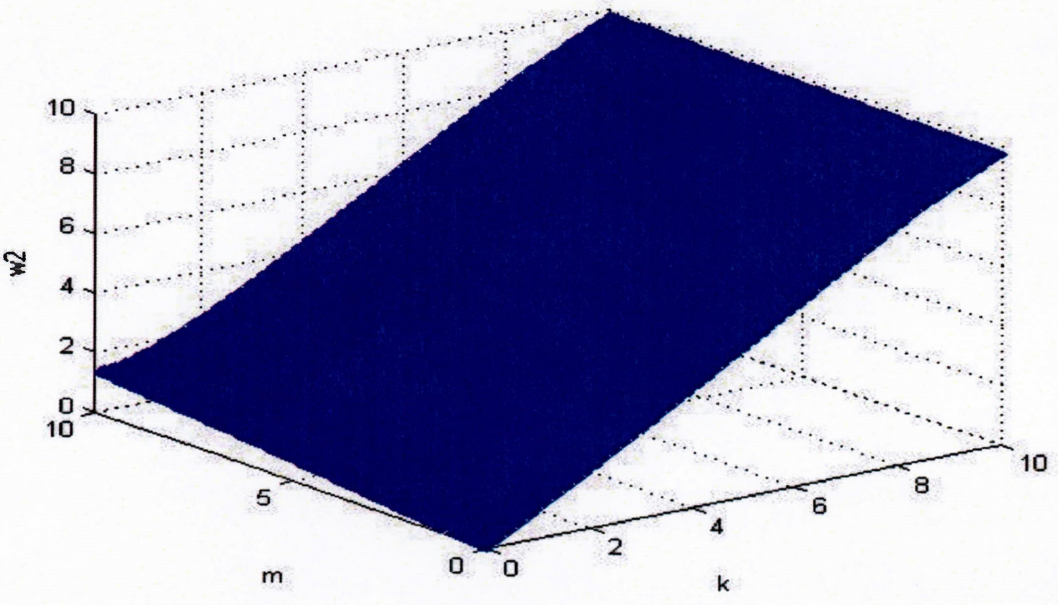

Figure 36: Thin cylinder with closed-circuit boundary condition. (3-D surface second propagating mode).

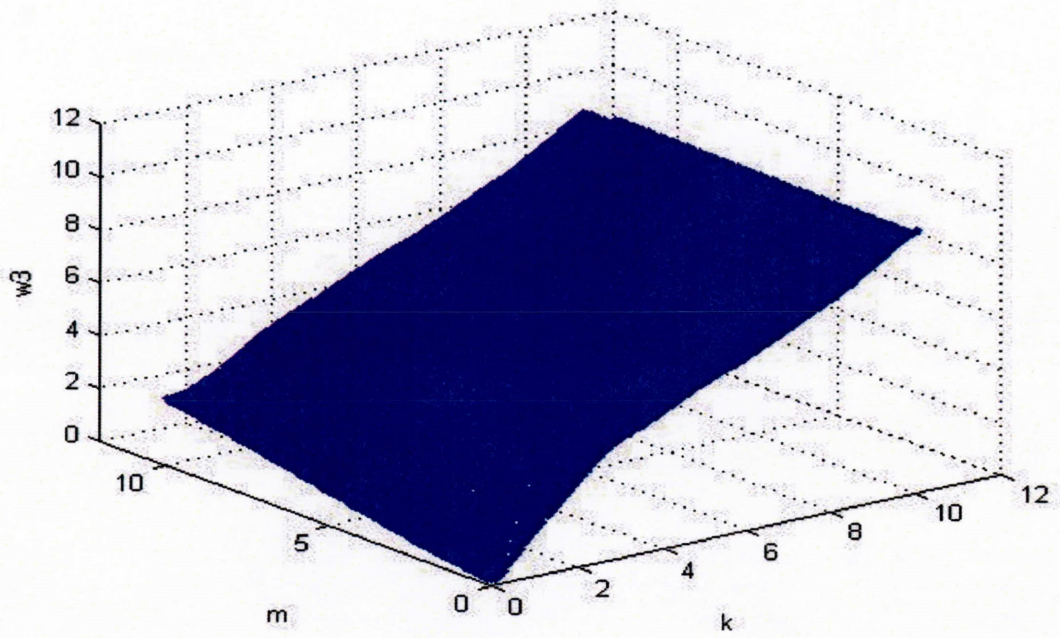

Figure 36: Thin cylinder with closed-circuit boundary condition. (3-D surface third propagating mode).

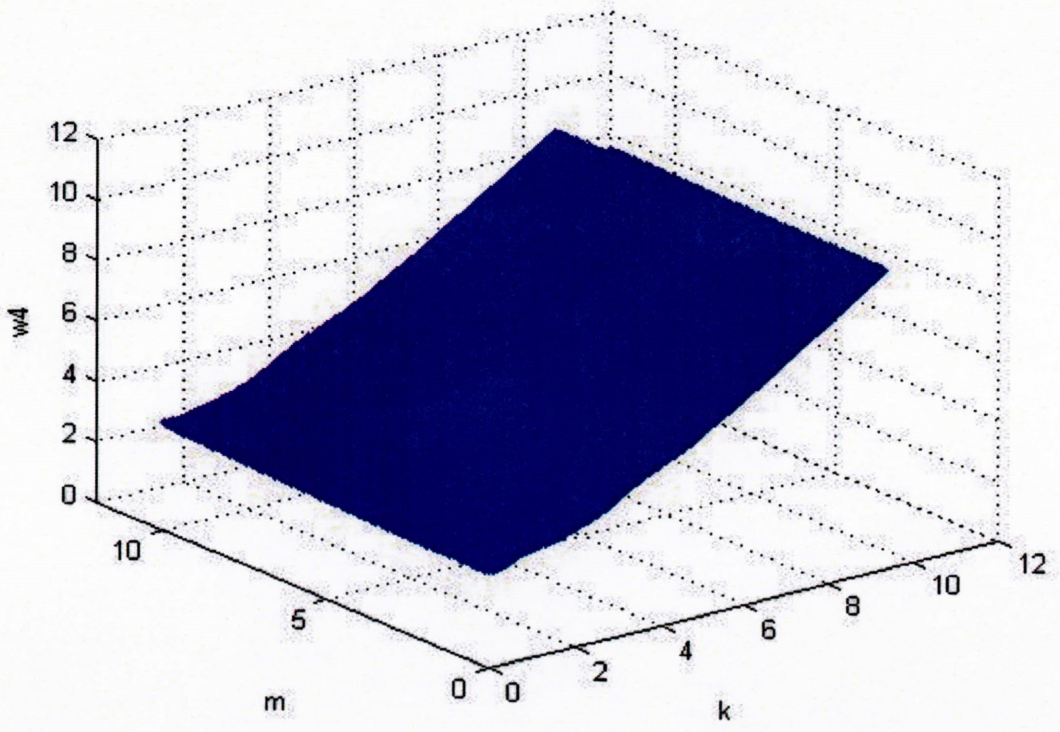

Figure 37: Thin cylinder with closed-circuit boundary condition. (3-D surface fourth propagating mode).

When analyzing this case (thin closed circuit cylinder) it can be seen that as m increases the trends do not change. This behavior is similar to the case of the thin open cylinder; this clearly states that the wave spectrum is essentially independent of m.

The electrical boundary conditions seem to have a minimum effect on the wave spectra (ω-k relationships) since both open and closed circuit cases have similar graphs if not identical. The only effect is seen on the higher order modes but this effect is minimal

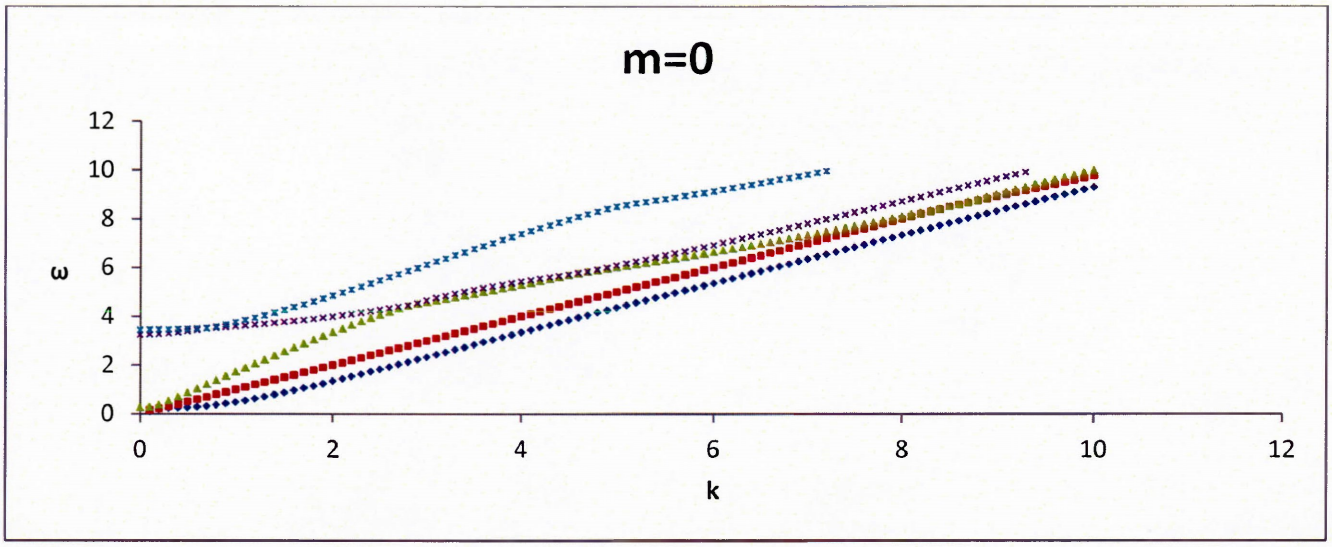

Figure 38(a): ω-k Relationship for *m=0* (Thin cylinder with closed-circuit case).

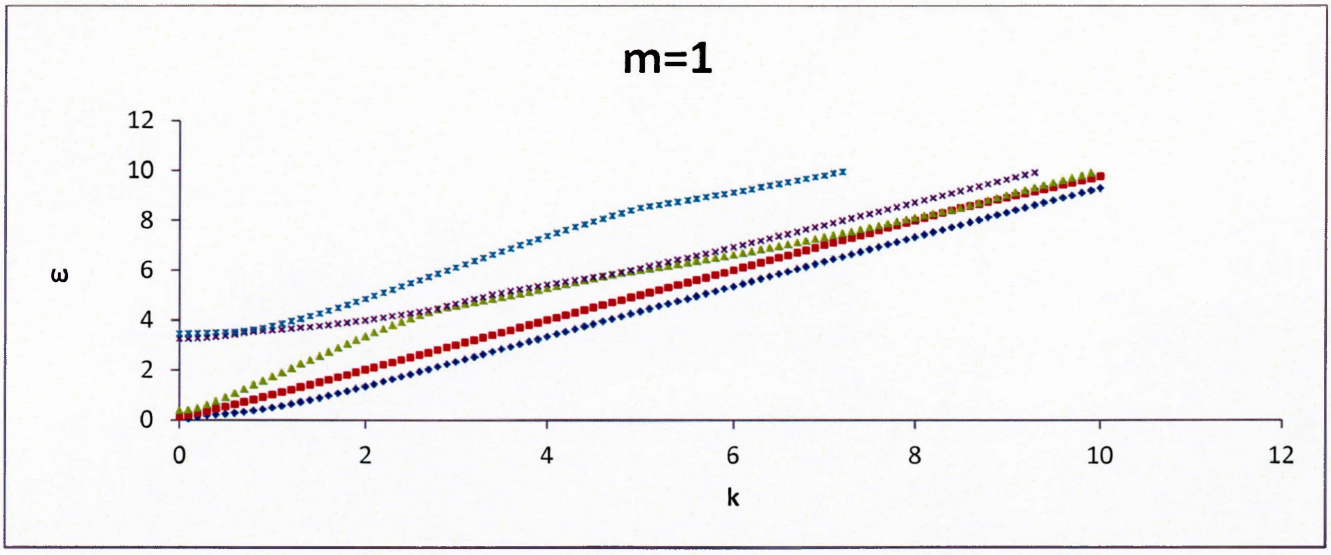

Figure 38(b): ω-k Relationship for *m=1* (Thin cylinder with closed-circuit case).

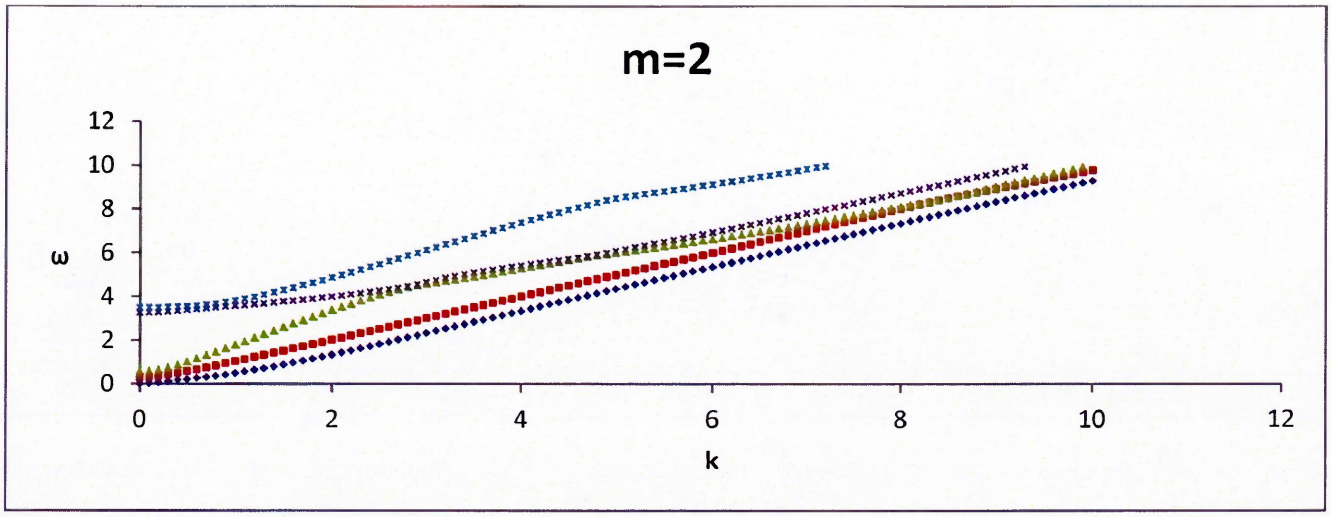

Figure 38(c): ω-k Relationship for *m=2* (Thin cylinder with closed-circuit case).

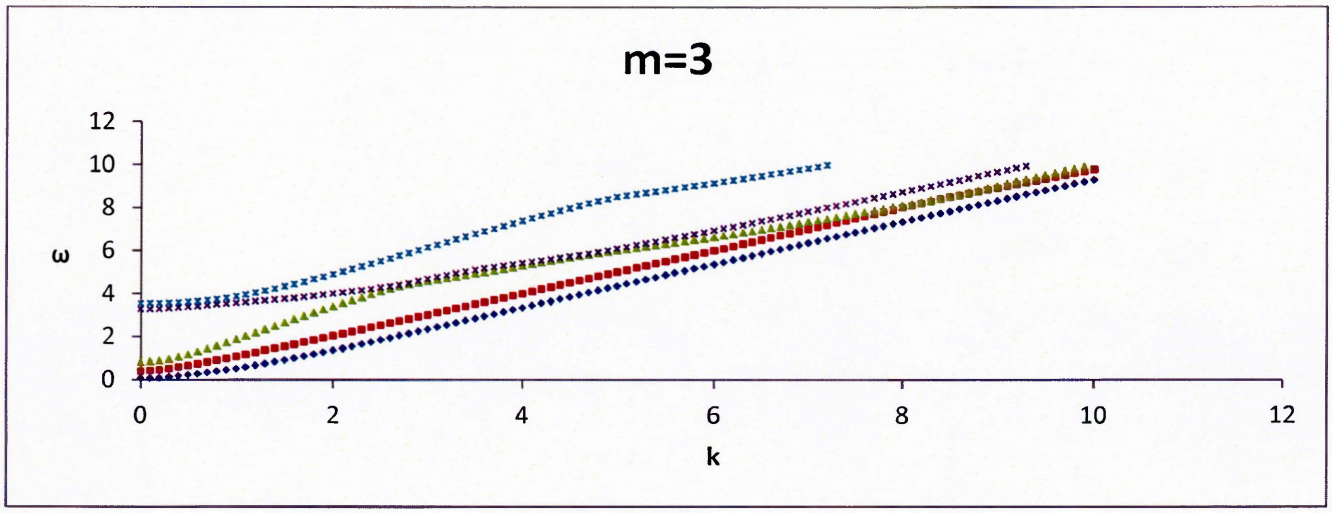

Figure 38(d): ω-k Relationship for *m=3* (Thin cylinder with closed-circuit case).

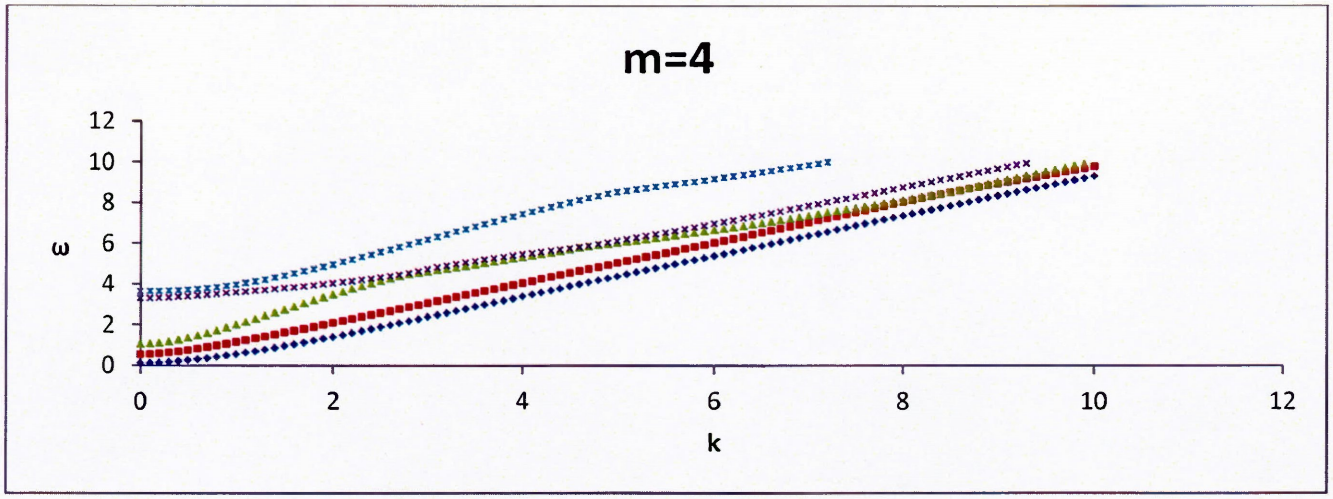

Figure 38(e): ω-k Relationship for *m=4* (Thin cylinder with closed-circuit case).

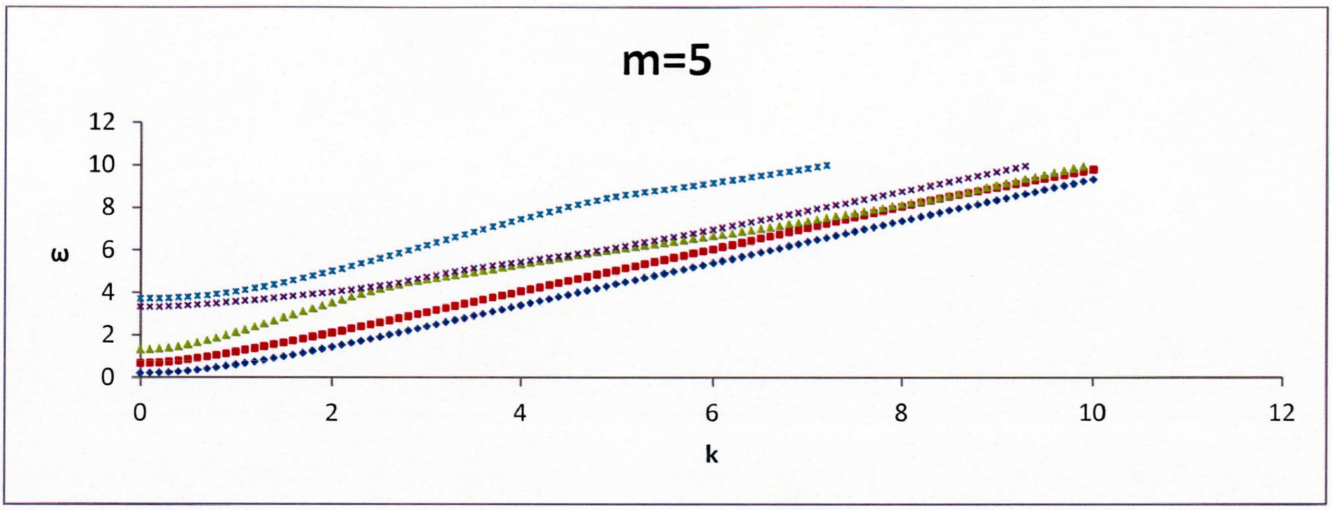

Figure 38(f): ω-k Relationship for *m=5* (Thin cylinder with closed-circuit case).

Figures 38(a-f) and 39(a-f), show the results for the thin closed circuit case. The behavior is similar as with the thin open circuit case.

When comparing thin and thick cylinders there exists a major difference between the presented waves spectra due mainly to geometry change. But when comparing closed and open circuit boundary conditions there are many similarities. Also when comparing the behavior of the thick (open or closed-circuit case) to the behavior of the thin (open or closed) the behavior is very different either when *m* is increasing or when *k* is increasing (*ω-m* relationship and *ω-k* relationship).

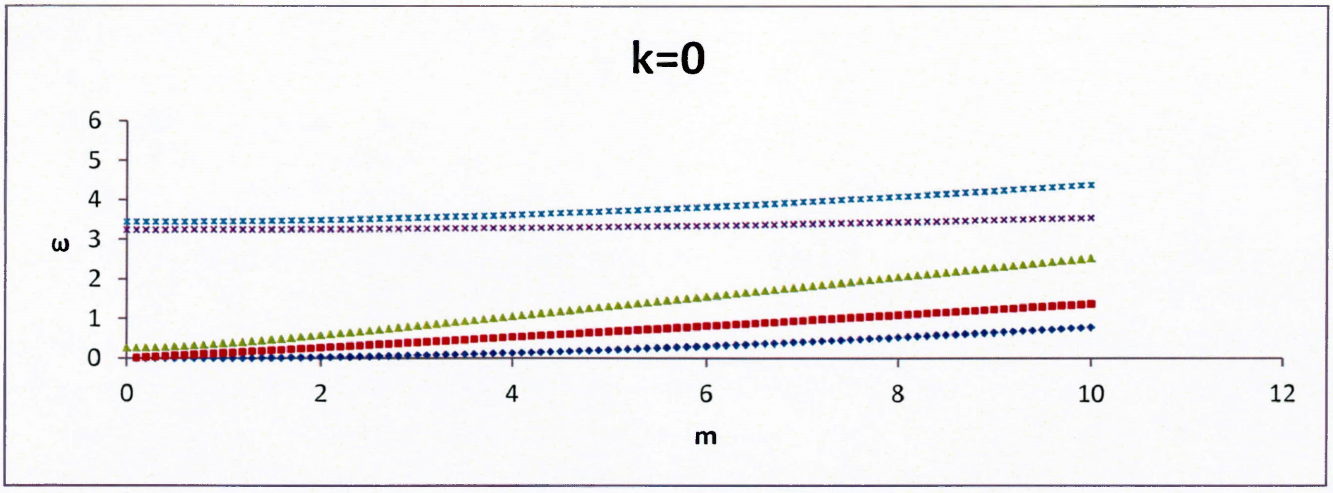

Figure 39(a): ω-k Relationship for *k=0* (Thin cylinder with closed-circuit case).

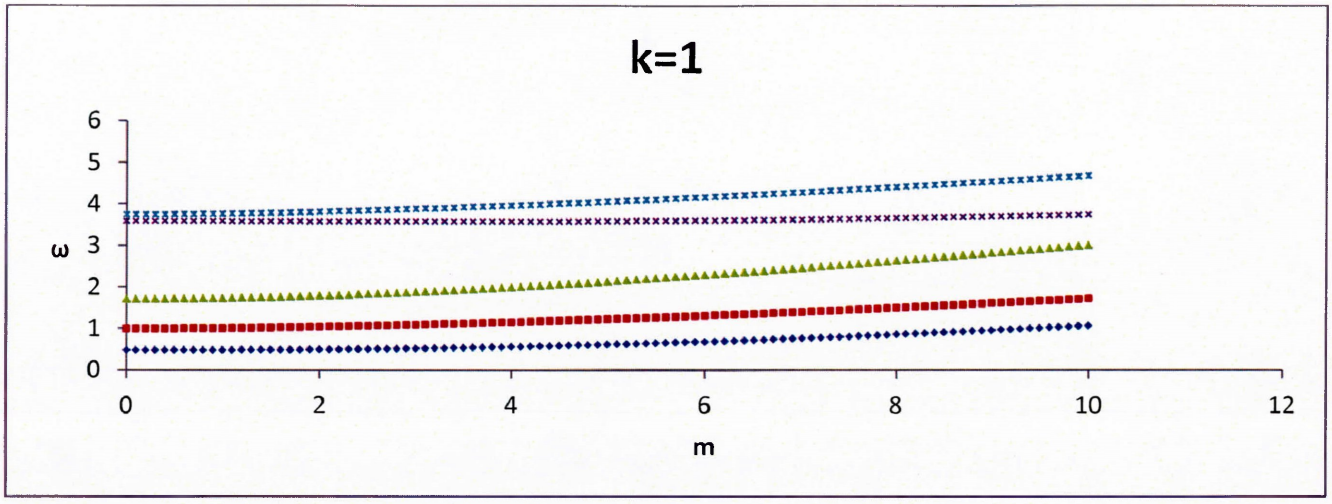

Figure 39(b): ω-k Relationship for *k=1* (Thin cylinder with closed-circuit case).

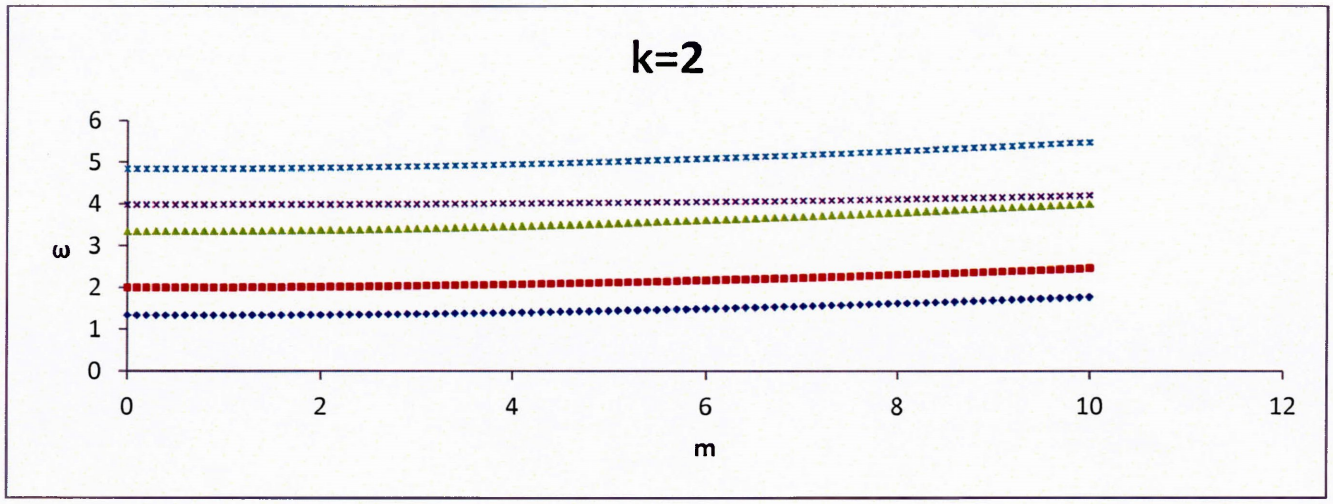

Figure 39(c): ω-k Relationship for *k=2* (Thin cylinder with closed-circuit case).

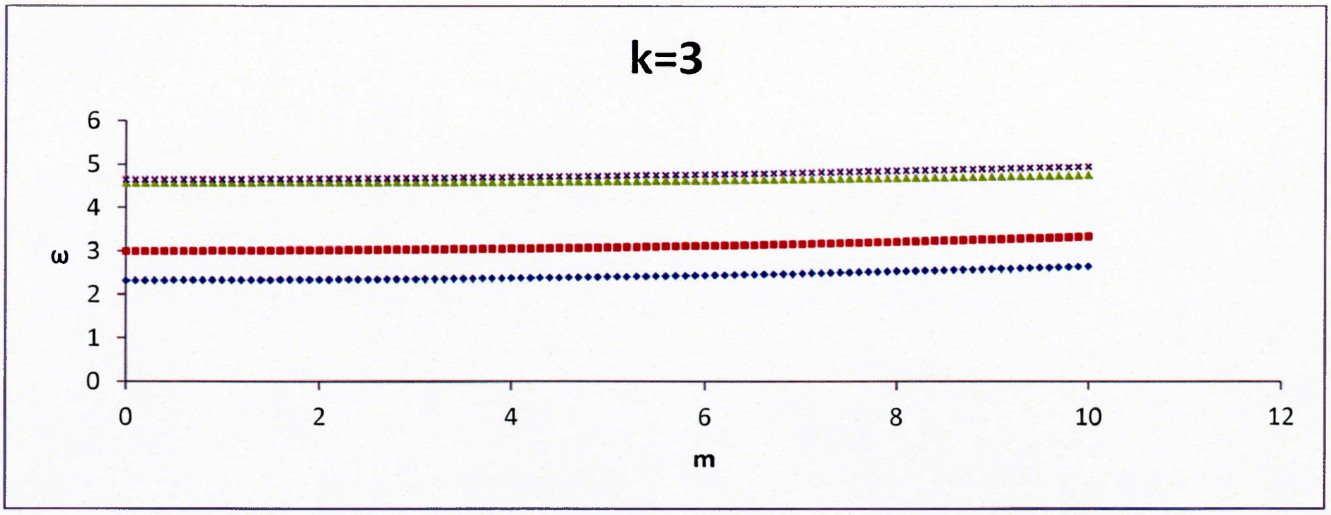

Figure 39(d): ω-k Relationship for *k=3* (Thin cylinder with closed-circuit case).

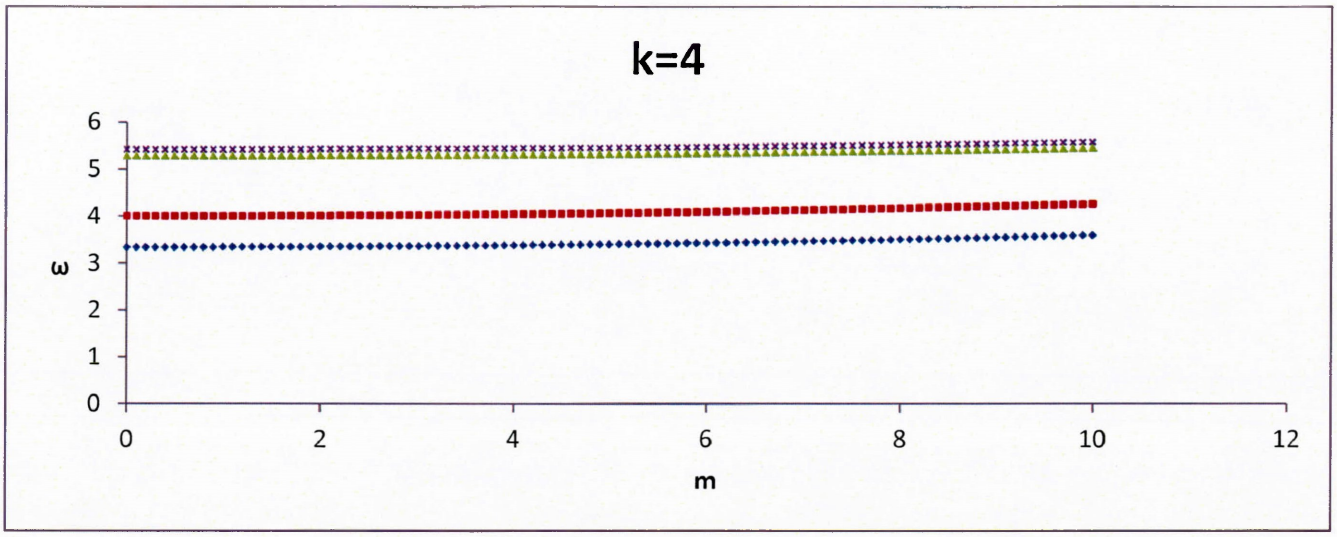

Figure 39(e): ω-k Relationship *k=4* (Thin cylinder with closed-circuit case).

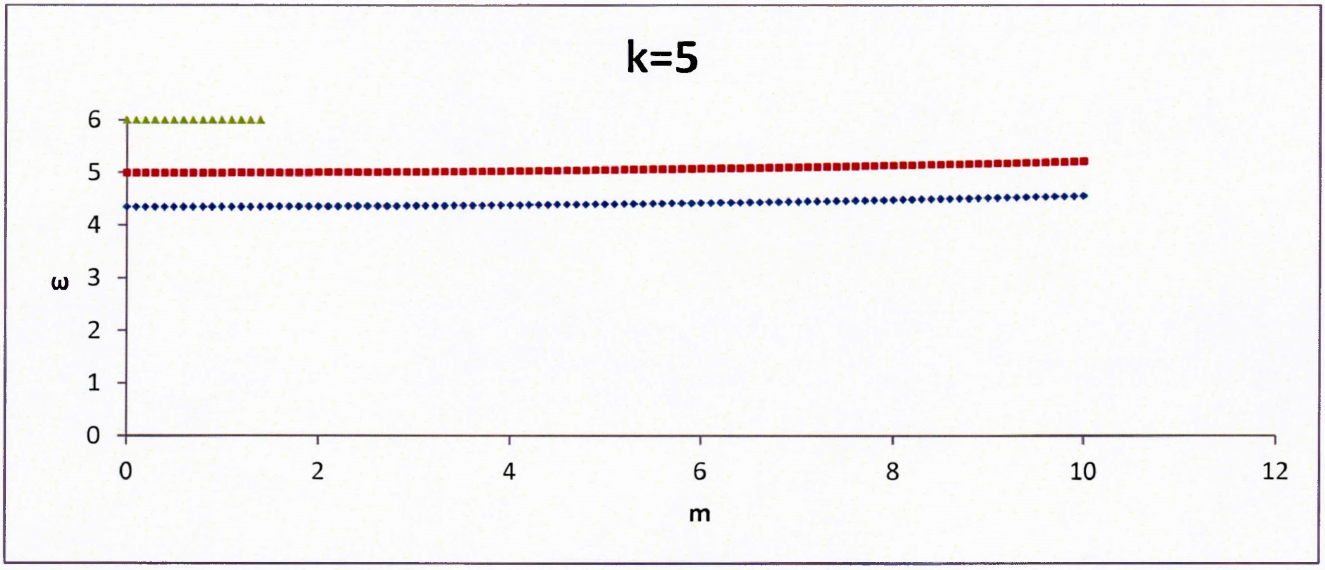

Figure 39(f): ω-k Relationship for *k=5* (Thin cylinder with closed-circuit case).

3.5.6 Wave Propagation along a Specified Direction (Thick Cylinder)

To better understand the 3D wave spectra, the wave spectra for different ratio of k/m are presented. They are the spectra for wave propagating in a direction inclined to the symmetrical axis of the cylinder.

Figures 40 (a-e) show the wave in a thick cylinder with open-circuit boundary condition. Three different ratios are studied here; namely k/m=0.5, k/m=1 and k/m=2, respectively.

For comparison purposes, the results for m=0 and k=0 are reproduced here and they are corresponding to the k/m=∞ and the case k/m=0 (Figures 40(a-e)).

Figures 40(a) and 40(b) are very similar in there trends since the ratio of k/m has changed from 0 to 0.5. The first mode shows a nice almost non-dispersive nature in a large range of k>1.8. The second and third modes show an almost non-dispersive behavior for values of k>1.8. The fourth and fifth modes are almost non-dispersive for values of k>3. When observing Figures 40(a-e), we can see that all the propagating modes have the same cut-off frequency. It is also noted that back-ward wave of the first mode exists only for small ratio of k/m.

The similarity among those wave spectra suggests that the spiral wave is not sensitive to its propagating direction.

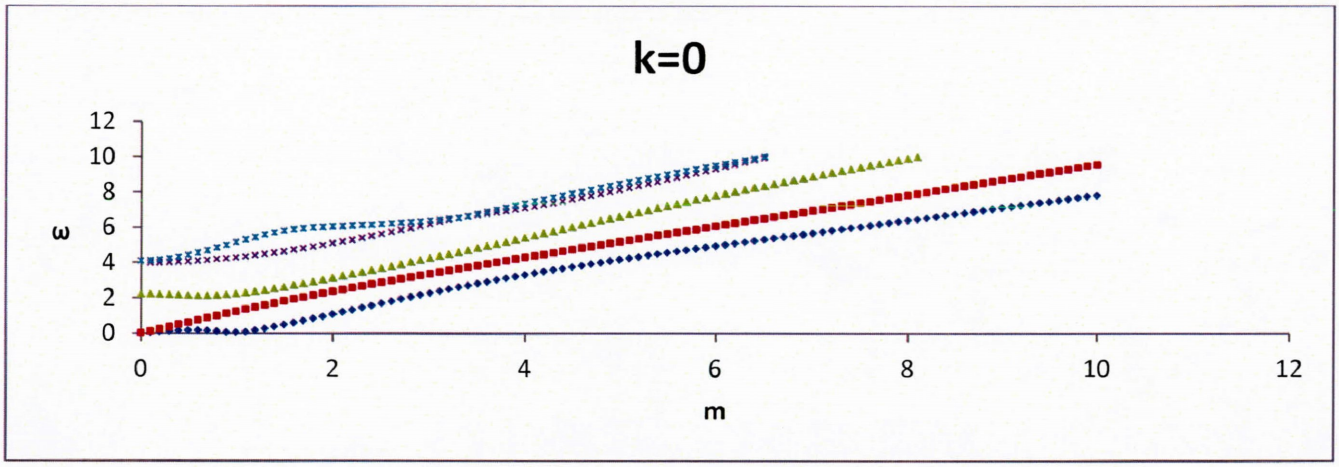

Figure 40(a): Thick cylinder with open-circuit boundary conditions (k=0).

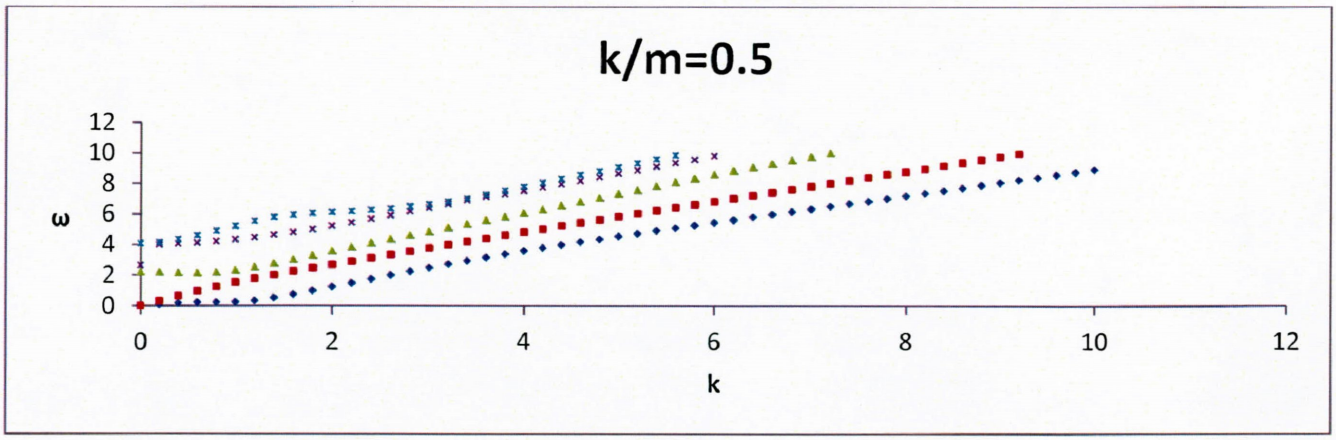

Figure 40(b): Thick cylinder with open-circuit boundary conditions (k/m=0.5).

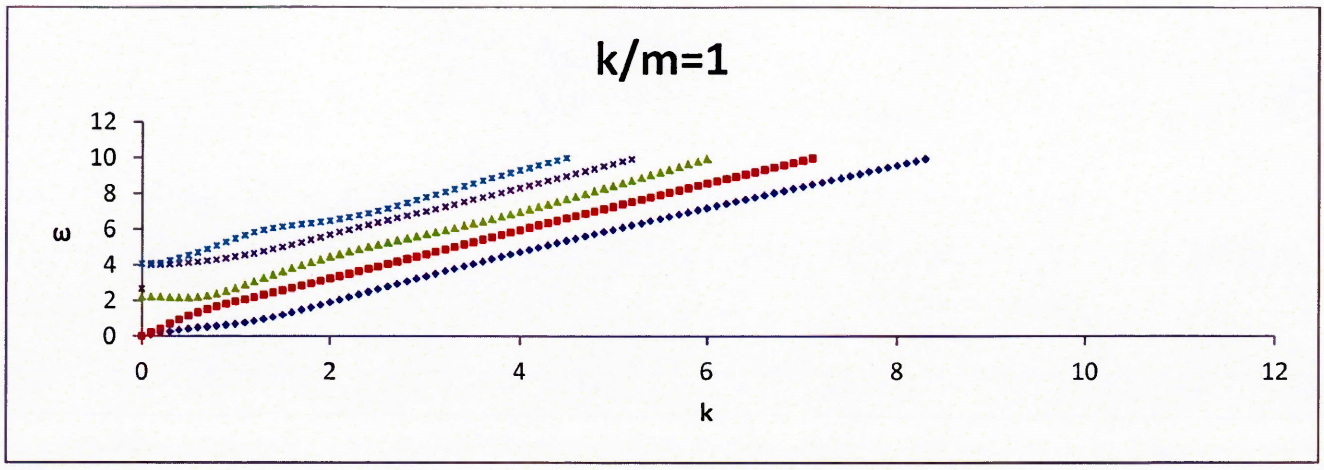

Figure 40(c): Thick cylinder with open-circuit boundary conditions (k/m=1).

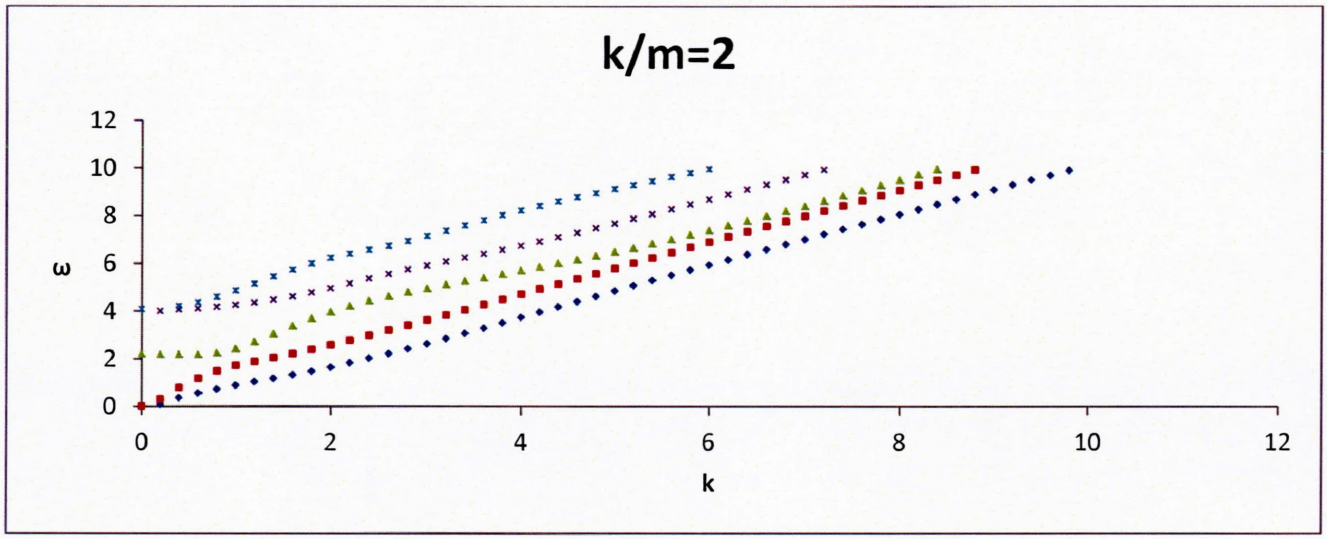

Figure 40(d): Thick cylinder with open-circuit boundary conditions (k/m=2).

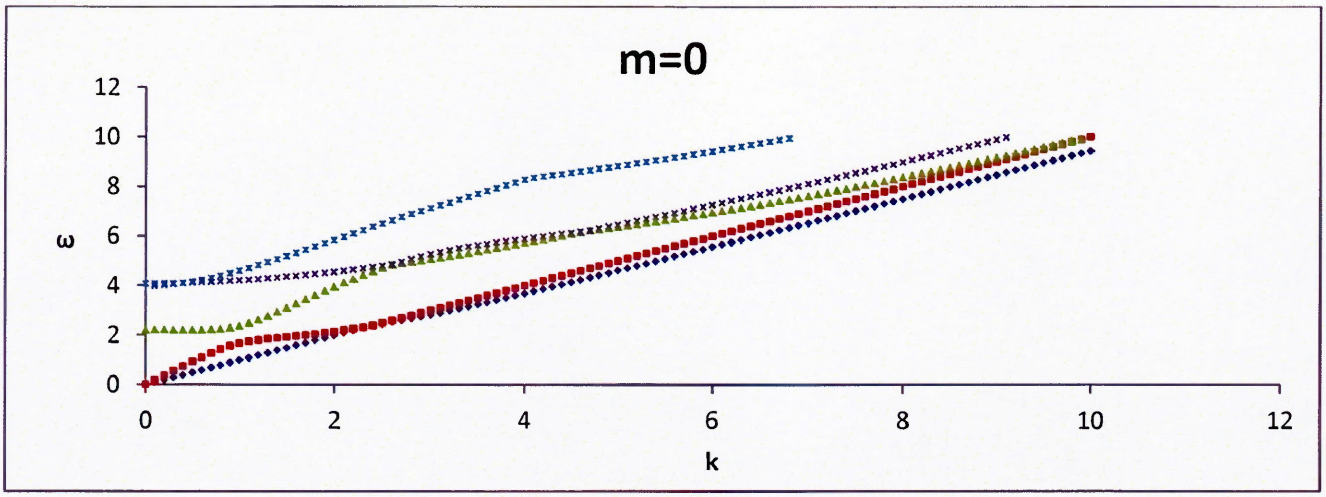

Figure 40(e): Thick cylinder with open-circuit boundary conditions (m=0).

3.5.7 Wave Propagation along a Specified Direction (Thin Cylinder)

Figures 41(a)-41(e) illustrate how the wave spectra changes when the ratio of k/m changes from 0.5 to 1 to 2 for a thin cylinder with open-circuit boundary conditions. The results for k=0 and m=0 are reproduced for comparison purpose.

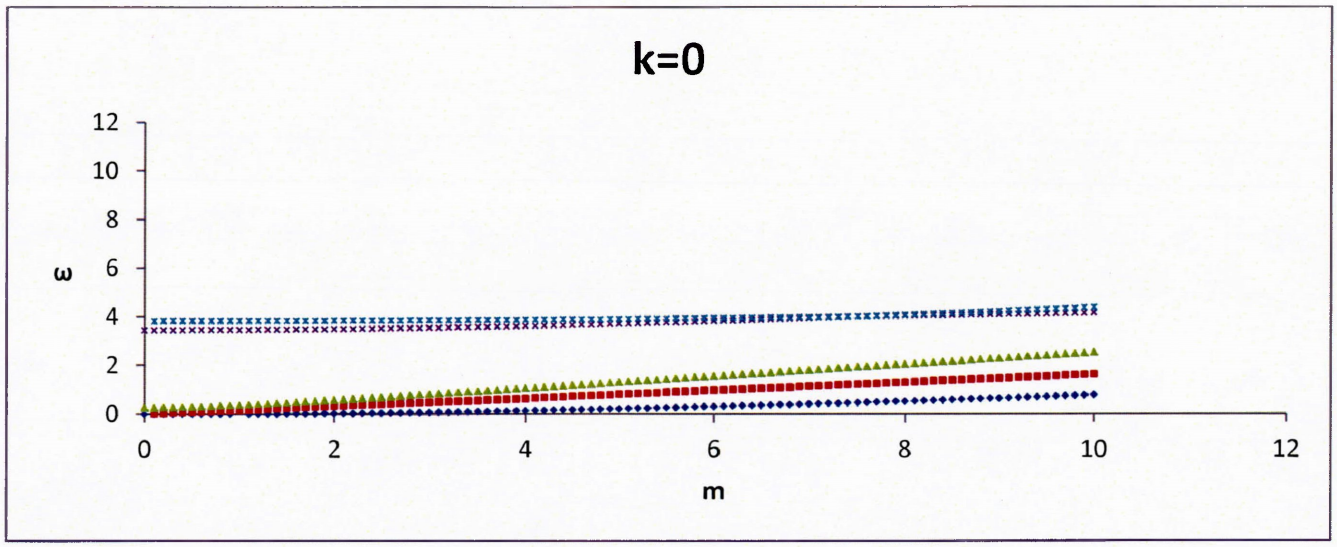

Figure 41(a): Thin cylinder with open-circuit boundary conditions (k=0).

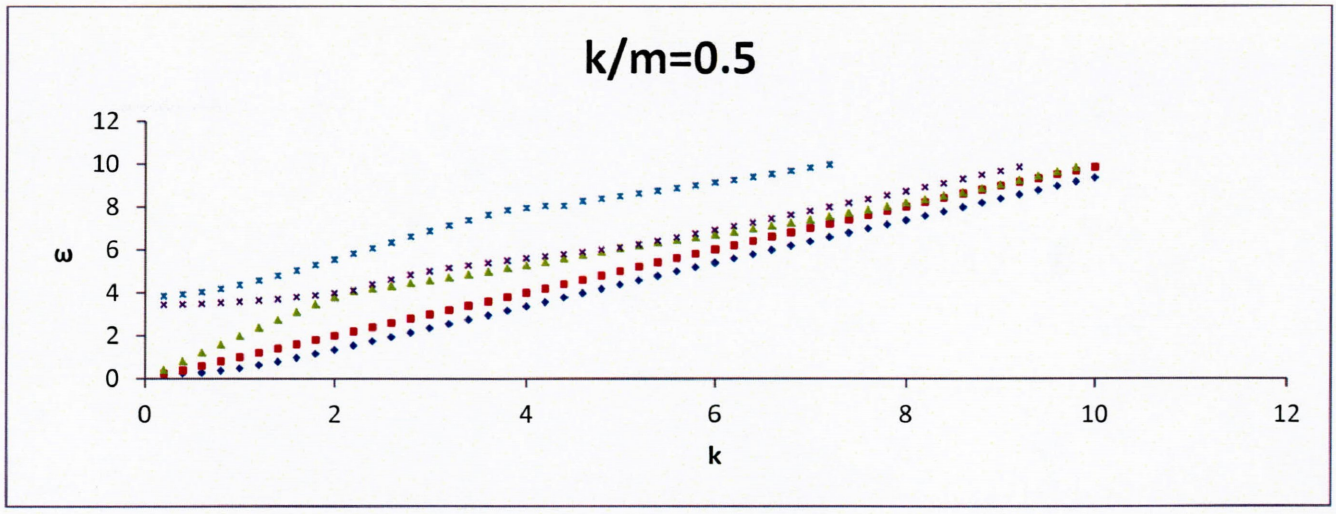

Figure 41(b): Thin cylinder with open-circuit boundary conditions (k/m=0.5).

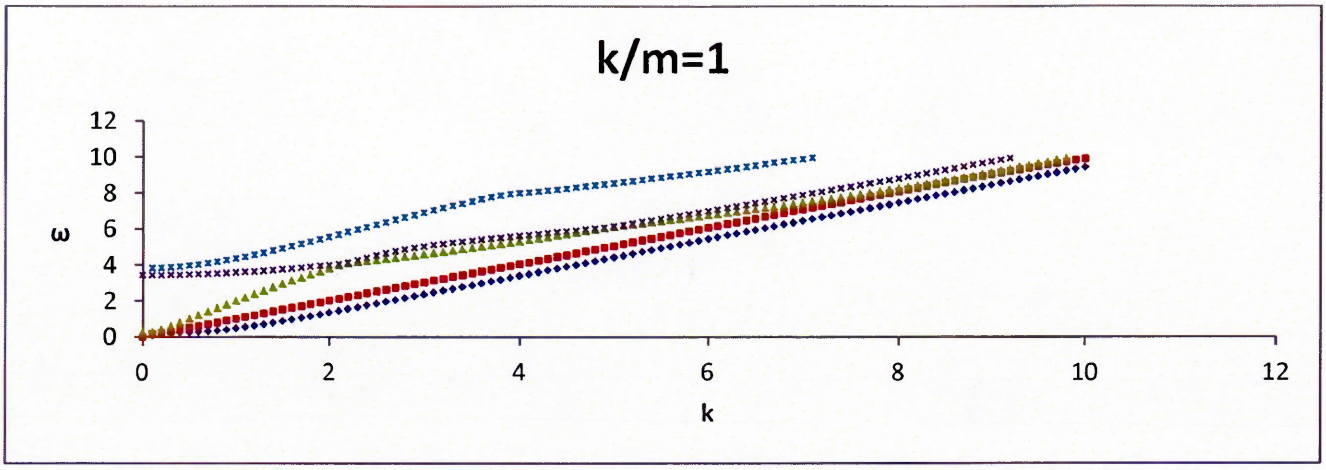

Figure 41(c): Thin cylinder with open-circuit boundary conditions (k/m=1).

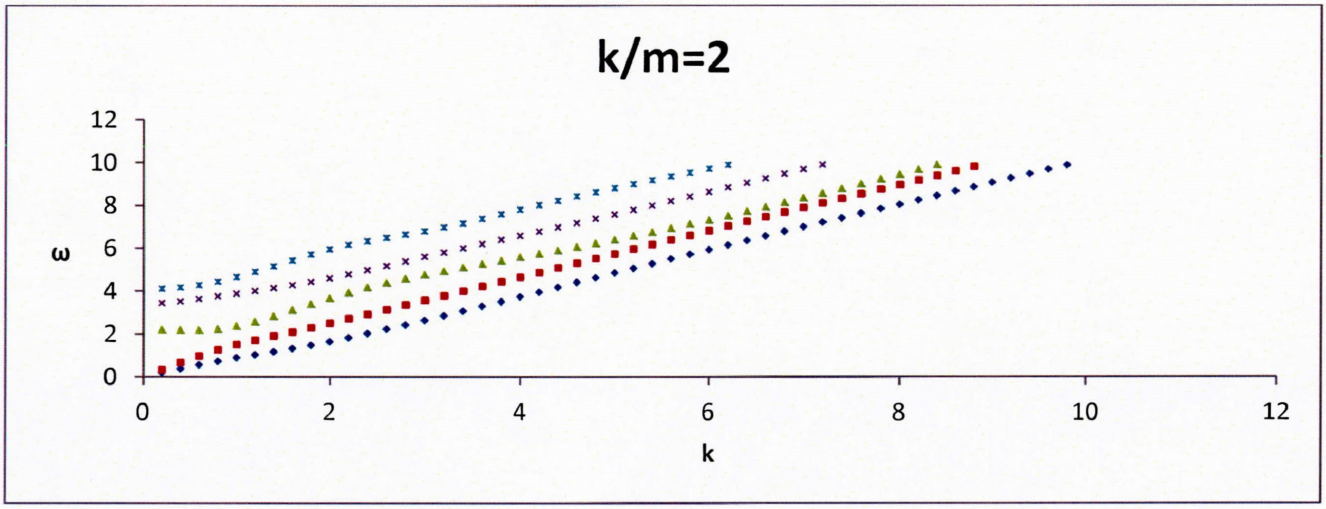

Figure 41(d): Thin cylinder with open-circuit boundary conditions (k/m=2).

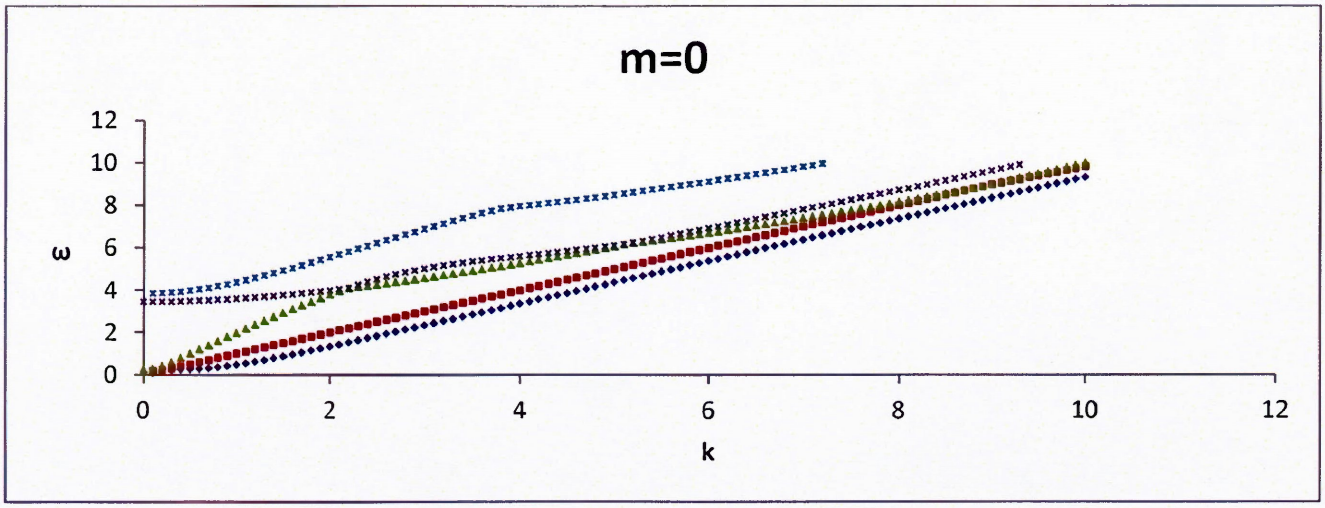

Figure 41(e): Thin cylinder with open-circuit boundary conditions (m=0).

Modes 1 and 2 are almost non-dispersive. Also, as k increases modes 3 and 4 seem to get closer to each other and also interact with each other.

Other than the case k=0 which corresponding wave propagating in the circumferential only, all the other wave spectra have the similar structures, it is suggested that, in the thin cylinder, the spiral wave propagation is not sensitive to its propagating direction. In the other words, the circumferential wave has a different wave structure than that of spiral waves. This is contrary to the case of a thick cylinder.

Chapter 4: Conclusions and Recommendations

4.1 Conclusions

The wave propagation in an infinitely long piezoelectric hollow cylinder and hollow circular annulus was studied in this thesis.

First, the frequency spectra of the thick and thin circular annulus (k=0) were investigated by applying the finite element method and the analytical solution method. The wave modes were presented by solving the second order eigenvalue problem to obtain the finite element method solution. The traction free mechanical boundary conditions along with the electrical (open and closed) boundary conditions have been applied to obtain the analytical solution.

Second, a convergence check has been done in order to determine the suitable number of elements required to carry out the results throughout the research. Convergence occurred at 20 elements, so 20 elements were used to carry out all the analysis. Then it was also necessary to cross check the results obtained from the developed FORTRAN program with the limited published results. The results were cross checked with published results for a hollow cylinder from reference [2]. This was done by setting all the electrical material properties to zero, this will result in an isotropic cylinder.

Third, the wave spectra for real, imaginary and complex wave number were presented. It was found that the electrical boundary conditions do not affect the wave spectra and only the geometry affects the wave spectra. When comparing the wave spectra of the open-circuit case and the closed-circuit case for a thick cylinder, it was found that the results are very similar. This was also seen in the case of the thin cylinder. This means that the electric boundary conditions have very minimum effects on the wave spectra. This was expected since the presented equations of motion are said to be decoupled when expressed in terms of the displacement and electric potential. When the wave spectra of the thin and thick cylinders are compared (open-circuit or closed circuit), it was found that there exist notable differences in the graphs. We can say that the wave spectra are sensitive to the geometry not the electrical boundary conditions in the case of circumferential wave propagation. Also, it was found that the lower modes at higher wave number m displace an almost non-dispersive relationship.

FEM results were presented for any given m. Therefore, m can be real, complex and imaginary. This means that the harmonic wave solution is not circumferentially periodic at complex, imaginary and non-integer real value m.

Lastly, the analyses were carried out on infinitely long piezoelectric cylinder. This is a more general study as compared with the simple case of a circular annulus. The wave propagation was studied in both the circumferential and axial direction (spiral wave). In order to validate the programs developed for this study, a cross check was performed to retrieve the results for the simple case of a circular annulus (k=0). This was achieved by setting k=0, w=0 and φ=0.

The method of solution (mathematical formulation) was carried out using both the finite element method and the analytical solution method. All the numerical results presented are using the finite element method since the analytical method computer code was not developed. The eigenvalue problem was found to be dependent on three parameters (ω, k and m). By giving k and m we can obtain ω. This will result in a three dimensional surface plot. Two dimensional plots were also presented. The first two dimensional plot was obtained by holding m as a constant and then the ω-k relationship is obtained. The second two dimensional plot is obtained by holding k as a constant and then the ω-m relationship is obtained. Results were also presented for k/m=0, 0.5, 1, 2 and infinity (propagation along a specific direction).

When the case of the thick cylinder (open-circuit and closed-circuit boundary conditions) is analyzed it was found that there are many similarities between the two cases. For example, in the ω-k relationships, as m is increased the cut-off frequencies also increased for each propagating mode. Also, it was found that lower order modes are almost non-dispersive for both open-circuit and closed circuit boundary condition cases (ω-k relationships and ω-m relationships). Therefore, the impact of the electrical boundary conditions on the wave spectra is minimal since there are many similarities that exist between the two cases.

For the thin cylinder case, it was found that there are many similarities between the open-circuit case and the closed-circuit case. The cut-off frequencies are independent of increasing m in the ω-k relationship since the cut-off frequencies do not change drastically when m is increased. Lower order modes (1st and 2nd mode) are found to be almost non-dispersive. The wave spectra for the ω-k relationships was found to be independent of m since there is very little change to the

wave spectra when m is increased. It was also found that in the ω-m relationships, that all the modes are almost non-dispersive. At high values of k, all the modes become an almost straight line which displays an almost perfect non-dispersive behavior. Also, the cut-off frequencies are separated into two groups. The first group contains modes 1, 2 and 3 and the second group contains modes 4 and 5. The impact of the electrical boundary conditions was found to be minimal on the wave spectra. This implies that the wave spectra are not sensitive to the electrical boundary conditions even though the equations of motion are coupled.

When the thick and thin cylinders are compared (open-circuit and closed-circuit case) the impact of this change was clearly seen on the wave spectra. Therefore, the wave spectra for thin cylinder with either closed-circuit or open circuit boundary conditions was found to be sensitive to the change of geometry of the cylinder.

The wave propagation was also studied along a specific direction for both the thin and the thick cylinders (open-circuit case). It was found that the spiral wave propagation is not sensitive to its propagating direction for all the presented cases except for the case k=0.

The presented study will serve as a benchmark for future work in this field of study. Suggested future recommendations are presented in the following section. The suggested future recommendations will outline what will be the next phase of this research.

4.2 Suggested Future Recommendations

1. The wave spectra presented should be extended to studying, for example, wave scattering and green's function.
2. Results for the presented wave spectra can be validated experimentally. This can be done by measuring the linear phase velocity in the circumferential direction at the surface of the cylinder. The relationship between the linear phase velocity c(r) and ω and m can be found in Equation (3.78) which was given in Chapter 2.
3. An experimental test loop can be developed to apply the knowledge in this study to real QNDT. Instead of using the conventional methods that are used to monitor the health of a given structure one can apply the knowledge from this research to QNDT. Understanding the wave propagation is important in determining where defects are in a given structure. By understanding the wave propagation in a perfect cylinder (no

defects) one can compare the wave spectra to the wave spectra of a real working cylinder. This comparison can help identify, possibly, the defect size and location.

References

1. Michael Y., Shatalov, Arthur G. Every and Alfred S. Yenwong-Fai, 2009, "Analysis of Non-Axisymmetric Wave Propagation in a Homogeneous Piezoelectric Solid Circular Cylinder of Transversely Isotropic Material," International Journal of Solids and Structures., Vol. 46, pp. 837-850.
2. Liu, G. and Qu J., 1998, "Guided Circumferential Waves in a Circular Annulus," J. Appl. Mech., Vol.65, pp.424-430.
3. Mindlin, R. D., and McNiven, H. D., 1960, "Axially Symmetric Waves in Elastic Rods," ASME Journal of Applied Mechanics, Vol. 27, pp. 145-151.
4. Mindlin, R. D., and Fox, E. A., 1960, "Vibrations and Waves in Elastic Bars of Rectangular Cross Section," J. Appl. Mech., Vol. 27, pp. 152-158.
5. Gazis, D., 1959, "Three Dimensional Investigation of the Propagation of Waves in Hollow Circular Cylinders, I. Analytical Foundation; II. Numerical Results." J. Acoust. Soc. Am., Vol. 14, pp. 1869-1876.
6. Miklowitz, J., 1978, "The Theory of Elastic Waves and Wave Guides, North-Holland Amsterdam".
7. Ditri, J. J., and Rose, J. L., 1992, "Excitation of Guided Elastic Wave Modes of Hollow Cylinders by Applied Surface Traction," J. Appl. Phys., Vol. 72, pp. 2589-2597.
8. Pochhammer, L., 1876. reineangew J.. Math. 81, 324.
9. Cook, E. G., and Valkenburg, H. E., 1954, "Surface Waves At Ultrasonic Frequencies," ASTM, Bull., Vol. 3, pp. 81-84.
10. Viktorov, I. A., 1958, "Rayleigh-type Waves on a Cylindrical Surface," Soviet Phys.—Acoust., Vol. 4, pp. 131-136.
11. Grace O. D., and Goodman R. R., 1965, "Circumferential Waves on Solid Cylinders," Department of Physics , Colorado State University.
12. Brekhovskikh, L. M., 1968, "Surface Waves Confined to the Curvature of the Boundary in Solid,"Soviet Phys., --Acous. Vol. 13, pp. 462-472.
13. Cerv, J., 1988, "Dispersion of Elastic Waves and Rayleigh-type Waves in a Thin Disc," Acta Technica Csav, Vol. 89, pp. 81-84.
14. Qu, J., Berthelot, Y., and Li, Z., 1996, "Dispersion of Guided Circumferential Waves in Circular Annulus," Review and Progress of Quantitative NDE, Vol. 15, pp. 169-176.
15. Mirsky, I., 1965 "Wave propagation in transversely isotropic circular cylinders. Part I: Theory," J. Acoust. Soc. Am., Vol. 37, pp. 1016-1021.
16. De Billy, M., 1995, "On the Influence of Anisotropy on Backscattering polar diagrams at resonance," Acustica, Vol. 81, pp. 281-284.
17. De Billy, M., 1995, "Resonance angular diagrams observed from anistropic cylinders submitted to an acoustic excitation," J. Acoust. Soc. Am., Vol. 97, pp. 852-855.
18. Kaduchak, G., and Loeffler C. M., 1996 "Backscattering of obliquely incident plane waves by a composite cylindrical shell constructed of isotropic and transversely isotropic layers," in the 131st meeting of the Acoustical Soc. Am, pp. 2545.

19. Tsai, Y. M., 1990, "Cylindrically guided waves in a transversely isotropic shaft," Review and Progress of Quantitative NDE, Vol. 9, pp.290-301.
20. Tsai, Y. M., 1991, "Longitudinal motion of a thick transversely isotropic hollow cylinder," J. Press. Ves. Tech., Vol. 113, pp. 585-589.
21. Dayal,V., 1993 "Longitudinal waves in homogeneous anisotropic cylinder bars immersed in fluid," J. Acoust. Soc. Am., Vol. 93, pp. 1249-1251.
22. Nagy, P. B. 1995, "Longitudinal guided wave propagation in a transversely isotropic rod immersed in fluid," J. Acoust. Soc. Am., Vol. 98, pp. 454-457.
23. Berliner, M. J. and Solecki, R., 1996, "Wave propagation in fluid-loaded, transversely isotropic cylinders. Part I: Analytical formulation," J. Acoust. Soc. Am., Vol. 99, pp. 1841-1847.
24. Berliner, M. J. and Solecki,R., 1996, "Wave propagation in fluid-loaded, transversely isotropic cylinders. Part II: Numerical Results," J. Acoust. Soc. Am., Vol. 99, pp. 1848-1853.
25. Voight, W., 1928, "Lehrbuch der Krystallphysik". Leipzig: B.G. Teubner; second edition.
26. Cady, W. G., 1946," Piezoelectricity". New York: McGraw-Hill; first edition.
27. Mason, W. P., 1950, "Piezoelectric Crystals and their Applications to Ultrasonics," Princeton, New Jersey: Van Nostrand.
28. Shaw, E. A. G., 1956, "On the resonant vibrations of thick barium titanate discs," J. Acoust. Am., Vol. 28, pp. 38-50.
29. EerNisse, E. P., 1967, "Variational Method for Electroelastic Vibration Analysis," IEEE Transactions on Sonics and Ultrasonics SU-14, pp. 153-160.
30. Allik, H., and Hughes, T. J. R., 1970, "Finite element method for Piezoelectric Vibration," International Journal of Numerical Methods in Engineering., Vol. 2, pp. 151-157.
31. Ostergaard, D. F. and Pawlak, T. P., 1986, "Three Dimensional Finite Elements for Analyzing Piezoelectric structures," Transactions of the Ultrasonic Symposium, Williamburg, Virginia, pp. 639-644.
32. Cheng, M. F., 1988, "Finite Element of Finite Axisymmetric Piezoelectric Cylinders," Master's Thesis, Tennessee Technical University, Cooksville, Tennessee.
33. Paul, H.S., 1986, "Vibrations of Circular Cylindrical Shells of Piezoelectric Silver Iodide Crystals," J. Acoust. Soc. Am., Vol. 40, pp. 1077-1080.
34. Wilson L. O. and Morrison J. A., 1977 "Wave propagation in Piezoelectric rods of Hexagonal Crystal Symmetry," Quarterly J. Mech. Appl. Mathematics XXX, pp. 388-395.
35. Paul, H.S. and Raju D. P., 1982, "Asymptotic Analysis of the Modes of Wave Propagation in a Piezoelectric Solid Cylinder," J. Acoust. Soc. Am., Vol. 71, pp. 255-263.
36. Ambardor, A. and Ferris C. D., 1978, "Wave Propagation in Piezoelectric two Layered Cylindrical Shell with hexagonal Symmetry," J. Acoust. Soc. Am., Vol. 63, pp. 781-792.
37. Paul, H.S. and Vankatesan, M., 1986, "Axisymmetric Vibration of a Piezoelectric Solid Cylinder Guided by a Thin Film," J. Acoust. Soc. Am., Vol. 80, pp. 1091-1096.

38. Buchanan, G. and Peddison, J., 1989, "Axisymmetric Vibration of infinite Piezoelectric Cylinders using one-dimensional Finite Elements," IEEE Transactions on Ultrasonic, Ferroelectrics, and Frequency Control., Vol.36, pp. 459-465.
39. Adelman, N. T., Stavsky, Y. and Segal, E. 1975, " Axisymmetric vibrations of radially polarized Piezoelectric Ceramic Cylinders," J. Sound and Vibration., Vol. 38, pp. 245-254.
40. Siao, J., Dong, S. and Song, J., 1994. Frequency spectra of laminated piezoelectric cylinders.ASME Journal of Vibrations and Acoustics 116, 364-370.
41. Bai, H., Taciroglu, E., Dong, S., Shah, A., June 2004. Elastodynamic Green's function for a laminated piezoelectric cylinder. International Journal of Solids and Structures, 41,6335–6350.
42. Michael Y., Shatalov, Arthur G. Every and Alfred S. Yenwong-Fai, 2009, "Analysis of Non-Axisymmetric Wave Propagation in a Homogeneous Piezoelectric Solid Circular Cylinder of Transversely Isotropic Material," International Journal of Solids and Structures., Vol. 46, pp. 837-850.
43. Liu, G. and Qu J., 1998, "Guided Circumferential Waves in a Circular Annulus," J. Appl. Mech., Vol.65, pp.424-430.
44. Tyutekin, V., 2003, "Helical Waves of an Elastic Cylindrical Shell," Andreev Acoustics Institute, Russian Academy of sciences.
45. Jiangon, Y., Bin, W. and Guoqiang, C., Augest 2008, "Wave Characteristics in Functionally graded Piezoelectric Hollow Cylinders," Arch Appl Mech (2009) 79: 807–824.
46. Jiangong, Y., Bin, W., July 2008, "Circumferential wave in magneto-electro-elastic functionally graded cylindrical curved plates," European Journal of Applied Mechanics A/ solids.
47. Honarvar, F., 1997, "Nondestructive Evaluation of Cylindrical Components by Resonance Acoustic Spectroscopy," J. Acoust. Soc. Am., Vol. 99, pp. 1945-1961.
48. Tiersten, H. F., 1968, "Linear Piezoelectric Plate. Plenum Press, New York".
49. Graff, K. F., 1975, "Waves in Elastic Solids. Dover, Oxford".
50. Abramowitz, M., Stegun, I. A., 1965, "Handbook of Mathematical Functions, Dover, New York".

Appendix A-Elements of the k-m Relationship Matrix (Circular Annulus)

$$Bj2 = J_m(\alpha_1 r_i)$$

$$By2 = Y_m(\alpha_1 r_i)$$

$$Bj1 = J_{m+1}(\alpha_1 r_i)$$

$$By1 = Y_{m+1}(\alpha_1 r_i)$$

$$Bj6 = J_m(\alpha_2 r_i)$$

$$By6 = Y_m(\alpha_2 r_i)$$

$$Bj5 = J_{m+1}(\alpha_2 r_i)$$

$$By5 = Y_{m+1}(\alpha_2 r_i) \tag{B1}$$

$$Q(1,1) = Bj2\left[\rho\omega^2 + \frac{(c_{11}-c_{12})m^2+(-c_{11}+c_{12})m}{r_i^2}\right] + Bj1\frac{1}{r_i}\left[\sqrt{\frac{\rho}{c_{11}}}w(c_{11}-c_{12})\right] \tag{B2}$$

$$Q(1,2) = By2\left[a\rho\omega^2 + \frac{(c_{11}-c_{12})m^2+(-c_{11}+c_{12})m}{r_i^2}\right] + By1\ \frac{1}{r_i}\left[\sqrt{\frac{\rho}{c_{11}}}w(c_{11}-c_{12})\right] \tag{B3}$$

$$Q(1,3) = Bj6\ i\left[\frac{(c_{11}-c_{12})m^2+(-c_{11}+c_{12})m}{r_i^2}\right] + Bj5\ \frac{im}{r_i}\left[c_{12}\sqrt{\frac{\rho}{c_{66}}}w - c_{12}\right] \tag{B4}$$

$$Q(1,4) = By6\ i\left[\frac{(c_{11}-c_{12})m^2+(-c_{11}+c_{12})m}{r_i^2}\right] + By5\ \frac{im}{r_i}\left[c_{12}\sqrt{\frac{\rho}{c_{66}}}w - c_{12}\right] \tag{B5}$$

$$Q(1,5) = 0 \tag{B6}$$

$$Q(1,6) = 0 \tag{B7}$$

$$Bj4 = J_m(\alpha_1 r_o)$$

$$By4 = Y_m(\alpha_1 r_o)$$

$$Bj3 = J_{m+1}(\alpha_1 r_o)$$

$$By3 = Y_{m+1}(\alpha_1 r_o)$$

$$Bj8 = J_m(\alpha_2 r_o)$$

$$By8 = Y_m(\alpha_2 r_o)$$

$$Bj7 = J_{m+1}(\alpha_2 r_o)$$

$$By7 = Y_{m+1}(\alpha_2 r_o) \tag{B8}$$

$$Q(2,1) = Bj4\left[\rho\omega^2 + \frac{(c_{11}-c_{12})m^2+(-c_{11}+c_{12})m}{r_o^2}\right] + Bj3\,\frac{1}{r_o}\left[\sqrt{\frac{\rho}{c_{11}}}w(c_{11}-c_{12})\right] \quad \text{(B9)}$$

$$Q(2,2) = By4\left[\rho\omega^2 + \frac{(c_{11}-c_{12})m^2+(-c_{11}+c_{12})m}{r_o^2}\right] + By3\,\frac{1}{r_o}\left[\sqrt{\frac{\rho}{c_{11}}}w(c_{11}-c_{12})\right] \quad \text{(B10)}$$

$$Q(2,3) = Bj8\left[\frac{(c_{11}-c_{12})m^2+(-c_{11}+c_{12})m}{r_o^2}\right] + Bj7\,\frac{im}{r_o}\left[c_{12}\sqrt{\frac{\rho}{c_{66}}}w - c_{12}\right] \quad \text{(B11)}$$

$$Q(2,4) = By8\left[\frac{(c_{11}-c_{12})m^2+(-c_{11}+c_{12})m}{r_o^2}\right] + By7\,\frac{im}{r_o}\left[c_{12}\sqrt{\frac{\rho}{c_{66}}}w - c_{12}\right] \quad \text{(B12)}$$

$$Q(2,5) = 0 \quad \text{(B13)}$$

$$Q(2,6) = 0 \quad \text{(B14)}$$

$$Q(3,1) = Bj2\,\frac{i}{r_i^2}[(c_{11}-c_{12})m^2 - (c_{11}-c_{12})m] + Bj1\,\frac{im}{r_i}\left[\sqrt{\frac{\rho}{c_{11}}}w(c_{11}-c_{12})\right] \quad \text{(B15)}$$

$$Q(3,2) = By2\,\frac{i}{r_i^2}[(c_{11}-c_{12})m^2 - (c_{11}-c_{12})m] + By1\,\frac{im}{r_i}\left[\sqrt{\frac{\rho}{c_{11}}}w(c_{11}-c_{12})\right] \quad \text{(B16)}$$

$$Q(3,3) = Bj6\left[\rho\omega^2 + \frac{(-c_{11}+c_{12})m^2+(c_{11}-c_{12})m}{r_i^2}\right] + Bj5\left[\sqrt{\frac{\rho}{c_{66}}}w\left(\frac{c_{11}-c_{12}}{r_i}\right)\right] \quad \text{(B17)}$$

$$Q(3,4) = By6\left[\rho\omega^2 + \frac{(-c_{11}+c_{12})m^2+(c_{11}-c_{12})m}{r_i^2}\right] + By5\left[\sqrt{\frac{\rho}{c_{66}}}w\left(\frac{c_{11}-c_{12}}{r_i}\right)\right] \quad \text{(B18)}$$

$$Q(3,5) = 0 \quad \text{(B19)}$$

$$Q(3,6) = 0 \quad \text{(B20)}$$

$$Q(4,1) = Bj4\,\frac{i}{r_o^2}[(c_{11}-c_{12})m^2 - (c_{11}-c_{12})m] + Bj3\,\frac{im}{r_o}\left[\sqrt{\frac{\rho}{c_{11}}}w(c_{11}-c_{12})\right] \quad \text{(B21)}$$

$$Q(4,2) = By4\,\frac{i}{r_o^2}[(c_{11}-c_{12})m^2 - (c_{11}-c_{12})m] + By3\,\frac{im}{r_o}\left[\sqrt{\frac{\rho}{c_{11}}}w(c_{11}-c_{12})\right] \quad \text{(B22)}$$

$$Q(4,3) = Bj8\left[\rho\omega^2 + \frac{(-c_{11}+c_{12})m^2+(c_{11}-c_{12})m}{r_o^2}\right] - Bj7\left[\sqrt{\frac{\rho}{c_{66}}}w\left(\frac{c_{11}-c_{12}}{r_o}\right)\right] \quad \text{(B23)}$$

$$Q(4,4) = By8\left[\rho\omega^2 + \frac{(-c_{11}+c_{12})m^2+(c_{11}-c_{12})m}{r_o^2}\right] - By7\left[\sqrt{\frac{\rho}{c_{66}}}w\left(\frac{c_{11}-c_{12}}{r_o}\right)\right] \quad \text{(B24)}$$

$$Q(4,5) = 0 \quad \text{(B25)}$$

$$Q(4,6) = 0 \quad \text{(B26)}$$

At the open circuit boundary condition

$$Q(5,1) = 0 \quad \text{(B27)}$$

$$Q(5,2) = 0 \quad \text{(B28)}$$

$$Q(5,3) = 0 \quad \text{(B29)}$$

$$Q(5,4) = 0 \quad \text{(B30)}$$

$$Q(5,5) = r^{m-1} \quad \text{(B31)}$$

$$Q(5,6) = -r^{-m-1} \quad \text{(B32)}$$

Equations (B31-B32) r=a=r_i

$$Q(6,1) = 0 \quad \text{(B33)}$$

$$Q(6,2) = 0 \quad \text{(B34)}$$

$$Q(6,3) = 0 \quad \text{(B35)}$$

$$Q(6,4) = 0 \quad \text{(B36)}$$

$$Q(6,5) = r^{m-1} \quad \text{(B37)}$$

$$Q(6,6) = -r^{-m-1} \quad \text{(B38)}$$

Equations (B37-B38) r=b=r_o

At the closed circuit boundary condition

$$Q(5,1) = 0 \quad \text{(B39)}$$

$$Q(5,2) = 0 \quad \text{(B40)}$$

$$Q(5,3) = 0 \quad \text{(B41)}$$

$$Q(5,4) = 0 \quad \text{(B42)}$$

$$Q(5,5) = r^{m} \quad \text{(B43)}$$

$$Q(5,6) = r^{-m} \quad \text{(B44)}$$

Equations (B43-B44) r==r_i

$$Q(6,1) = 0 \quad \text{(B45)}$$

$$Q(6,2) = 0 \quad \text{(B46)}$$

$$Q(6,3) = 0 \quad \text{(B47)}$$

$$Q(6,4) = 0 \tag{B48}$$

$$Q(6,5) = r^{m} \tag{B49}$$

$$Q(6,6) = r^{-m} \tag{B50}$$

Equations (B45-B50) $r=r_o$

Appendix B-Definitions of the Differential Operators $[L_r]$, $[L_\theta]$ *and* $[L_z]$

$$[L_r] = \begin{bmatrix} \frac{\partial}{\partial r} & 0 & 0 & 0 \\ \frac{1}{r} & 0 & 0 & 0 \\ 0 & 0 & 0 & 0 \\ 0 & 0 & 0 & 0 \\ 0 & 0 & 0 & 0 \\ 0 & \frac{\partial}{\partial r} - \frac{1}{r} & 0 & 0 \\ 0 & 0 & 0 & -\frac{\partial}{\partial r} \\ 0 & 0 & 0 & 0 \\ 0 & 0 & 0 & 0 \end{bmatrix}$$

$$[L_\theta] = \begin{bmatrix} 0 & 0 & 0 & 0 \\ 0 & \frac{1}{r}\frac{\partial}{\partial \theta} & 0 & 0 \\ 0 & 0 & 0 & 0 \\ 0 & 0 & \frac{1}{r}\frac{\partial}{\partial \theta} & 0 \\ 0 & 0 & 0 & 0 \\ \frac{1}{r}\frac{\partial}{\partial \theta} & 0 & 0 & 0 \\ 0 & 0 & 0 & 0 \\ 0 & 0 & 0 & -\frac{1}{r}\frac{\partial}{\partial \theta} \\ 0 & 0 & 0 & 0 \end{bmatrix}$$

$$[L_z] = \begin{bmatrix} 0 & 0 & 0 & 0 \\ 0 & 0 & 0 & 0 \\ 0 & 0 & \frac{\partial}{\partial z} & 0 \\ 0 & \frac{\partial}{\partial z} & 0 & 0 \\ \frac{\partial}{\partial \theta} & 0 & 0 & 0 \\ 0 & 0 & 0 & 0 \\ 0 & 0 & 0 & 0 \\ 0 & 0 & 0 & 0 \\ 0 & 0 & 0 & -\frac{\partial}{\partial z} \end{bmatrix}$$

$$[\boldsymbol{B_1}] = \begin{bmatrix} N_{,r} & 0 & 0 & 0 \\ \frac{1}{r}N & 0 & 0 & 0 \\ 0 & 0 & 0 & 0 \\ 0 & 0 & N_{,r} & 0 \\ 0 & N_{,r} - \frac{N}{r} & 0 & 0 \\ 0 & 0 & 0 & -N_{,r} \\ 0 & 0 & 0 & 0 \\ 0 & 0 & 0 & 0 \\ 0 & 0 & 0 & 0 \end{bmatrix}$$

$$[\boldsymbol{B_2}] = \begin{bmatrix} 0 & 0 & 0 & 0 \\ 0 & \frac{1}{r}N & 0 & 0 \\ 0 & 0 & 0 & 0 \\ 0 & 0 & \frac{1}{r}N & 0 \\ 0 & 0 & 0 & 0 \\ \frac{1}{r}N & 0 & 0 & 0 \\ 0 & 0 & 0 & 0 \\ 0 & 0 & 0 & -\frac{1}{r}N \\ 0 & 0 & 0 & 0 \end{bmatrix}$$

$$[\boldsymbol{B_3}] = \begin{bmatrix} 0 & 0 & 0 & 0 \\ 0 & 0 & 0 & 0 \\ 0 & 0 & N & 0 \\ 0 & N & 0 & 0 \\ N & 0 & 0 & 0 \\ 0 & 0 & 0 & 0 \\ 0 & 0 & 0 & 0 \\ 0 & 0 & 0 & 0 \\ 0 & 0 & 0 & -N \end{bmatrix}$$

Appendix C-Stiffness Matrices and Mass Matrix

$$[K_{11}] = \int [B_1{}^T][C][B_1]\, r\, dr$$

$$[K_{12}] = \int [B_1{}^T][C][B_2]\, r\, dr$$

$$[K_{13}] = \int [B_1{}^T][C][B_3] r\, dr$$

$$[K_{21}] = \int [B_2{}^T][C][B_1] r\, dr$$

$$[K_{22}] = \int [B_2{}^T][C][B_2]\, r\, dr$$

$$[K_{23}] = \int [B_2{}^T][C][B_3]\, r\, dr$$

$$[K_{31}] = \int [B_3{}^T][C][B_1]\, r\, dr$$

$$[K_{32}] = \int [B_3{}^T][C][B_2]\, r\, dr$$

$$[K_{33}] = \int [B_3{}^T][C][B_3]\, r\, dr$$

$$[M] = \int [N^T][\rho]\,[N\,] r\, dr$$

Appendix D-Elements of the *k-ω-m* Relationship Matrix (Cylinder)

r=r_i

$$Q(1,1) = \left[-c_{11}\Psi_{21}\alpha_1^2 - c_{13}k^2\Psi_{11} - e_{31}k^2\Psi_{31} + \frac{(c_{11}\Psi_{21}-c_{12}\Psi_{21})m^2+(c_{12}\Psi_{21}-c_{11}\Psi_{21})m}{r^2}\right]J_m(\alpha_1 r)$$

$$+\left[\frac{c_{11}\Psi_{21}-c_{12}\Psi_{21}}{r}\right]\alpha_1 J_{m+1}(\alpha_1 r)$$

$$Q(1,2) = \left[-c_{11}\Psi_{22}\alpha_2^2 - c_{13}k^2\Psi_{12} - e_{31}k^2\Psi_{32} + \frac{(c_{11}\Psi_{22}-c_{12}\Psi_{22})m^2+(c_{12}\Psi_{22}-c_{11}\Psi_{22})m}{r^2}\right]J_m(\alpha_2 r)$$

$$+\left[\frac{c_{11}\Psi_{22}-c_{12}\Psi_{22}}{r}\right]\alpha_2 J_{m+1}(\alpha_2 r)$$

$$Q(1,3) = \left[-c_{11}\Psi_{23}\alpha_3^2 - c_{13}k^2\Psi_{13} - e_{31}k^2\Psi_{33} + \frac{(c_{11}\Psi_{23}-c_{12}\Psi_{23})m^2+(c_{12}\Psi_{23}-c_{11}\Psi_{23})m}{r^2}\right] J_m(\alpha_3 r)$$

$$+\left[\frac{c_{11}\Psi_{23}-c_{12}\Psi_{23}}{r}\right]\alpha_1 J_{m+1}(\alpha_3 r)$$

$$Q(1,4) = \left[\frac{I(c_{11}-c_{12})m^2+I(c_{12}-c_{11})m}{r^2}\right]J_m(\beta r) + \left[\frac{I(c_{12}-c_{11})}{r}\right]\beta J_{m+1}(\beta r)$$

$$Q(1,5) = \left[-c_{11}\Psi_{21}\alpha_1^2 - c_{13}k^2\Psi_{11} - e_{31}k^2\Psi_{31} + \frac{(c_{11}\Psi_{21}-c_{12}\Psi_{21})m^2+(c_{12}\Psi_{21}-c_{11}\Psi_{21})m}{r^2}\right]Y_m(\alpha_1 r)$$

$$+\left[\frac{c_{11}\Psi_{21}-c_{12}\Psi_{21}}{r}\right]\alpha_1 Y_{m+1}(\alpha_1 r)$$

$$Q(1,6) = \left[-c_{11}\Psi_{22}\alpha_2^2 - c_{13}k^2\Psi_{12} - e_{31}k^2\Psi_{32} + \frac{(c_{11}\Psi_{22}-c_{12}\Psi_{22})m^2+(c_{12}\Psi_{22}-c_{11}\Psi_{22})m}{r^2}\right]Y_m(\alpha_2 r)$$

$$+\left[\frac{c_{11}\Psi_{22}-c_{12}\Psi_{22}}{r}\right]\alpha_2 Y_{m+1}(\alpha_2 r)$$

$$Q(1,7) = \left[-c_{11}\Psi_{23}\alpha_3^2 - c_{13}k^2\Psi_{13} - e_{31}k^2\Psi_{33} + \frac{(c_{11}\Psi_{23}-c_{12}\Psi_{23})m^2+(c_{12}\Psi_{23}-c_{11}\Psi_{23})m}{r^2}\right]Y_m(\alpha_3 r)$$

$$+\left[\frac{c_{11}\Psi_{23}-c_{12}\Psi_{23}}{r}\right]\alpha_1 Y_{m+1}(\alpha_3 r)$$

$$Q(1,8) = \left[\frac{I(c_{11}-c_{12})m^2+I(c_{12}-c_{11})m}{r^2}\right]Y_m(\beta r) + \left[\frac{I(c_{12}-c_{11})}{r}\right]\beta Y_{m+1}(\beta r)$$

$$Q(2,1) = \left[\frac{I(c_{11}-c_{12})\Psi_{21}m^2+I(c_{12}-c_{11})\Psi_{21}m}{r^2}\right]J_m(\alpha_1 r) + \left[\frac{I(c_{12}-c_{11})}{r}\right]m\Psi_{21}\alpha_1 J_{m+1}(\alpha_1 r)$$

$$Q(2,2) = \left[\frac{I(c_{11}-c_{12})\Psi_{22}m^2+I(c_{12}-c_{11})\Psi_{22}m}{r^2}\right]J_m(\alpha_2 r) + \left[\frac{I(c_{12}-c_{11})}{r}\right]m\Psi_{22}\alpha_2 J_{m+1}(\alpha_2 r)$$

$$Q(2,3) = \left[\frac{I(c_{11}-c_{12})\Psi_{23}m^2+I(c_{12}-c_{11})\Psi_{23}m}{r^2}\right] J_m(\alpha_3 r) + \left[\frac{I(c_{12}-c_{11})}{r}\right]m\Psi_{23}\alpha_3 J_{m+1}(\alpha_3 r)$$

$$Q(2,4) = \left[\frac{1}{2}(c_{11} - c_{12})\beta^2 + \frac{(c_{12}-c_{11})m^2+(c_{11}-c_{12})m}{r^2}\right] J_m(\beta\, r) + \left[\frac{(c_{12}-c_{11})}{r}\right] \beta\, J_{m+1}(\beta\, r)$$

$$Q(2,5) = \left[\frac{I(c_{11}-c_{12})\Psi_{21}m^2+I(c_{12}-c_{11})\Psi_{21}m}{r^2}\right] Y_m(\alpha_1\, r)\ \ m\Psi_{21}\alpha_1 Y_{m+1}(\alpha_1\, r)$$

$$Q(2,6) = \left[\frac{I(c_{11}-c_{12})\Psi_{22}m^2+I(c_{12}-c_{11})\Psi_{22}m}{r^2}\right] Y_m(\alpha_2\, r)\ + \left[\frac{I(c_{12}-c_{11})}{r}\right] m\Psi_{22}\alpha_2 Y_{m+1}(\alpha_2\, r)$$

$$Q(2,7) = \left[\frac{I(c_{11}-c_{12})\Psi_{23}m^2+I(c_{12}-c_{11})\Psi_{23}m}{r^2}\right] Y_m(\alpha_3\, r)\ m\Psi_{23}\alpha_3 Y_{m+1}(\alpha_3\, r)$$

$$Q(2,8) = \left[\frac{1}{2}(c_{11} - c_{12})\beta^2 + \frac{(c_{12}-c_{11})m^2+(c_{11}-c_{12})m}{r^2}\right] Y_m(\beta\, r) + \left[\frac{(c_{12}-c_{11})}{r}\right] \beta\, Y_{m+1}(\beta\, r)$$

$$Q(3,1) =$$
$$\left[\frac{1}{r}k\, I(c_{44}\Psi_{21} + c_{44}\Psi_{11} + e_{15}\Psi_{31})\right] J_m(\alpha_1\, r) + [-I(c_{44}\Psi_{21} + c_{44}\Psi_{11} + e_{15}\Psi_{31})]k\ \alpha_1 J_{m+1}(\alpha_1\, r)$$

$$Q(3,2) =$$
$$\left[\frac{1}{r}k\, I(c_{44}\Psi_{22} + c_{44}\Psi_{12} + e_{15}\Psi_{32})\right] J_m(\alpha_2\, r) + [-I(c_{44}\Psi_{22} + c_{44}\Psi_{12} + e_{15}\Psi_{32})]k\ \alpha_2 J_{m+1}(\alpha_2\, r)$$

$$Q(3,3) =$$
$$\left[\frac{1}{r}k\, I(c_{44}\Psi_{23} + c_{44}\Psi_{13} + e_{15}\Psi_{33})\right] J_m(\alpha_3\, r) + [-I(c_{44}\Psi_{23} + c_{44}\Psi_{13} + e_{15}\Psi_{33})]k\ \alpha_3\, J_{m+1}(\alpha_3\, r)$$

$$Q(3,4) = \left[\frac{-kc_{44}m}{r}\right] J_m(\beta\, r)$$

$$Q(3,5) = \left[\frac{1}{r}k\, I(c_{44}\Psi_{21} + c_{44}\Psi_{11} + e_{15}\Psi_{31})\right] Y_m(\alpha_1\, r) + [-I(c_{44}\Psi_{21} + c_{44}\Psi_{11} + e_{15}\Psi_{31})]k\ \alpha_1$$

$$Y_{m+1}(\alpha_1\, r)$$

$$Q(3,6) = \left[\frac{1}{r}k\, I(c_{44}\Psi_{22} + c_{44}\Psi_{12} + e_{15}\Psi_{32})\right] Y_m(\alpha_2\, r) + [-I(c_{44}\Psi_{22} + c_{44}\Psi_{12} + e_{15}\Psi_{32})]k\ \alpha_2$$

$$Y_{m+1}(\alpha_2\, r)$$

$$Q(3,7) = \left[\frac{1}{r}k\, I(c_{44}\Psi_{22} + c_{44}\Psi_{12} + e_{15}\Psi_{32})\right] Y_m(\alpha_3\, r) + [-I(c_{44}\Psi_{22} + c_{44}\Psi_{12} + e_{15}\Psi_{32})]k\ \alpha_2$$

$$Y_{m+1}(\alpha_3\, r)$$

$$Q(3,8) = \left[\frac{-k\, c_{44}m}{r}\right] Y_m(\beta\, r)$$

Q(4,1)=

$$\left[-\frac{1}{r}k\, I(-e_{15}\Psi_{11} + \varepsilon_{11}\Psi_{31} - e_{15}\Psi_{21})\right] J_m(\alpha_1\, r) + [I(-e_{15}\Psi_{11} + \varepsilon_{11}\Psi_{31} - e_{15}\Psi_{21})]k\ \alpha_1$$

$$J_{m+1}(\alpha_1\, r)$$

Q(4,2)=

$$\left[-\frac{1}{r}k\,I(-e_{15}\Psi_{12}+\varepsilon_{11}\Psi_{32}-e_{15}\Psi_{22})\right]J_m(\alpha_2\,r)+[I(-e_{15}\Psi_{12}+\varepsilon_{11}\Psi_{32}-e_{15}\Psi_{22})]k\,\alpha_2$$

$$J_{m+1}(\alpha_2\,r)$$

Q(4,3)=

$$\left[-\frac{1}{r}k\,I(-e_{15}\Psi_{13}+\varepsilon_{11}\Psi_{33}-e_{15}\Psi_{23})\right]J_m(\alpha_3\,r)+[I(-e_{15}\Psi_{13}+\varepsilon_{11}\Psi_{33}-e_{15}\Psi_{23})]k\,\alpha_3$$

$$J_{m+1}(\alpha_3\,r)$$

Q(4,4)=$\left[\frac{-k\,e_{15}m}{r}\right]J_m(\beta\,r)$

Q(4,5)=

$$\left[-\frac{1}{r}k\,I(-e_{15}\Psi_{11}+\varepsilon_{11}\Psi_{31}-e_{15}\Psi_{21})\right]Y_m(\alpha_1\,r)+[I(-e_{15}\Psi_{11}+\varepsilon_{11}\Psi_{31}-e_{15}\Psi_{21})]k\,\alpha_1$$

$$Y_{m+1}(\alpha_1\,r)$$

Q(4,6)=

$$\left[-\frac{1}{r}k\,I(-e_{15}\Psi_{12}+\varepsilon_{11}\Psi_{32}-e_{15}\Psi_{22})\right]Y_m(\alpha_2\,r)+[I(-e_{15}\Psi_{12}+\varepsilon_{11}\Psi_{32}-e_{15}\Psi_{22})]k\,\alpha_2$$

$$Y_{m+1}(\alpha_2\,r)$$

Q(4,7)=

$$\left[-\frac{1}{r}k\,I(-e_{15}\Psi_{13}+\varepsilon_{11}\Psi_{33}-e_{15}\Psi_{23})\right]Y_m(\alpha_3\,r)+[I(-e_{15}\Psi_{13}+\varepsilon_{11}\Psi_{33}-e_{15}\Psi_{23})]k\,\alpha_3$$

$$Y_{m+1}(\alpha_3\,r)$$

Q(4,8)=$\left[\frac{-k\,e_{15}m}{r}\right]Y_m(\beta\,r)$

Matrix elements Q(5,1) to Q(8,8) have the same definitions as Q(1,1) to Q(4,8) but $r=r_o$ (outer radius) instead of $r=r_i$